

Fall 11-23-2015

Applications of High Performance Affinity Chromatography with High Capacity Stationary Phases Made by Entrapment

John A. Vargas Badilla

University of Nebraska-Lincoln, johnvargasbadilla@gmail.com

Follow this and additional works at: <http://digitalcommons.unl.edu/chemistrydiss>



Part of the [Analytical Chemistry Commons](#)

Vargas Badilla, John A., "Applications of High Performance Affinity Chromatography with High Capacity Stationary Phases Made by Entrapment" (2015). *Student Research Projects, Dissertations, and Theses - Chemistry Department*. 65.
<http://digitalcommons.unl.edu/chemistrydiss/65>

This Article is brought to you for free and open access by the Chemistry, Department of at DigitalCommons@University of Nebraska - Lincoln. It has been accepted for inclusion in Student Research Projects, Dissertations, and Theses - Chemistry Department by an authorized administrator of DigitalCommons@University of Nebraska - Lincoln.

APPLICATIONS OF HIGH PERFORMANCE AFFINITY CHROMATOGRAPHY WITH HIGH
CAPACITY STATIONARY PHASES MADE BY ENTRAPMENT

by

John A. Vargas Badilla

A DISSERTATION

Presented to the Faculty of

The Graduate College at the University of Nebraska

In Partial Fulfillment of Requirements

For the Degree of Doctor of Philosophy

Major: Chemistry

Under the Supervision of Professor David S. Hage

Lincoln, Nebraska

August, 2015

APPLICATIONS OF HIGH PERFORMANCE AFFINITY CHROMATOGRAPHY WITH
HIGH CAPACITY STATIONARY PHASES MADE BY ENTRAPMENT

John A. Vargas Badilla, Ph.D.

University of Nebraska, 2015

Advisor: David S. Hage

High performance affinity chromatography (HPAC) is a technique that uses a biologically-related agent such as a transport protein or an antibody as the stationary phase in an HPLC system. In recent years, HPAC has been shown to be a valuable bioanalytical tool for studying solute-protein interactions. Human serum albumin (HSA), the most abundant protein in blood (with concentrations of 35 to 50 mg/mL in serum), has been shown to interact with many drugs, affecting their transport, excretion and metabolism. A physical method for immobilizing proteins in HPAC supports has been optimized in this dissertation by using HSA as a model protein.

This method involved the encapsulation of this protein inside the pores or near the surface of hydrazide-activated silica by using mildly oxidized glycogen as a capping agent for the hydrazide groups. Previous work has shown that this approach is able to retain the activity of the entrapped protein and to produce binding that is comparable to what is seen for the protein in its soluble form.

The entrapment process was optimized in a slurry based-format by altering the purification method for the oxidized glycogen, as well as increasing the concentration of protein and decreasing the total reaction volume that were used in this format. Through these changes, it was possible to obtain HPAC stationary phases with a nine-fold increase in their retention factor for warfarin. An

on-column entrapment approach was also examined, in which HSA and oxidized glycogen were reacted with hydrazide-activated silica in a flow-based format. This second approach provided retention factors for warfarin that were up to three-fold higher than those obtained by the slurry method. The ability of the on-column method to produce higher capacity stationary phases was then exploited for making chromatographic supports capable of separating sugars by using immobilized lectins. This on-column approach was also used for studying the effects of glycation of HSA on its binding properties with various sulfonylurea drugs that are used to treat diabetes. It was found that normal HSA and HSA with various levels of glycation, as immobilized by entrapment, did show changes in their drug binding parameters that depended on the level of glycation.

Finally, organic monoliths containing silver nanoparticles (AgNPs) were placed on glass slides and within microchannels and used for detecting a near infrared fluorescent dye. Up to ten-fold enhancement in the fluorescence signal of the dye was obtained for monoliths containing AgNPs when compared to control monoliths. This higher sensitivity can be exploited in making stationary phases or detection elements in microfluidic devices that can be utilized in the analysis of small samples and in applications such as flow-based biointeraction studies.

ACKNOWLEDGEMENTS

I would like to express my most sincere gratitude to my advisor, Dr. David S. Hage, for his mentorship throughout the past five years. Thank you for giving me the opportunity of pursuing my dream of obtaining my degree in a higher level institution of education while doing research in the field of bioanalytical chemistry. Thank you, Dr. Hage for your guidance in the completion of my research work and coursework. I want to especially thank you for your patience and support while accommodating to my needs.

I would also like to thank my committee members, Dr. Robert Powers, Dr. Rebecca Lai, Dr. Liangcheng Du and Dr. Gregory R. Bashford, for the patience and dedication they have shown in guiding me while I pursued my degree at UNL. I would like to especially thank Dr. Powers who accepted me into his laboratory for my first rotation when I came to Nebraska. That experience enriched my education by adding to my knowledge about high end NMR technology. I also learned a lot about working in a team in his laboratory.

I want to thank my family for all of their love and support over my years of graduate studies. Thank you, Loraine for your unconditional support during the thirteen years that we have been married and especially during my journey of pursuing a graduate degree. You were always there for me, even in the hard times. Your support while I attended graduate school is incommensurable and helped me to balance the duties of graduate school with the duties of parenting our two children. Thank you to my son John and my daughter Maite for brightening my life everyday with their laughter, joy and love every time I came back home from school. They have been my driving force for moving forward to the completion of my degree. I would also like to thank my Mom and Dad for encouraging me and supporting me to follow my dreams. Mom, you have instilled me with the faith in Jesus from an early age, which have helped me to walk

through life. Dad, you have shown me the example of working hard with honesty and caring for the others. You both have set up an example of a good family and good values for me. Thank you also to my brother, who has always been there, supporting me as part of a united family.

I would like to express my special gratitude to the Universidad de Costa Rica for giving me support for being in the United States with my family while I was pursuing my Ph.D. in Chemistry. I am proud to belong to this institution and am looking forward to giving my best as a faculty member. We are all grateful for having the experience of living in Lincoln, Nebraska, for five years. We all learned a lot during this process and also enjoyed this living experience.

TABLE OF CONTENTS

CHAPTER 1. INTRODUCTION	1
1.1. HIGH PERFORMANCE AFFINITY CHROMATOGRAPHY	1
1.2. COVALENT IMMOBILIZATION AND IMMOBILIZATION EFFECTS	2
1.3. ENTRAPMENT	3
1.4. QUANTITATIVE AFFINITY CHROMATOGRAPHY	4
1.5. OVERALL GOALS AND SUMMARY OF WORK	9
REFERENCES	10
CHAPTER 2. APPROACHES FOR INCREASING PROTEIN CONTENT DURING IMMOBILIZATION THROUGH ENTRAPMENT	14
2.1. INTRODUCTION	14
2.1.1. Examples of binding agents for HPAC	15
2.1.2. Preparation of stationary phases for HPAC by entrapment	21
2.2. EXPERIMENTAL SECTION	27
2.2.1. Reagents	27
2.2.2. Apparatus	27
2.2.3. Preparation of entrapped protein supports	28
2.2.4. Chromatographic methods	30
2.3. RESULTS AND DISCUSSION	32
2.3.1. Initial measurement of protein content by the BCA assay	32
2.3.2. Measurement of protein content in supports by fluorescence	33

2.3.3. Comparison of the fluorescence method with thermogravimetric analysis	38
2.3.4. Purification of oxidized glycogen	40
2.3.5. Size fractionation of oxidized glycogen	45
2.3.6. Optimization of protein entrapment based on measurements of protein content ..	50
2.3.7. Optimization of protein entrapment based on retention factor measurements	51
2.4. CONCLUSIONS.....	59
REFERENCES	60
CHAPTER 3. OPTIMIZATION OF A FLOW-BASED FORMAT FOR ENTRAPMENT	68
3.1. INTRODUCTION	68
3.2. EXPERIMENTAL SECTION	69
3.2.1. Reagents.....	69
3.2.2. Apparatus	70
3.2.3. Preparation of columns containing entrapped proteins.....	71
3.2.4. Chromatographic methods.....	72
3.3. RESULTS AND DISCUSSION	73
3.3.1. Optimization of the on-column entrapment method.....	73
3.3.2. Estimation of protein content following on-column entrapment.....	84
3.3.3. Column stability and comparison with previous HSA columns.....	90
3.4. CONCLUSIONS	94
REFERENCES	96
CHAPTER 4. RAPID ANALYSIS OF DRUG-PROTEIN BINDING BASED ON COLUMNS PREPARED BY ENTRAPMENT.....	102

4.1. INTRODUCTION	102
4.2. EXPERIMENTAL SECTION	108
4.2.1. Materials	108
4.2.2. Apparatus	108
4.2.3. Preparation of <i>in vitro</i> glycated HSA.....	110
4.2.4. Support preparation.....	111
4.2.5. Chromatographic studies	112
4.3. THEORY	114
4.3.1. Zonal elution.....	114
4.3.2. Frontal analysis	120
4.4. RESULTS AND DISCUSSION	121
4.4.1. Estimation of the amount of an entrapped protein in a column	121
4.4.2. Estimating the global affinity constant and site-specific binding constants for acetohexamide with entrapped normal HSA	130
4.4.3. Estimation of global affinity constants and the site-specific binding constants for sulfonylurea drugs with entrapped samples of normal or glycated HSA	135
4.5. CONCLUSIONS	141
REFERENCES	143
 CHAPTER 5. MICROFLUIDIC DEVICES WITH ENHANCED FLUORESCENCE	
DETECTION WITH MONOLITH SUPPORTS AND SILVER NANOPARTICLES	148
5.1. INTRODUCTION	148
5.2. EXPERIMENTAL SECTION.....	151

5.2.1. Materials	151
5.2.2. Solution preparation.....	152
5.2.3. Apparatus	152
5.2.4. Construction of microfluidic devices.....	153
5.2.5. Monolith preparation	154
5.3. THEORY	159
5.3.1. Fluorescence spectroscopy.....	159
5.3.2. Surface-enhanced fluorescence.....	162
5.4. RESULTS AND DISCUSSION	167
5.4.1. Initial alignment of NIR fluorescence microscope stage	167
5.4.2. Fluorescence measurements of IR 800CW in microchannels and monoliths.....	172
5.4.3. Fluorescence enhancement in EDMA/GMA monoliths	186
5.4.3.1. Adjustment of the fluorescence microscope controller	186
5.4.3.2. Preparation of monoliths with AgNP.....	187
5.4.4. Fluorescence enhancement by AgNPs for monoliths in microfluidic chips.....	201
5.5. CONCLUSIONS.....	208
REFERENCES	210
CHAPTER 6. SUMMARY AND FUTURE WORK	218
6.1. SUMMARY.....	218
6.2. FUTURE WORK.....	220

CHAPTER 1. INTRODUCTION

1.1. HIGH PERFORMANCE AFFINITY CHROMATOGRAPHY

High performance affinity chromatography (HPAC) is an analytical technique that combines the instrumentation, speed and efficiency of high performance liquid chromatography (HPLC) with the highly selective nature of affinity chromatography (AC) [1,2]. This liquid chromatographic technique uses the reversible interactions that are common in many biological systems, such as enzyme-substrate and antibody-antigen interactions. One of the components of such a system is coupled to a chromatographic matrix and placed into a column where it makes up the stationary phase (or “affinity ligand”). The other component is dissolved in the mobile phase and used as an applied target or analyte. The interactions between the affinity ligand and the analyte are usually quite strong and specific, allowing for the use of affinity chromatography in the purification and analysis of target compounds in complex samples [1-5].

The affinity ligand can be either a biological agent, such as a protein, or a synthetic molecule that mimics some of the binding properties of a natural compound. Examples of proteins that have been used as affinity ligands are human serum albumin (HSA), α 1-acid glycoprotein (AGP), and antibodies (or immunoglobulins). Lectins from plants are affinity ligands that also belong to this category. Examples of synthetic molecules that have been used as affinity ligands are boronic acids, metal ion chelates and biomimetic dyes [5-7].

When the affinity ligand (e.g., a protein) is immobilized onto a support that is suitable for use in high performance liquid chromatography (e.g., porous silica beads), the

resulting technique is known as HPAC. This method can be used in separations to conveniently isolate, measure, or study specific target-ligand interactions even when the applied targets are present in complex biological samples. Automation in HPAC can allow a drastic reduction in analysis times and the sample sizes that are required for the study of biological interactions when compared with other well-established techniques such as ultrafiltration and equilibrium dialysis. Another advantage of HPAC is its ability to reuse the same biological agent for many studies [1,2].

1.2. COVALENT IMMOBILIZATION AND IMMOBILIZATION EFFECTS

Covalent attachment is frequently used for immobilizing a ligand to an HPAC support. Functional groups such as amine, sulfhydryl, carbonyl or hydroxyl groups are commonly used for this process. Among these groups, amines have been widely used in the immobilization of proteins to silica supports for use in HPAC [4,8-13]. The Schiff base method is one example of such a technique [14]. The stability of the linkage between amine groups on a protein and aldehyde groups on a modified support has made this method attractive for work with proteins and antibodies [14]. However, covalent coupling methods can often have issues like multisite attachment, improper ligand orientation and immobilization near the active site of a ligand, which can lead to a decrease in or loss of the ligand's activity [5].

Multisite attachment refers to the coupling of an affinity ligand to a support through more than one functional group on the same ligand. This effect can stabilize the attachment of an affinity ligand to the support but can also deform the active site of the affinity ligand,

affecting its binding capacity. Improper orientation occurs when the site of attachment for an affinity ligand is at or near its active region. Steric hindrance occurs when this active site is blocked by the support or by neighboring affinity ligands. These factors can render the active site more difficult to reach by the target analyte. These problems (e.g., multisite attachment or improper orientation) may be present to some extent when immobilizing affinity ligands that are proteins and when using amine-based coupling methods, because amine groups may be present at many locations in such binding agents [5].

1.3. ENTRAPMENT

To overcome effects such as steric hindrance and improper attachment that can occur during the use of covalent immobilization methods, and to obtain protein-based stationary phases with high activities, alternative immobilization methods based on entrapment have been explored [5,15-19]. This approach involves the physical containment or encapsulation of an affinity ligand in a support that contains small pores or a highly cross-linked polymer network [5]. Entrapment has been extensively used in work with sol-gels for drug release and for applications involving low performance separations. However, most of these materials are not suitable for use in HPAC because of their inability to withstand high pressures and their slow mass transfer properties [15-17].

Recent work was conducted using entrapment with HPLC-grade silica and was tested by using HSA as a model affinity ligand [20]. This method has been employed for examining the interactions of HSA with sulfonylurea drugs by HPAC [21]. The entrapment procedure that was used in these studies involved placing HSA into a slurry containing hydrazide-activated porous silica and glycogen that had been mildly oxidized

by treatment with periodic acid to form aldehyde groups on the glycogen. The aldehyde groups on the glycogen were able to react with the hydrazide groups on the silica to form stable covalent bonds, while the HSA remained free in solution. During this reaction, some of the HSA became entrapped in a soluble form near the surface of the support or within the pores of the silica particles with no apparent loss of activity. Because glycogen is a large and highly branched carbohydrate polymer, the entrapped HSA was blocked by this polymer from leaving the support, but it was still possible for this protein to be reached by small molecules that could pass into and out of the pores of the support or reach its surface [20,21]. Besides providing good activity and avoiding many of the undesirable effects of covalent immobilization, this entrapment approach could be extended to other proteins and relatively large affinity ligands [20].

1.4. QUANTITATIVE AFFINITY CHROMATOGRAPHY

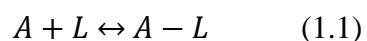
Although affinity chromatography was initially used for the isolation of biological compounds, over the past few decades a great deal of work has been done using this method for chemical analysis in areas such as biochemistry, pharmaceutical science, clinical chemistry, and environmental testing. In addition, the role of affinity chromatography in these fields has involved an increasing emphasis on the use of this method as a tool for studying the strength and rates of biological interactions, as well as in characterizing the number and types of binding sites that are involved in these interactions [2,4,22-24].

Several parts of this dissertation are concerned with the use of affinity chromatography and HPAC for the study and characterization of biological interactions. This type of application is also known as quantitative affinity chromatography or analytical

affinity chromatography. One advantage of using HPAC for this type of work is the ability to often reuse the same preparation of an immobilized affinity ligand for multiple experiments. This feature reduces the total amount of affinity ligand that is needed to conduct a series of experiments and reduces the cost per analysis. In addition, using the same affinity ligand preparation for many experiments helps to improve the reproducibility and precision by minimizing batch-to-batch and run-to-run variations. Finally, the ability of HPAC to make use of HPLC instrumentation allows for the automation of this method and reduces contamination of the columns between experiments by continuously washing the stationary phase with the mobile phase [25].

One experimental format that is used in HPAC for studying biological interactions is zonal elution (or “ZE”). This method involves making small injections of a probe compound or the analyte into a column that contains the immobilized affinity ligand. The outcome of this experiment is a peak for the probe or analyte that can be monitored by on-line detection. The most common parameter that is obtained from this chromatogram is the retention time of the injected compound, which is then used to help characterize the binding of this compound to the affinity ligand in the presence of a given mobile phase (e.g., a buffer that mimics physiological conditions or the natural environment of the affinity ligand) [1,25].

The binding between the applied analyte (A) and an affinity ligand (L) immobilized in a chromatographic column can be described by the following equations for a system with a 1:1 interaction,



$$K_a = \frac{k_a}{k_d} = \frac{[A-L]^*}{[A][L]^*} \quad (1.2)$$

where $A-L$ is the analyte-ligand complex, K_a is the association equilibrium constant for the formation of this complex, k_a and k_d are the association and dissociation rate constants for this complex, and $[L]^*$ or $[A-L]^*$ represent the surface concentrations of the affinity ligand and analyte-ligand complex at equilibrium [8,9]. These equations indicate that the retention of an analyte or target compound in an affinity column is determined by several parameters, such as the strength of the ligand-target interaction (e.g., K_a) and the amount of the immobilized affinity ligand that is present (e.g., $[L]^*$).

An analyte's retention in an affinity column can be described experimentally by its retention factor k , which is calculated as follows,

$$k = \frac{(t_r - t_m)}{t_m} \quad (1.3)$$

where t_r is the retention time of the analyte, and t_m is the column void time. The value of the retention factor is related to the association equilibrium constant and the amount of active affinity ligand in the column, as is indicated for a 1:1 reaction in Equation (1.4),

$$k = K_a \frac{m_L}{V_M} \quad (1.4)$$

where m_L is the moles of active affinity ligand, and V_M is the column void volume. The ratio m_L/V_M in this equation is the effective concentration of the affinity ligand in the column [8,9]. If the mobile phase during a zonal elution experiment contains other agents (e.g., competing solutes), it is further possible to use this type of study to obtain information on how these agents may affect the analyte-ligand interaction [8,9,25].

Another important format that can be used for studying a biological interaction by HPAC is frontal analysis (or "FA"). In this approach, a solution containing a known

concentration of a target analyte is continuously applied to an affinity column at a constant flow rate. As the target binds to the immobilized affinity ligand, the column becomes saturated and the amount of target that is eluting from the column gradually increases. This forms a breakthrough curve, which is essentially a titration of the active ligand in the column. If relatively fast association and dissociation kinetics are present on the time scale of this experiment, the mean position of the breakthrough curve can be used to determine the amount of active affinity ligand that is in the column and the association equilibrium constant of the affinity ligand for the target [5,25].

When frontal analysis is used to study a biological interaction, the moles of the target that are required to reach the mean point of the breakthrough curve are often measured at several concentrations of the applied target, and the resulting data are fit to various models to determine if this interaction involves one or more binding sites. The model that best describes the data is then used to determine the equilibrium constant(s) for the target-ligand interactions and the amount of each type of binding site in the column. For example, in the case of a target analyte (A) that has a single type of binding site on an affinity ligand (L), the frontal analysis results should provide a good fit to the following equation,

$$\frac{1}{m_{Lapp}} = \frac{1}{K_a m_L [A]} + \frac{1}{m_L} \quad (1.5)$$

where m_{Lapp} is the apparent moles of the analyte that are required to reach the mean breakthrough point for the column at a given molar concentration for the applied analyte, $[A]$. The parameters K_a and m_L in Equation (1.5) are the same as described earlier and can be determined from the slope and intercept of a best-fit line to the data for a system with a

single type of binding site. The goodness of the fit for the data to this equation can be assessed by using such tools as the correlation coefficient and the sum of the squares of the residuals. These and other tools can also be used to compare the fit of the data to other possible models, such as one involving two different types of binding sites [10,13,25].

The binding capacity of an affinity column can be determined from the value of mL that is obtained by frontal analysis [1,25,26]. When determining the binding capacity in this way, it is important to use a relatively slow flow rate that ensures that all of the applied analyte has sufficient time to interact with the immobilized affinity ligand [5]. The specific activity of the immobilized ligand can be found by dividing the measured binding capacity by the total amount of immobilized affinity ligand that is present. For instance, if the affinity ligand is a protein, the total amount of the binding agent that is present can be measured by an independent method such as a bicinchoninic acid (BCA) protein assay [5,18].

1.5. OVERALL GOALS AND SUMMARY OF WORK

It has been demonstrated recently that the entrapment of affinity ligands on hydrazide-activated silica, by capping this support with oxidized glycogen, can be a valuable approach for immobilizing proteins such as HSA for HPAC [20,21]. However, this method still needs further optimization for its use with alternative affinity ligands and in new applications. To expand the use of this technique for preparing other HPAC stationary phases, it is necessary to conduct studies to answer the following questions. First, “What methods can be used to increase the amount of the entrapped affinity ligand?” Second, “What are some novel applications of affinity columns that have been prepared by

entrapment, such as with regards to the study of biological interactions?” Third, “What are some alternative ways of carrying out the entrapment process?”

There are several benefits to seeking the answers to these questions. One possible outcome from this type of research would be the ability to prepare affinity microcolumns that are suitable for the analysis of extremely small samples or that could achieve low limits of detection. The use of entrapment to prepare small affinity columns with high binding capacities would also be useful in situations where a limited amount of ligand is available, such as in the immobilization of proteins from individual samples of human serum. The creation of new approaches for entrapment, such as the use of on-line systems for column preparation, would be useful in automating these methods and would also be of interest in applications such as personalized medicine for studies of protein-drug interactions and the measurement or characterization of biomarkers in samples that are taken from individuals with diseases such as diabetes or cancer.

Chapter 2 of this dissertation will look at ways for increasing the amount of a protein that can be immobilized through entrapment. The optimization of a flow-based entrapment procedure will be described in Chapter 3. A fast method for studying drug-protein binding, as based on entrapped protein columns, will be presented in Chapter 4. Finally, a platform that can be used for on-column detection in microscale chromatography or post-column sensing in microfluidic devices, and using fluorescent dyes and monolithic supports, is examined in Chapter 5.

REFERENCES

1. D.S. Hage, P.F. Ruhn, An introduction to affinity chromatography, in: D.S. Hage (Ed.) Handbook of Affinity Chromatography, 2nd ed., CRC Press, Boca Raton, FL, 2006, pp. 3-13.
2. R.R. Walters, Affinity chromatography, *Anal. Chem.*, 57 (1985) 1099A-1114A.
3. G.T. Hermanson, A.K. Mallia, P.K. Smith, Immobilized Affinity Ligand Techniques, Academic Press, Waltham, MA, 1992.
4. D.S. Hage, J.A. Anguizola, C. Bi, R. Li, R. Matsuda, E. Papastavros, E. Pfaunmiller, J. Vargas, X. Zheng, Pharmaceutical and biomedical applications of affinity chromatography: recent trends and developments, *J. Pharm. Biomed. Anal.*, 69 (2012) 93-105.
5. H.S. Kim, D. Hage, S., Immobilization methods for affinity chromatography, in: D.S. Hage (Ed.) Handbook of Affinity Chromatography, 2nd ed., CRC Press, Boca Raton, FL, 2006, pp. 36-78.
6. X.C. Liu, W.H. Scouten, Boronate affinity chromatography, in: D.S. Hage (Ed.) Handbook of Affinity Chromatography, 2nd ed., CRC Press, Boca Raton, FL, 2006, pp. 215-229.
7. N.E. Labrou, K. Mazitsos, Y.D. Clonis, Dye-ligand and biomimetic affinity chromatography, in: D.S. Hage (Ed.) Handbook of Affinity Chromatography, 2nd ed., CRC Press, Boca Raton, FL, 2006, pp. 231-255.

8. D.S. Hage, High-performance affinity chromatography: a powerful tool for studying serum protein binding, *J. Chromatogr. B*, 768 (2002) 3-30.
9. D.S. Hage, J. Anguizola, O. Barnaby, A. Jackson, M.J. Yoo, E. Papastavros, E. Pfaunmiller, M. Sobansky, Z.H. Tong, Characterization of drug interactions with serum proteins by using high-performance affinity chromatography, *Curr. Drug Metabol.*, 12 (2011) 313-328.
10. D.S. Hage, J.A. Anguizola, A.J. Jackson, R. Matsuda, E. Papastavros, E. Pfaunmiller, Z.H. Tong, J. Vargas-Badilla, M.J. Yoo, X.W. Zheng, Chromatographic analysis of drug interactions in the serum proteome, *Anal. Methods*, 3 (2011) 1449-1460.
11. D.S. Hage, J. Austin, High-performance affinity chromatography and immobilized serum albumin as probes for drug- and hormone-protein binding, *J. Chromatogr. B*, 739 (2000) 39-54.
12. D.S. Hage, A. Jackson, M.R. Sobansky, J.E. Schiel, M.J. Yoo, K.S. Joseph, Characterization of drug-protein interactions in blood using high-performance affinity chromatography, *J. Sep. Sci.*, 32 (2009) 835-853.
13. D.S. Hage, S.A. Tweed, Recent advances in chromatographic and electrophoretic methods for the study of drug-protein interactions, *J. Chromatogr. B*, 699 (1997) 499-525.
14. G.T. Hermanson, *Bioconjugate Techniques*, 2nd ed., Academic Press, Haltham, MA, 2008.

15. D. Avnir, T. Coradin, O. Lev, J. Livage, Recent bio-applications of sol-gel materials, *J. Mater. Chem.*, 16 (2006) 1013-1030.
16. J. Livage, T. Coradin, C. Roux, Encapsulation of biomolecules in silica gels, *J. Phys. Condens. Matter*, 13 (2001) R673-R691.
17. L. Betancor, H.R. Luckarift, Bioinspired enzyme encapsulation for biocatalysis, *Trends Biotechnol.*, 26 (2008) 566-572.
18. R.A. Thompson, S. Andersson, S. Allenmark, Direct liquid chromatographic separation of enantiomers on immobilized protein stationary phases. VII. Sorbents obtained by entrapment of cross-linked bovine serum albumin in silica, *J. Chromatogr.*, 465 (1989) 263-270.
19. S. Andersson, S. Allenmark, P. Erlandsson, S. Nilsson, Direct liquid chromatographic separation of enantiomers on immobilized protein stationary phases . VIII. A comparison of a series of sorbents based on bovine serum albumin and its fragments, *J. Chromatogr.*, 498 (1990) 81-91.
20. A.J. Jackson, H. Xuan, D.S. Hage, Entrapment of proteins in glycogen-capped and hydrazide-activated supports, *Anal. Biochem.*, 404 (2010) 106-108.
21. A.J. Jackson, J. Anguizola, E.L. Pfaunmiller, D.S. Hage, Use of entrapment and high-performance affinity chromatography to compare the binding of drugs and site-specific probes with normal and glycosylated human serum albumin, *Anal. Bioanal. Chem.*, 405 (2013) 5833-5841.

22. C.A.C. Wolfe, D.S. Hage, W. Clarke, Affinity methods in clinical and pharmaceutical Analysis, in: D.S. Hage (Ed.) Handbook of Affinity Chromatography, 2nd ed., CRC Press, Boca Raton, FL, 2006, pp. 461-486.
23. N. Jordan, I.S. Krull, Affinity chromatography in biotechnology, in: D.S. Hage (Ed.) Handbook of Affinity Chromatography, 2nd ed., CRC Press, Boca Raton, FL, 2006, pp. 487-516.
24. M.A. Nelson, D.S. Hage, Environmental analysis by affinity chromatography, in: D.S. Hage (Ed.) Handbook of Affinity Chromatography, 2nd ed., CRC Press, Boca Raton, FL, 2006, pp. 517-545.
25. D.S. Hage, J. Chen, Quantitative affinity chromatography, in: D.S. Hage (Ed.) Handbook of Affinity Chromatography, 2nd ed., CRC Press, Boca Raton, FL, 2006, pp. 595-628.
26. D.S. Hage, M.A. Nelson, H. Xuan, Application and elution in affinity chromatography, in: D.S. Hage (Ed.) Handbook of Affinity Chromatography, 2nd ed., CRC Press, Boca Raton, FL, 2006, pp. 79-97

CHAPTER 2.

APPROACHES FOR INCREASING PROTEIN CONTENT DURING IMMOBILIZATION THROUGH ENTRAPMENT

2.1. INTRODUCTION

The interaction of small solutes with proteins in serum is important for many drugs and biological agents. Serum proteins such as human serum albumin (HSA) and α 1-acid glycoprotein (AGP) are known to bind to many small endogenous compounds in the body, as well as pharmaceutical agents. Drug-protein interactions in serum are often significant, with approximately 43% of the 1500 most common drugs having at least 90% binding to proteins in serum. These interactions can affect the free concentration of a drug in blood and can play an important role in determining the distribution, activity, excretion, and metabolism of such an agent in the body [1-3].

The study of drug-protein interactions has been carried out in the past by using techniques such as equilibrium dialysis, ultrafiltration, and other solution-based reference methods (e.g., various spectroscopic methods) [4,5]. High performance affinity chromatography (HPAC) is a type of affinity chromatography that utilizes solid supports consisting of small, rigid particles that can withstand the high pressures that are typical of HPLC. These supports can provide the enhanced mass transfer properties that are needed in HPLC for chromatographic separations and are better suited for analytical applications than less rigid and larger diameter supports [7]. Supports that can be used in HPAC include silica, azalactone beads, hydroxylated polystyrene media, and some types of monolithic

columns [5,7-9]. The study of drug-protein interactions by HPAC with proteins such as HSA and AGP has provided binding parameters that show good agreement with values obtained by using soluble HSA or AGP [5].

One advantage of HPAC is that the same protein or binding agent preparation can often be used for multiple experiments. Thus, only a small amount of a protein is often required in HPAC to conduct a large number of studies. This feature is useful when a limited amount of the binding agent is available and helps to provide good precision by minimizing run-to-run variations in this binding agent. The speed and precision of HPAC, as well as its ability to be automated, also make this method attractive for analytical applications and drug-protein binding studies [8,10-12].

2.1.1. Examples of binding agents for HPAC

HSA is commonly used as an immobilized affinity ligand in HPAC to study drug-protein binding. HSA was used in this study as a model binding agent for identifying ways of improving immobilization methods (i.e., entrapment, in this case) and for achieving a higher protein content in columns that are to be used in HPAC. HSA is the most abundant protein in serum and binds to numerous drugs and endogenous compounds. HSA makes up about 60% of the total protein content in blood and has a typical concentration that ranges from 35 to 50 g/L. This protein has a molar mass of 66,438 g/mol and consists of a single polypeptide chain of 585 amino acids, which form a structure that is stabilized by 17 disulfide bonds. The binding of drugs to serum proteins like HSA often improves their solubility and is an important source of interactions that may occur between some drugs and endogenous agents such as fatty acids. These agents may compete directly or indirectly for the same binding sites on serum proteins. This fact makes the binding by HSA and

other serum proteins with drugs a subject of great interest to the pharmaceutical industry [1-3]. Figure 2.1 shows the structure of HSA and the location of its two major binding sites for drugs: Sudlow sites I and II. Sudlow site I (also known as the warfarin-azapropazone site) tends to bind bulky heterocyclic compounds, while Sudlow site II (also known as the indole-benzodiazepine site) often binds to aromatic carboxylic acids [8,13,14].

The lectin concanavalin A (Con A) was a second binding agent that was considered in this study. Lectins are non-immune system proteins that are often isolated from plants and that can agglutinate cells and/or precipitate complex carbohydrates. Lectins have the ability to bind to specific sugar moieties and have been used extensively as affinity ligands for fractionating and isolating glycoproteins and glycopeptides. For example, Con A can bind to mannosyl and glucosyl residues, while the lectin wheat germ agglutinin (WGA) recognizes N-acetyl-glucosamine (GlcNAc) and sialic acid (NeuNAc) residues [15-19].

Figure 2.1 Structure of HSA, including its two major binding sites for drugs (i.e., Sudlow sites I and II). This structure includes a molecule of the drug *R*-warfarin (shown in blue) that is bound to Sudlow site I. The image is based on PDB entry 2bxd and was generated using Uniprot file ID: P02758 [6].

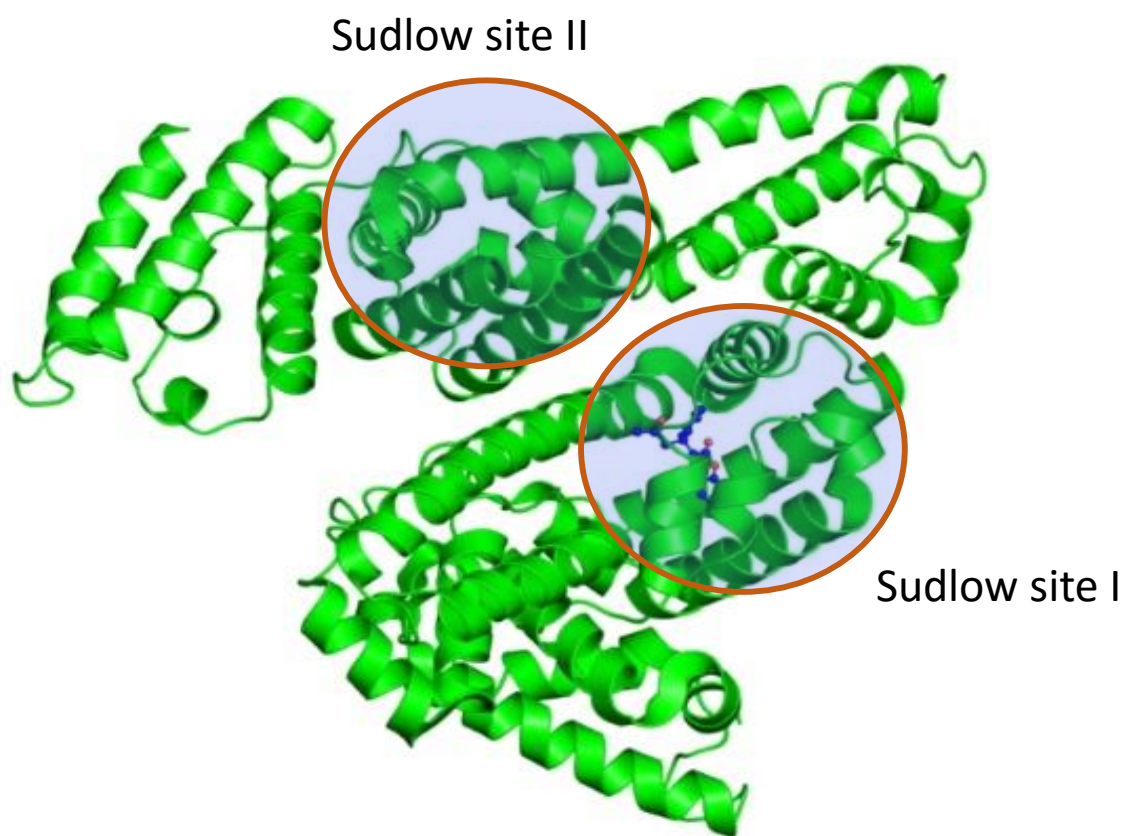


Figure 2.2 The tetrameric structure of Con A, which was co-crystallized with the glycopeptide Man-WYD. The four monomer chains are represented by different colors. Each identical monomeric unit also includes Ca^{2+} (green), Mn^{2+} (purple) and the glycopeptide moiety. This image is based on PDB entry 4czs [24].



Con A is obtained from the jack bean and is the first lectin whose structure was determined. It contains 237 amino acid residues and has a molar mass of 25.5 kDa. The monomers of Con A can aggregate to form dimers and tetramers. Each monomer has one binding site for a saccharide, one transition metal (usually Mn^{2+}) and one Ca^{2+} ion [20,21]. This binding site can interact with mannosyl and glucosyl residues of polysaccharides and glycoproteins (i.e., groups containing C3, C4 and C6 hydroxyl groups) and can be used to capture *N*-glycosylated peptides/proteins with broad specificity [22]. Figure 2.2 shows the structure of the tetrameric form of Con A [23,24].

2.1.2. Preparation of stationary phases for HPAC by entrapment

The use of binding agents such as HSA or Con A in HPAC starts by immobilizing such a protein on a suitable support. Porous silica with a particle size of 7 μm and a pore size of 300 nm was selected for use in this work as the support material, due to its good mechanical stability and mass transfer properties. This same material has also been used in many previous studies with HPAC based on the same or similar proteins to those that were used in this current study [3,25-27]. The particle size and pore size selected for this support in this study have been found in a prior report to provide the highest protein content for similar supports that have been prepared by using protein entrapment [28].

The porous silica that was used as a starting material for this work was converted to a hydrazide-activated form for use in protein entrapment, according to a previously published procedure [29]. As can be seen in Figure 2.3, the first step was to treat the silica particles with 3-glycidoxypropyltrimethoxysilane, followed by the addition of dilute sulfuric acid to generate diol-bonded silica. This material was then dried and could be stored as an intermediate support for several months prior to its use for protein entrapment.

The next step was to oxidize part of the diol-bonded silica with periodic acid to create aldehyde groups on the surface of the support. This was followed by the reaction of these aldehyde groups with a homobifunctional hydrazide reagent to create hydrazide-activated silica. In this study, oxalic dihydrazide was added to the aldehyde-activated silica to form the hydrazide-activated support, and sodium borohydride was later added to reduce and remove any aldehyde groups that were still on the support.

In the next step of the entrapment process, a slurry containing the hydrazide-activated silica in pH 5.0, 0.10 M potassium phosphate buffer was combined with the protein that was to be entrapped (e.g., HSA or Con A) and a mildly oxidized form of glycogen, which was used as a capping agent. During the entrapment process, aldehyde groups on the oxidized glycogen were allowed to react with hydrazide groups on the support. At the same time, part of the protein became trapped by the glycogen in the support and remained in a soluble form (see Figure 2.4) [28,30].

Previous work has shown that this entrapment process can place proteins onto a silica support while maintaining their biological activity [30]. The purpose of this current study was to further optimize this method to increase the final protein content. A high protein content was desired because it should result in higher resolution and binding strengths for the resulting HPAC columns. The activity of HSA columns that were made by this method was monitored by using warfarin and carbamazepine, whose interactions with HSA are well-characterized [26,31-36]. The activity of columns prepared with Con A were measured by using 4-methylumbelliperyl α -D-mannopyranoside (MUM), which can be detected by absorbance or fluorescence; and has a relatively high affinity for Con A [17].

Figure 2.3 Scheme for the preparation of hydrazide-activated silica from porous silica particles. Adapted with permission from Ref. [29].

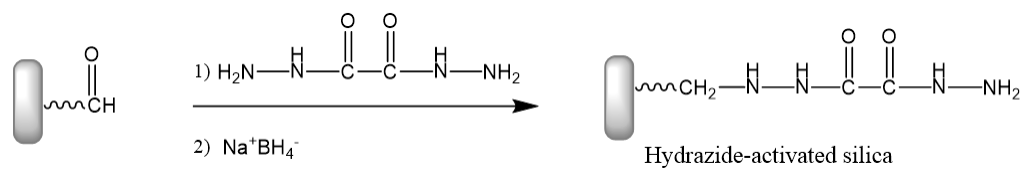
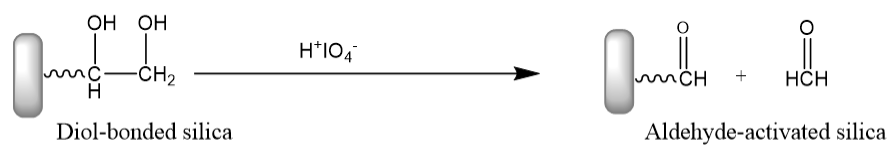
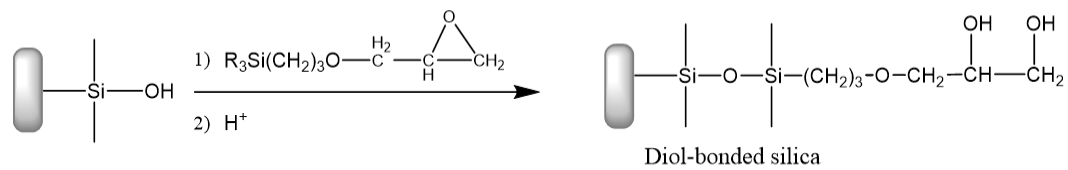
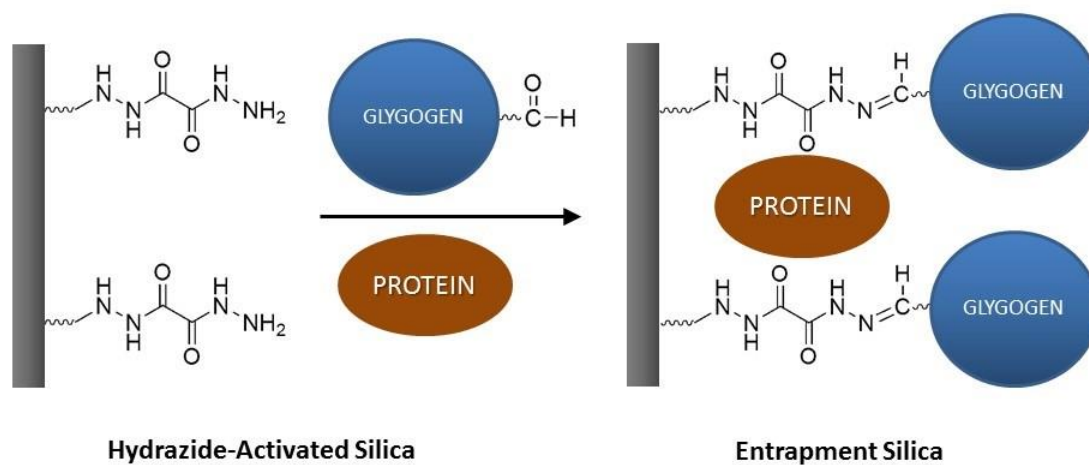


Figure 2.4 Scheme for protein entrapment by the reaction of mildly-oxidized glycogen with hydrazide-activated silica. Adapted with permission from Ref. [28].



2.2. EXPERIMENTAL SECTION

2.2.1. Reagents

HSA (essentially fatty acid free, purity $\geq 96\%$), Con A (type V, lyophilized powder, purity $\geq 99\%$), bovine serum albumin (BSA, fraction V, purity $\geq 96\%$), glycogen (bovine liver, type IX, total glucose $\geq 85\%$, dry basis), racemic warfarin (purity $\geq 98\%$), MUM (purity $\geq 96\%$), 4-methylumbelliperyl α -D-galactopyranoside (MUGA, purity $\geq 98\%$), periodic acid reagent (H_5IO_6 , purity 99%), Lucifer yellow CH (LyCH, purity $\geq 85\%$), fluorescein isothiocyanate (FITC, isomer I, purity 90%) and FITC-BSA conjugate (purity 90%) were purchased from Sigma-Aldrich (St. Louis, MO, USA). Nucleosil Si-300 silica (7 μm particle diameter, 300 \AA pore size, 100 m^2/g surface area) was obtained from Macherey Nagel (Düren, Germany). A micro-bicinchoninic acid (BCA) protein assay kit was purchased from Pierce (Rockford, IL, USA). All other chemicals were of the purest grades available. Econo-Pac 10DG disposable desalting columns (3.3 mL void volume, 6 kDa exclusion limit; BioRad, Hercules, CA, USA) and Vivaspin 6 ultrafiltration tubes (30 kDa cutoff; Sartorius, Göttingen, Germany) were used for glycogen purification. All buffers and aqueous solutions were prepared using water from a Nanopure system (Barnstead, Dubuque, IA, USA). Buffers were filtered using 0.20 μm GNWP nylon membranes from Millipore (Billerica, MA, USA) and were degassed by sonication under vacuum for at least 20 min prior to use.

2.2.2. Apparatus

The chromatographic system consisted of a 1200 isocratic pump from Agilent (Santa Clara, CA, USA) and a Series 200 UV-Vis detector plus a vacuum degasser from Perkin-Elmer (Waltham, MA, USA). Samples were injected using a Rheodyne LabPro valve (Cotati, CA, USA) that was equipped with a 5 μ L or a 20 μ L loop. An Isotemp 9100 circulating water bath (Fisher Scientific, Pittsburgh, PA, USA) and a water jacket from Alltech (Deerfield, IL, USA) were used for temperature control of the columns. The chromatographic data was collected using LabView 8 software (National Instruments, Austin, TX, USA) and analyzed using PeakFit 4.12 (Systat Software, San Jose, CA, USA).

A Pack in a Box system (ChromTech, Apple Valley, MN, USA) was used for packing the supports into columns. A UV-160A spectrophotometer (Shimadzu, Kyoto, Japan) was used for the BCA protein assay. A Cary Eclipse fluorescence spectrophotometer (Varian, Palo Alto, CA, USA) with a microplate reader adaptor was used for the protein assay based on fluorescence. The thermogravimetric analysis of silica samples was performed using a TGA7 system (Perkin Elmer, Waltham, MA, USA) equipped with nitrogen flow for inert analysis conditions and data collection software.

2.2.3. Preparation of entrapped protein supports

The columns containing entrapped proteins were prepared from Nucleosil 300-7, HPLC-grade porous silica that had been converted into diol silica, as based on a previous procedure [29]. The diol silica was dried and stored for future use. Batches of this silica were converted into hydrazide-activated silica by following a procedure that has also been described in the literature [29].

The initial conditions used for entrapment were based on previous work [28] and involved making a slurry containing 0.08 g of hydrazide-activated silica and 0.8 mL of 10 mg/mL HSA in pH 5.0, 0.10 M potassium phosphate buffer. This slurry was degassed in a sonication bath for 10 min to ensure there was no trapped air within the support. Next, 0.28 mL of a 4.25 mg/ml solution of mildly oxidized glycogen in the pH 5.0, 0.10 phosphate buffer was added (i.e., an amount equivalent to 15 mg glycogen/g silica). The glycogen had been previously oxidized with periodic acid reagent in a pH 5.0 buffer containing 20 mM sodium acetate and 15 mM sodium chloride, as well as 17 mg of glycogen and 135 mg of the periodic acid reagent in 4 mL of this buffer; this oxidation was done for a period of 16 h in the dark. The volume of solution for the entrapment reaction was then adjusted to 2 mL by adding pH 5.0, 0.10 M phosphate buffer. This slurry was placed on a rotation mixer for 16 h at 4 °C. Finally, 50 µL of oxalic dihydrazide (at a concentration of 1 mg/mL in pH 5.0, 0.10 M phosphate buffer) was added and allowed to mix with this slurry for 1 h to cap any remaining aldehyde groups on the glycogen and to decrease possible non-specific binding of other solutes to the column. Control supports were prepared in the same manner, but with only buffer being used in place of the protein solution during the entrapment step.

Several conditions were varied in this study to increase the amount of entrapped protein. These conditions included the method that was used to isolate the oxidized glycogen, the concentration of the protein that was used during the entrapment method, and the mass ratio of the protein versus silica that was utilized. The entrapped protein supports and control supports were suspended in pH 7.4, 0.067 M potassium phosphate buffer and were downward slurry packed into 1.0 cm × 2.1 mm i.d. stainless

steel columns. A pH 7.4, 0.067 M potassium phosphate buffer was used as the packing solution. As the support slurry entered the column, the pressure was increased gradually until it reached a maximum of 3500 psi and was held at this pressure for 50 min while passing the pH 7.4 phosphate buffer through the column. The pressure was then decreased gradually to avoid disturbing the packed support. The column was later taken off of the packing system, and its assembly was completed. Before carrying out any experiments with these supports, each column was placed in an HPLC system and pH 7.4, 0.067 M potassium phosphate buffer was passed through the column at 0.5 mL/min for at least 1 h or until a stable baseline was achieved.

2.2.4. Chromatographic methods

The application and elution buffer that was used in the chromatographic studies with the entrapped HSA columns was pH 7.4, 0.067 M potassium phosphate [26,31-36]. The application and elution buffer for the work with the entrapped Con A columns was pH 5.0, 0.50 M sodium acetate that contained 1 mM calcium chloride and 1 mM manganese chloride [37,38]. All columns were equilibrated with their corresponding buffer at 0.50 mL/min for at least 1 h before injections were made (Note: more time was required to reach a stable baseline when the column was conditioned for the first time). The temperature was maintained at 37 °C for the HSA columns and at 20 °C for the Con A columns, as well as for their respective control columns, during these experiments. The injected analytes were dissolved in the same application/elution buffers as were used on each of these columns. The wavelengths used for detection were 307 nm for warfarin, 316 nm for MUM or MUGA, and 205 nm or 220 nm for sodium nitrate.

In the zonal elution studies, several sample concentrations and flow rates were tested for use with each probe or analyte to find conditions in which the measured retention factors remained constant even when making small changes in these parameters. The sample volumes that were used were 5 μL or 20 μL . No significant variations in the retention factors were seen when using the following conditions for the zonal elution studies: flow rate, 0.50 mL/min; sample concentrations, 10-20 μM warfarin, 5-10 μM MUM or MUGA, and 2.5-5.0 μM sodium nitrate. These conditions for providing linear elution conditions and results that were independent of the flow rate agreed with previous observations that have been made in prior studies with HSA columns [33,36,39,40].

The retention time for each injected solute was estimated by analyzing the chromatograms with PeakFit 4.12 and fitting the data by using an exponentially-modified Gaussian and half-Gaussian modified Gaussian (EMG+CMG) function, followed by determination of each peak's first statistical moment or centroid. All of the retention factors were determined for data acquired over at least three injections on the entrapped protein columns and control columns. The solutes that were used as non-retained markers were sodium nitrate for the HSA columns and MUGA for the Con A columns. The extra-column void time of the system was found by measuring the elution time of the non-retained solutes when a zero volume union was placed into the chromatographic system instead of the column [39].

The protein content of each stationary phase was measured initially by using a BCA protein assay [41,42]. An alternative method was also developed, as described later in this chapter, that involved labeling some of the protein with fluorescein, entrapping this labeled

protein, and then measuring the fluorescence of a slurry that was prepared with the entrapped and labeled protein support.

2.3. RESULTS AND DISCUSSION

2.3.1. Initial measurement of protein content by the BCA assay

The protein coverage of the supports was first measured by a BCA assay. This method is based on the ability of proteins to reduce Cu^{2+} to Cu^+ in an alkaline solution (i.e., the biuret reaction), with the Cu^+ then forming a complex with the BCA reagent to form a colored complex that absorbs light at 562 nm [41,42]. The initial batches of the entrapped HSA support that were made in this study gave only a small apparent protein content when measured by this assay, as well as weak retention for warfarin on a column that contained this support. An increase in the reaction volume that was used during the protein entrapment did lead to some increase in the retention factor for warfarin, however, the apparent protein content of the support was still small.

One major issue in these early experiments was that it was difficult to determine the protein content of the supports by the BCA protein assay. This occurred because both the control support and support containing the entrapped protein gave a high response in this assay. It was hypothesized that this behavior was caused by the presence of the hydrazide groups on the support which, like the peptide backbone of proteins, could reduce Cu^{2+} to Cu^+ in the BCA assay. The large response for the control support in this assay created only small differences in the final absorbances that were measured for the supports with entrapped proteins versus the control supports. This, in turn, produced high variability

in the final results. To resolve this issue, a search was made for another method that could be used to measure the protein content of these supports.

2.3.2. Measurement of protein content in supports by fluorescence

A method based on fluorescence was also developed and tested to estimate the protein content of supports that were prepared through entrapment. This method involved labeling a portion of the protein with fluorescein, entrapping this protein, and then measuring the fluorescence of a slurry that contained the support with the entrapped and labeled protein. A procedure for labeling HSA or BSA with FITC [43], was adapted for this work, as based on directions provided by the manufacturer of the FITC reagent [44]. In this procedure, a solution containing 8.8 mg of the protein in 4 mL of freshly prepared pH 9.0, 0.10 M sodium carbonate/bicarbonate buffer was combined with 1 mL of 1 mg/mL FITC in the same buffer, giving a molar ratio for FITC vs. albumin of 20:1. This mixture was stirred in the dark for 2 h at room temperature.

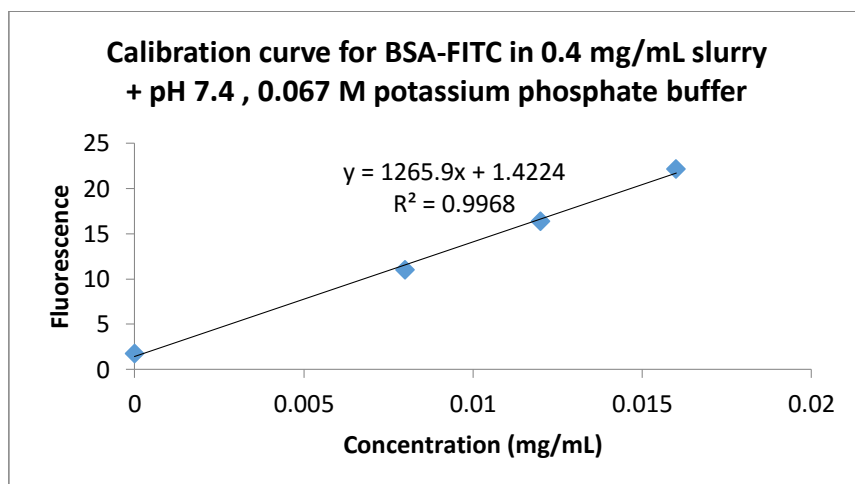
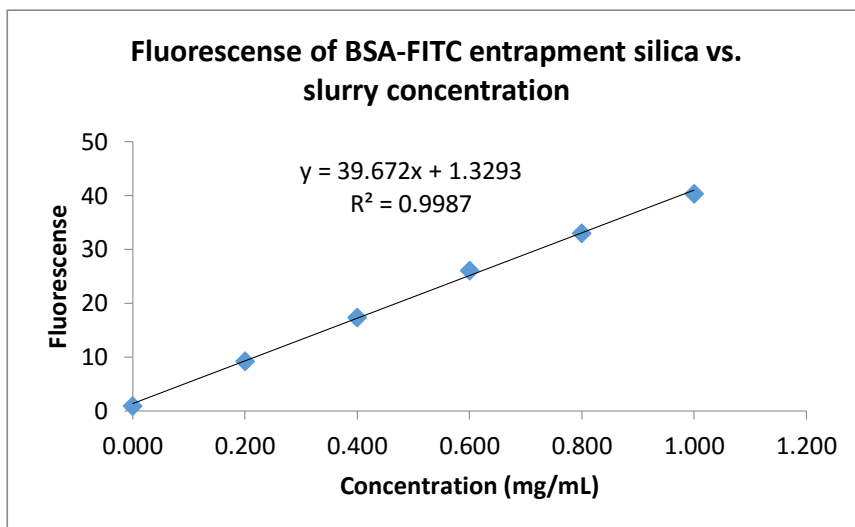
An Econo-Pac 10DG disposable desalting column was used to separate the unreacted FITC from the fluorescein-protein conjugate and to carry out buffer exchange. In this part of the procedure, a 3 mL portion of the reaction mixture containing the excess FITC and the fluorescein-protein conjugate was applied to the desalting column and eluted with pH 7.4, 0.010 M phosphate buffered saline, according to instructions by the supplier of the column. The first yellow fraction (about 4 mL, and which contained the labeled protein) was collected; this fraction was further purified by using an ultrafiltration tube with a 30 kDa MW cutoff and pH 5.0, 0.10 M potassium phosphate buffer. The initial volume of the sample plus the buffer in this tube was 3 mL. The centrifugation step for this tube proceeded at 2.5×10^3 g and 25 °C until the volume of solution in the tube was reduced

to 0.5 mL. The process of adding more buffer and centrifugation was repeated until no free FITC from the original solution that held the fluorescein-protein conjugate was detected, as based on absorbance measurements of the filtrate at 495 nm. Three filtration cycles were necessary to complete this process.

The labeling ratio for the protein conjugate (i.e., the ratio of fluorescein-to-protein, or F/P, in the final conjugate) was determined by making absorbance measurements at both 280 nm (for the protein) and at 495 nm (for the fluorescein), as well as for solutions containing only the protein or FITC at these same wavelengths. When BSA was used in this labeling method, the ratio of fluorescein-to-protein in the resulting conjugate was determined to be 2.37 (± 0.10) mol/mol ($n = 3$).

To test for the response of the proposed fluorescence assay in the presence of silica, several dilutions of an FITC-BSA conjugate were placed into a slurry containing 40 mg/mL of diol-bonded silica in pH 7.4, 0.067 M potassium phosphate buffer. These solutions were placed into a 96-well plate in 250 μ L aliquots and measured for their fluorescence, using 495 nm as the excitation wavelength and 521 nm as the emission wavelength. As demonstrated in Figure 2.5 (top), a linear response with a value for r^2 that was greater than 0.98 was obtained for these results, along with a low response for the blank. In addition, reproducible results were acquired for samples that contained up to 0.05 mg/mL FITC-BSA. To investigate the effect of settling by the support over time, measurements were taken after letting the slurry stand in the well plates from 1 min to 10 min. The response for each slurry concentration did vary over time in this study, but the response was consistent when this time was kept constant for all samples and standards.

Figure 2.5 Typical results for a method based on fluorescence for measuring the protein content of supports prepared through the entrapment of BSA-FITC. The upper graph shows the response that was obtained for various slurry concentrations of silica that contained entrapped BSA-FITC. The calibration plot in the bottom shows the response that was obtained when various amounts of FITC were added to a 0.4 mg/mL slurry of silica. The buffer used in this study was pH 7.4, 0.067 M potassium phosphate buffer. Based on this method, the protein content of the support containing entrapped and labeled BSA was estimated to be 24 (\pm 3) mg of BSA-FITC/g silica.



This assay was used to optimize the conditions for entrapping proteins such as BSA or HSA in silica, as accomplished by using a preparation of FITC-BSA for the entrapment process. This sample was originally employed under the same conditions as were initially used to entrap HSA. The resulting slurry was diluted to minimize the effects of light scattering by the support and to provide samples that gave measurements within the linear range of the assay. Solutions containing commercial FITC-BSA or FITC-BSA that was prepared in-house and the control silica were used to prepare the calibration plots. Slurries of the entrapped BSA-FITC that had silica concentrations ranging from 1 to 10 mg/mL gave signals of 5 to 60 fluorescence units and a linear response in this assay. Slurries that were made with the control support or diol-bonded silica gave a background response of less than 2 fluorescence units over the same range of slurry concentrations. The fluorescence measurements were taken within 30 s of placing the samples into the wells to avoid any change in the signal over time (Note: only a small effect of time on the signal was observed in this case because of dilute slurry concentrations that were being used).

Determination of the entrapped protein content by fluorescence was used for monitoring the protein content that was obtained when using various entrapment conditions for both FITC-BSA and FITC-HSA (Note: the FITC-BSA was made under the same conditions as described for FITC-HSA). In the final conditions that were used for these assays, slurries were made from the supports containing entrapped FITC-BSA or FITC-HSA and were diluted to a slurry concentration that yielded a fluorescence signal between 20 and 50 units. A calibration curve was made using a slurry of the control support that had the same silica concentration as the sample. The same preparation of the labelled protein that was used for entrapment was also used to make the standards for the calibration

plot. The best-fit lines for all the resulting calibration plots had r^2 values that were greater than 0.98. An example of such a plot is given in the bottom of Figure 2.5.

2.3.3. Comparison of the fluorescence assay with thermogravimetric analysis

To further test the fluorescence assay, thermogravimetric analysis (TGA) was used for measuring the protein content of several samples of HSA silica that had also been analyzed by the BCA protein assay and the fluorescence method. TGA is a destructive technique that monitors the loss in mass for a sample as the temperature of the sample is increased [45]. The results are given in the form of a thermogram, or a plot of mass vs. temperature. This technique is quite sensitive for detecting small differences in mass with temperature, which makes it useful for studying changes in sample composition that occur as a function of temperature [46,47].

The following conditions were found to be useful for analyzing the protein content of silica by TGA. First, the sample was placed in a TGA pan and its mass was recorded while going from room temperature to 110 °C at 5 °C/min. Second, this sample was held at 110 °C for 20 min to eliminate any traces of water that were present and to condition the sample; the mass was then again recorded and used as the “initial mass”. Third, the temperature was increased from 110 °C to 650-850 °C at 20 °C/min while the mass was recorded; the result that was obtained when the mass no longer changed with the temperature was used as the “final mass”. During this process, nitrogen at a flow rate of 20 mL/min was used to purge oxygen from the analysis chamber.

The losses in mass that were measured by TGA for the silica that contained entrapped proteins and for the control silica were compared. The difference in this mass

should have represented the amount of protein that was entrapped in the silica, because the control silica had no protein but was prepared with all other reagents being the same as were used for the entrapment process. An HSA silica support and a control silica support that were prepared by the Schiff base method were also analyzed by TGA for comparison of their results with those obtained for the same materials with a BCA protein assay.

The thermogravimetric data were normalized and the percent mass loss for the silica samples containing protein or for the control silica supports were calculated as shown by Equation 2.1,

$$\text{Protein \%} = (\%W_{e1} - \%W_{e2}) - (\%W_{c1} - \%W_{c2}) \quad (2.1)$$

where $\%W_{e1}$ and $\%W_{e2}$ are the weight percent values for the supports that were prepared by entrapment (or that contained immobilized protein) at the initial temperature for the study (i.e., after conditioning the support at 110 °C) and at the final temperature that was used for the analysis, respectively. The values of $\%W_{c1}$ and $\%W_{c2}$ in Equation 2.1 are the weight percent values that were measured at the same initial and final temperatures for the corresponding control support. As this equation indicates, the difference in these masses should have corresponded to the amount of protein that was lost through combustion from the entrapped protein support during the TGA analysis. The initial and final temperatures that were used in this calculation were selected so that the weight of the support was initially constant (i.e., after the support had been held at 110 °C), and the weight had reached a plateau after being heated (i.e., which usually occurred after 650 °C). The same temperatures were used for both the entrapped protein supports and the control supports.

Some examples of thermograms that were obtained for a control support and a support that contained entrapped proteins are presented in Figure 2.6. Table 2.1 compares the results that were obtained by the TGA method with those for the BCA assay and the fluorescence method, as described in the previous section. As can be seen in this table, there was a good agreement between the results that were obtained by the three methods. These results offered additional evidence that the fluorescence method, or TGA, could be used as an alternative to the BCA assay for measuring the protein content of supports that were prepared through entrapment.

2.3.4. Purification of oxidized glycogen

Various factors were considered in an attempt to increase the amount of protein that could be immobilized through the entrapment method. One of these factors was the way in which the oxidized glycogen was isolated after its oxidation with periodate and before its use in the entrapment method. The oxidized glycogen that was to be used for entrapment was initially purified by placing a 3 mL portion of the oxidized glycogen solution onto a gel filtration column (i.e., an Econo-Pac 10DG disposable desalting column, 3.3 mL void volume, 6 kDa exclusion mass). A pH 5.0, 0.10 M potassium phosphate buffer was next added, as previously described for the purification of oxidized glycogen [28] and buffer exchange, and by following the directions provided by manufacturer of this column. However, this purification method appeared to give a low protein content in the entrapment method, as described in Section 2.3.1.

Figure 2.6 Typical results obtained by TGA for a support containing entrapped FITC-BSA and a control silica. The experimental conditions are described in the text.

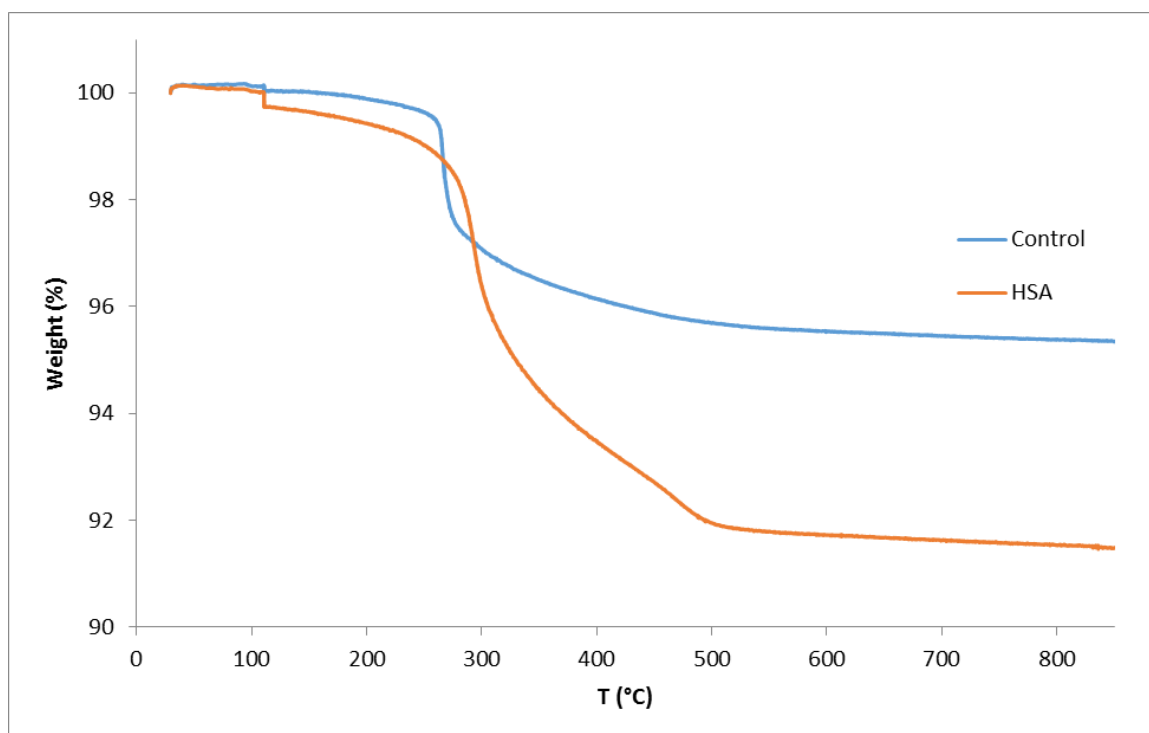


Table 2.1. Protein content of various supports prepared under the same conditions but that were measured by several methods.

Immobilization method	Type of protein or analysis method, and protein content (mg/g silica)		
	HSA, TGA ¹	BSA-FITC, Fluorescence ²	HSA, BCA assay ²
Entrapment method	22.1	23.9 (\pm 2.9)	
Schiff base method	35.3		30.7 (\pm 3.5)

¹These results were obtained for one set of samples of the protein supports (containing HSA) and the control supports

²This result is based on at least three replicate samples.

To increase this protein content, the elution fraction from the gel filtration column that had the highest amount of oxidized glycogen was determined by measuring the absorbance at 280 nm for 1 mL portions of the collected fractions. Fractions 2-4 (with a total volume of 3 mL) were found to have the highest absorbance and were used for entrapment. However, no significant increase in the protein content of the entrapped supports was achieved under these modified conditions. It was also observed that some cloudiness started to appear in the collected and oxidized glycogen fraction after about two days of storage at 4 °C. Allowing this solution to sit for one week resulted in extensive precipitation. It is believed that this behavior indicated that there was still some periodic acid left in the glycogen mixture, which continued to lead to further oxidation of the glycogen and its cross-linking or aggregation over time.

To avoid these problems, an alternative method of purification for the oxidized glycogen was examined based on ultrafiltration. In this method, a 4 mL portion of a reaction mixture that contained oxidized glycogen and periodic acid in pH 5.0, 20 mM sodium acetate buffer containing with 15 mM sodium chloride was placed into an ultrafiltration tube with a MW cutoff of 30 kDa. This tube was centrifuged at 3×10^3 g and 20 °C, with pH 5.0, 0.10 M potassium phosphate buffer being added as needed. The volume of the solution in the tube was filled to the 5 mL mark with this pH 5.0 buffer before each centrifugation cycle, and the centrifugation was continued until the solution volume in the tube was 2.5 mL. This process was then repeated, following the addition of more pH 5.0 buffer to the tube. During this process, some haziness was often observed in the oxidized glycogen solution, which may have indicated the beginning of some aggregation or cross-linking. To overcome this problem, the procedure was modified by

carrying out three centrifugation cycles in the presence of water before the pH 5.0 buffer was used. This new procedure involved at least seven centrifugation cycles, each requiring 10 to 15 min to complete. The purified oxidized glycogen solution that was obtained by this method was used within two days of preparation and did not show any cloudiness over at least one week of storage. This was the type of oxidized glycogen that was used in all later work in this dissertation.

2.3.5. Size fractionation of oxidized glycogen

Glycogen is a branch-on-branch polysaccharide with a homogeneous branched structure that is formed by $\alpha(1\rightarrow4)$ linked D-glucose with $\alpha(1\rightarrow6)$ branching at about every 8 to 12 glucose residues. Glycogen has an average degree of branching of 7-9% and an average molar mass of 10^5 to 10^8 Da, with a broad size distribution in size that depends on the type of animal from which the glycogen was obtained [48,49]. Experiments were carried out to see if there were any molecules of oxidized glycogen that were too small to be used as capping agents for porous silica during entrapment. Of particular interest were glycogen molecules that had molecular weights under 300 kDa, due to the pore size of the silica supports that were used in this study.

To study the effects of the presence or absence of these smaller glycogen molecules, oxidized glycogen was prepared and purified by using a modified form of the ultrafiltration method that was described in the previous section. This preparation was then labeled that same day with LyCH (i.e., a hydrazide-containing dye that can couple with compounds that have free aldehyde groups), according a method adapted from the literature for use with oxidized glycoproteins [50-52]. Briefly, a 3 mg/mL solution of LyCH was prepared

by dissolving this reagent in pH 6.5, 0.10 M potassium phosphate buffer and heating the mixture to about 50 °C. A 17 mg portion of oxidized glycogen was purified by using an ultrafiltration tube with a MW cutoff of 30 kDa and was exchanged through this process into pH 6.5, 0.10 M potassium phosphate buffer. The final volume of this solution was 4 mL and its glycogen concentration was approximately 4.2 mg/mL.

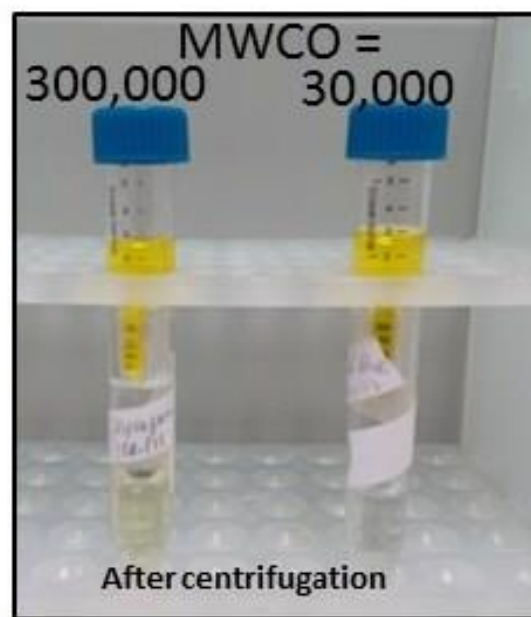
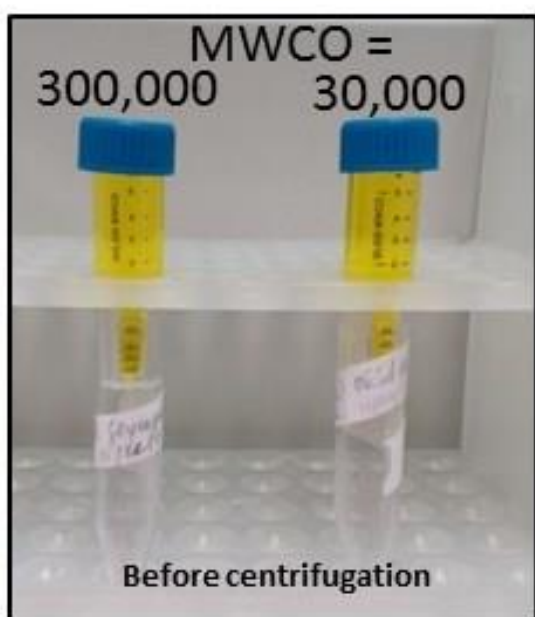
For the labeling reaction, 1 mL of the oxidized glycogen solution was mixed with 1 mL of the LyCH solution for 2 h. The reaction mixture was purified by gel filtration to remove the excess LyCH. The same type of gel filtration column that was used initially in the purification of oxidized glycogen was used to remove the excess LyCH. The fraction due to the first yellow band that eluted from this column contained unreacted LyCH; this fraction was discarded. A second yellow band that corresponded to the labelled and oxidized glycogen eluted between 14 and 22 mL and was collected. Absorbance measurements that were made at 428 nm on these fractions were used to monitor the elution process. The LyCH-glycogen conjugate was further purified by ultrafiltration and the buffer was exchanged with water by using a tube with a 30 kDa cutoff and the procedure described in the previous section that used a series of washes with water. The centrifugation cycles were stopped when no yellow color and no absorbance at 428 nm was detected in the filtrate, indicating that all of the excess and unreacted LyCH had been removed from the oxidized glycogen solution. After this process, the yellow solution of the LyCH-labelled oxidized glycation was diluted to 6 mL with water, and 3 mL of this solution was transferred to an ultrafiltration tube with a 300 kDa cutoff. Water was added to raise the volume of the solution in the tube to 6 mL, and this tube was centrifuged until the solution in the tube reached 2.5 mL (see

Figure 2.7).

The fraction of the labeled and oxidized glycogen that passed through the 300 kDa cutoff membrane of the second ultrafiltration tube was found by using the absorbance values and the volumes of the filtrate and retentate. The absorbance of the filtrate was corrected by subtracting the absorbance of the filtrate from the tube with the 30 kDa cutoff, which was used as a blank. The result indicated that only 2.1% of the oxidized glycogen, as obtained from bovine liver, had sizes under 300 kDa. These results showed that the molecular weight for most of the oxidized glycogen that was used for protein entrapment was greater than or equal to 300 kDa. In related experiments, it was determined that the process of washing and concentrating the oxidized glycogen solutions by ultrafiltration and centrifugation was about three times faster on the tubes that had 300 kDa cutoff membranes

vs. those with a 30 kDa cutoff. However, the 30 kDa filters were also acceptable for this work and were used in the following studies.

Figure 2.7 Ultrafiltration and centrifugation studies carried out with oxidized glycogen that was labelled with LyCH and that had been previously purified by gel filtration and ultrafiltration using a tube with a 30,000 Da MW cutoff (MWCO). The image on the left show this solution before it was subjected to ultrafiltration and centrifugation using tubes with 300,000 Da or 30,000 Da cutoff values; the image on the right shows the result after the centrifugation/ultrafiltration step that was performed for measuring the fraction of the glycogen that was smaller than 300,000 Da.



2.3.6. Optimization of protein entrapment based on measurements of protein content

Several experiments were next carried out to maximize the final content of proteins such as HSA that could be immobilized by entrapment within silica. This work was initially carried by using normal HSA and FITC-labelled BSA or HSA as model proteins. Modifying and changing the purification method for the oxidized glycogen from gel filtration to ultrafiltration, as described in the previous section, provided a 1.8-fold increase in the protein content that could be obtained through entrapment for FITC-BSA, as shown in Table 2.2. This improvement can be explained by the multiple washing steps that were now used in the ultrafiltration method, which should have helped to more effectively eliminate periodic acid after the oxidation process. This, in turn, should have avoided any further reaction of this reagent with glycogen, and prevented any aggregation or cross-linking of the oxidized glycogen before it could react with the hydrazide-activated silica.

Two other changes that were made in the entrapment procedure, as indicated in Table 2.2, involved decreasing the volume of solution that was used in the entrapment reaction (e.g., from 2.0 mL to 1.7 mL) and introducing a step in which the protein was allowed to incubate with the hydrazide-activated silica before the oxidized glycogen was added. This combination of changes helped to increase the protein content by 2.5-fold versus the initial conditions. Lowering the solution volume further to 1.0 mL during entrapment gave a 3.9-fold increase in the final protein content for HSA. Increasing the protein/silica amount that was used for entrapment to 400 mg/g silica for HSA plus decreasing the solution volume to 0.72 mL gave an apparent increase of 3.2-fold in the protein content when compared to the initial reaction conditions (Note: this latter change

may not have been statistically significant due to the large variation in the measured protein content that was obtained when using the BCA assay). Decreasing the solution volume further to 0.2 mL gave a 6.4- to 7.4-fold increase in protein content for the FITC-labeled HSA and BSA when compared to the results that were obtained with the initial reaction conditions for FITC-BSA.

2.3.7. Optimization of protein entrapment based on retention factor measurements

The conditions that could be used for entrapment were also optimized by using HSA as a model protein and by comparing the amount of active protein in the supports, as determined through retention factor measurements. In this approach, columns that were prepared with each type of support, and its control support, were compared for their retention of warfarin, which is a drug that has well-characterized binding to HSA. In this method, the retention time (t_r) was measured for warfarin on both a column containing entrapped HSA and on a control column. The value of the retention factor (k) on each type of column was then calculated according to the following expressions:

$$k_1 = \frac{(t_{r1} - t_{m1})}{(t_{m1} - t_v)} \quad (2.2) \qquad k_2 = \frac{(t_{r2} - t_{m2})}{(t_{m2} - t_v)} \quad (2.3)$$

$$k = k_1 - k_2 \quad (2.4)$$

where k_1 and k_2 are the retention factors for warfarin on the columns containing the entrapment protein or control support, respectively; t_{r1} and t_{r2} are the retention times for warfarin on these columns; t_{m1} and t_{m2} are the void times of these columns (e.g., as measured by using the elution times of a non-retained solute); and t_v is the void time of the system (e.g., as measured by injecting a non-retained solute with no column present in the system).

Table 2.2. Protein content obtained under various conditions when using the entrapment method

Experiments - Initial conditions for entrapment and changes made in these conditions	Type of protein	Protein content (mg/g silica) ¹
1 Initial conditions: Total volume, ² 2.0 mL HSA/silica ratio, 100 mg/g Oxidized glycogen purified by gel filtration	FITC-BSA	5.9 (\pm 0.2)
2 Oxidized glycogen purification method changed from gel filtration to ultrafiltration	FITC-BSA	10.6 (\pm 0.6)
3 Total volume ² decreased from Expt. 2 to 1.7 mL; Pre-incubation step for protein with the support (4 h) added to the entrapment procedure	FITC-BSA	15 (\pm 2)
4 Total volume ² changed from Expt. 3 to 1 mL	HSA	23 (\pm 11)
	Con A	44 (\pm 15)
5 Total volume ² decreased from Expt. 4 to 0.72 mL; HSA/silica ratio increased to 400 mg/g	HSA	19 (\pm 10)
6 Total volume ² decreased from Expt. 5 to 0.2 mL and HSA/silica ratio kept at 400 mg/g	FITC-HSA	39 (\pm 3)
	FITC-BSA	44 (\pm 3)

¹These results are the average for three measurement of the protein content by using the fluorescence for the fluorescein-protein conjugates or the BCA assay for the unmodified HSA or Con A. The numbers in parentheses represent a range of \pm 1 S.D.

²This value refers to the total volume of the solutions that were added to the support.

The retention factor for the control column was used to account for any non-specific interactions that warfarin may have had with the support. By subtracting this value from the retention factor that was measured on the entrapped protein column, as indicated in Equation 2.2, a value for the corrected retention factor was obtained that should have been related only to the interactions of warfarin with the immobilized HSA. In this study, these measurements were made by using $1.0 \text{ cm} \times 2.1 \text{ mm}$ columns that contained the entrapped protein support or the control support.

Table 2.3 shows how the corrected retention factor for warfarin changed when examining entrapped HSA columns that were prepared by using five sets of entrapment conditions. The first column of experimental data (i.e., Experiment 1) shows the results that were obtained after 1) the purification method for glycogen had been changed from gel filtration to ultrafiltration, 2) an initial incubation time for the protein with the support of 4 h had been introduced, and 3) the solution volume had been reduced from 2.0 mL to 1.0 mL. This corresponds to the same set of conditions that were present for Experiment 4 in Table 2.2.

Further modifications were then made in the entrapment procedure. Examples of modifications that were examined included decreasing the total reaction volume, increasing the concentration of the protein solution, and increasing the relative amount of the protein with respect to the support. A vortex mixer was used to allow the solution volumes to be kept below 0.72 mL in Experiments 2-5, but this volume was decreased to values as low as 0.2 mL (see Experiments 4-5). The concentration of protein that was used for the entrapment process increased from the reference amount of 8 mg/mL in Experiment 1 to a value of 100 mg/mL in Experiment 5. The relative amount of protein

with respect to the support was also increased from the value of 100 mg/g in Experiment 1 to values that ranged from 120 to 400 mg/g in the other experiments.

Overall, these changes in the entrapment conditions allowed an increase to be obtained in the corrected retention factor for warfarin from a value of 3.0 in Experiment 1 to a value of around 50 in Experiment 5. Some trends that were noted in these experiments are summarized in Figure 2.8. For instance, a 16-fold increase in the retention factor for warfarin was seen as the concentration of HSA that was used for entrapment was increased by 13-fold. Also there was a 12.5- to 16-fold increase in this retention factor as the ratio of HSA-to-silica was increased by 3.3- 4.0-fold.

In the final conditions that were selected for the entrapment method, the hydrazide-activated silica that was produced from a 50 mg batch of diol silica was transferred to a 2 mL vial, spun and decanted. The remaining reaction was carried out at room temperature (about 20 °C) and used a programmable vortex mixer that could run unattended to combine and mix the reagents with the silica. In the case of HSA, the activated support was mixed with 100 μ L of 200 mg/mL HSA in pH 5.0, 0.10 M potassium phosphate buffer, plus another 100 μ L of the same buffer with no protein present (Note: the additional buffer was used to obtain the same overall HSA concentration as was later used during the entrapment step). This slurry was mixed for 4 h on the programmable vortex mixer, with the excess solution then being decanted from the support. Second, 100 μ L of 200 mg/mL HSA in pH 5.0, 0.10 M potassium phosphate buffer and 100 μ L of 8.5 mg/mL oxidized glycogen in pH 5.0, 0.10 M potassium phosphate buffer were added (total reaction volume, 0.20 mL; HSA concentration, 100 mg/mL; oxidized glycogen concentration, 4.25 mg/mL), and the slurry was mixed for another 16 h at room temperature using the vortex mixer. To make

the control support, pH 5.0, 0.10 M potassium phosphate buffer was used in place of the protein solution. Finally, 50 μL of a 1 mg/mL oxalic dihydrazide solution in pH 5.0, 0.10 M potassium phosphate buffer was added to the slurry, and the mixing was continued for another 1 h.

Table 2.3. Corrected retention factors for warfarin measured on 1.0 cm × 2.1 mm columns containing HSA entrapped within silica under various conditions

Entrapment conditions	Experiment ¹				
	1	2	3	4	5
Total volume (mL)	1	0.72	0.3	0.2	0.2
Mass of silica (mg/mL) ²	80	88	167	250	250
Concentration of HSA (mg/mL) ³	8	35	20	40	100
Mass ratio of HSA/silica (mg/g) ⁴	100	396	120	160	400
Concentration of oxidized glycogen (mg/mL) ³	1.2	1.3	3.0	4.2	3.75
Mass ratio of oxidized glycogen/silica (mg/g) ⁴	15	15	18	17	15
Retention factor ⁵	3.0 (± 0.6)	15.8 (± 1.4)	4.0 (± 0.9)	9.5 (± 2.6)	49.9 (± 7.9)

¹The results for experiments 1, 2 and 5 in this Table were obtained with the same entrapment conditions as the last three experiments for HSA that are listed in Table 2.2.

²This value is the equivalent mass of diol-bonded silica that was present per unit of volume of the reaction mixture.

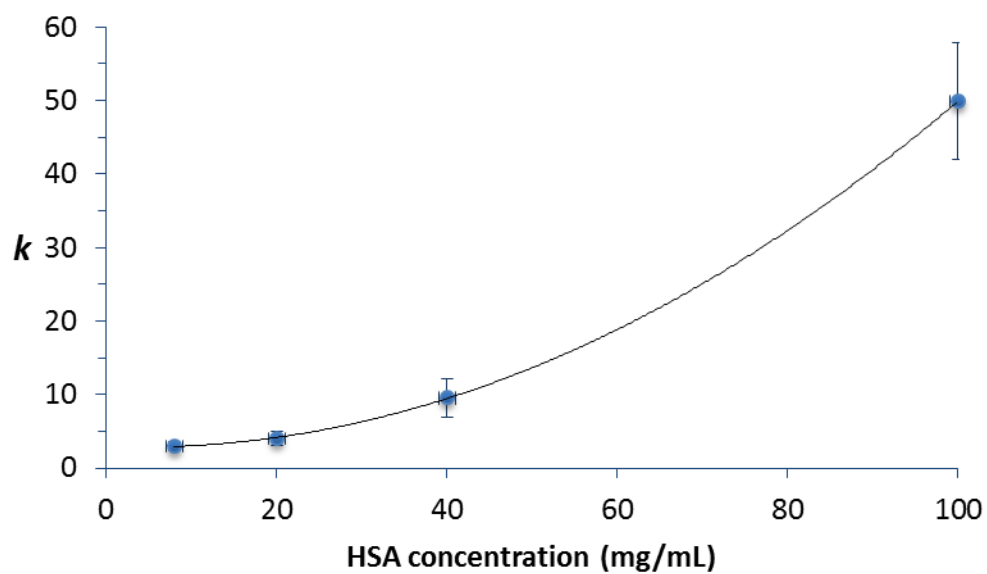
³These concentrations are based on total volume of all solutions that were added.

⁴These mass ratios are based on the equivalent mass of diol-bonded silica that was used.

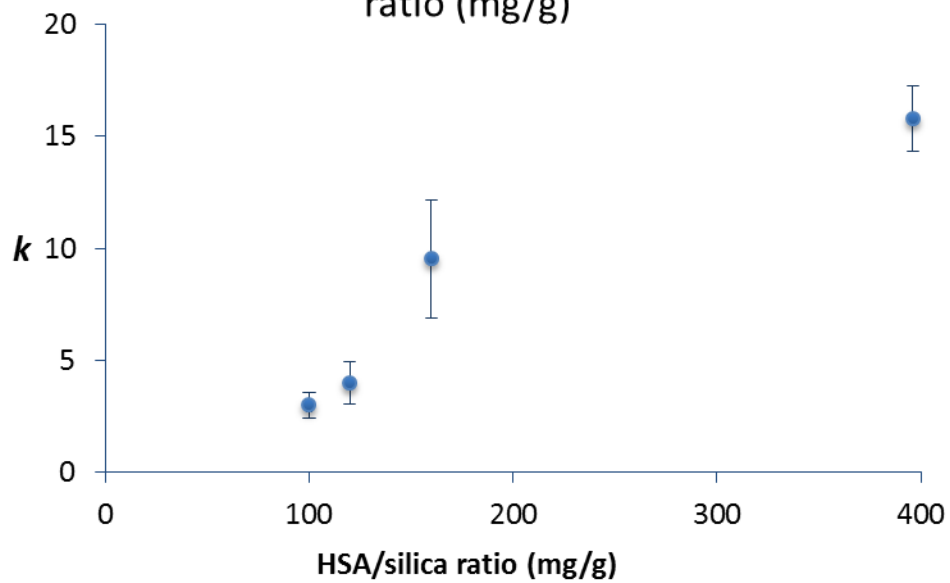
⁵These results are the averages of two or three determinations. The value for Experiment 5 is the average for two different batches of the entrapped HSA supports.

Figure 2.8 Variation in corrected retention factor (k) measured for warfarin on columns containing entrapped HSA that were prepared by varying the concentration of HSA that was used for entrapment or the relative amount of HSA versus the support that was used for entrapment. The errors bars represent a range of ± 1 S.D.

Variation in retention factor with HSA concentration (mg/mL)



Variation in retention factor with HSA/silica ratio (mg/g)



2.4. CONCLUSIONS

Several factors were examined to maximize the amount of proteins such as BSA and HSA that could be immobilized onto porous silica by entrapment. Some of the conditions that were modified were the purification method that was used for the oxidized glycogen, the concentration of protein that was used in the reaction mixture for entrapment, and the ratio of the protein vs. support that was used for entrapment. Alternative ways of monitoring the total amount of protein or active protein in the resulting supports were also considered. Examples of these methods included the use of fluorescence and thermogravimetric analysis. In the following chapter, the measurement of retention factors with probe compounds for the entrapped proteins will be explored as another method for determining the protein content.

It was found that improvements in the protein content could be achieved by changing several parameters. This included altering the purification method from gel filtration chromatography to ultrafiltration, using a pre-incubation step for the protein with the support, increasing the concentration of HSA in the entrapment method, and decreasing the solution volume in the reaction mixture. Changing these conditions gave up to a 7.4-fold increase in the amount of entrapped protein that could be obtained versus the initial reaction conditions. Increasing the concentration of the protein and increasing the protein/support mass ratio gave an even further increase in the apparent protein content, as represented by an increase of 16-fold in the retention factor for warfarin on entrapped HSA columns. This entrapment procedure can be adapted for use with other proteins or supports by using methods similar to those described in this chapter.

REFERENCES

1. D.S. Hage, J.A. Anguizola, A.J. Jackson, R. Matsuda, E. Papastavros, E. Pfaunmiller, Z.H. Tong, J. Vargas-Badilla, M.J. Yoo, X.W. Zheng, Chromatographic analysis of drug interactions in the serum proteome, *Anal. Methods*, 3 (2011) 1449-1460.
2. N.A. Kratochwil, W. Huber, F. Muller, M. Kansy, P.R. Gerber, Predicting plasma protein binding of drugs: a new approach, *Biochem. Pharmacol.*, 64 (2002) 1355-1374.
3. D.S. Hage, M. Bian, R. Burks, E. Karle, C. Ohnmacht, C. Wa, Bioaffinity chromatography, in: D.S. Hage (Ed.) *Handbook of Affinity Chromatography*, 2nd ed., CRC Press, Boca Raton, FL, 2006, pp. 101-126.
4. D.S. Hage, J. Chen, Quantitative affinity chromatography, in: D.S. Hage (Ed.) *Handbook of Affinity Chromatography*, 2nd ed., CRC Press, Boca Raton, FL, 2006, pp. 595-628.
5. D.S. Hage, A. Jackson, M.R. Sobansky, J.E. Schiel, M.J. Yoo, K.S. Joseph, Characterization of drug-protein interactions in blood using high-performance affinity chromatography, *J. Sep. Sci.*, 32 (2009) 835-853.
6. J. Ghuman, P.A. Zunszain, I. Petitpas, A.A. Bhattacharya, M. Otagiri, S. Curry, Structural basis of the drug-binding specificity of human serum albumin, *J. Mol. Biol.*, 353 (2005) 38-52.

7. P.-E. Gustavsson, P.-O. Larsson, Support materials for affinity chromatography, in: D.S. Hage (Ed.) Handbook of Affinity Chromatography, 2nd ed., CRC Press, Boca Raton, FL, 2006, pp. 16-33.
8. R.R. Walters, Affinity chromatography, *Anal. Chem.*, 57 (1985) 1099 A-1114 A.
9. R. Mallik, D.S. Hage, Development of an affinity silica monolith containing human serum albumin for chiral separations, *J. Pharmaceut. Biomed. Anal.*, 46 (2008) 820-830.
10. D.S. Hage, P. Ruhn, F., An introduction to affinity chromatography, in: D.S. Hage (Ed.) Handbook of Affinity Chromatography, 2nd ed., CRC Press, Boca Raton, FL, 2006, pp. 3-13.
11. G.T. Hermanson, A.K. Mallia, P.K. Smith, Immobilized Affinity Ligand Techniques, Academic Press, Haltham, MA, USA, 1992.
12. D.S. Hage, J.A. Anguizola, C. Bi, R. Li, R. Matsuda, E. Papastavros, E. Pfaunmiller, J. Vargas, X. Zheng, Pharmaceutical and biomedical applications of affinity chromatography: recent trends and developments, *J. Pharm. Biomed. Anal.*, 69 (2012) 93-105.
13. T. Peters Jr, All about albumin: Biochemistry, genetics, and medical applications, Academic press, San Diego, CA, USA, 1996.
14. P.A. Zunszain, J. Ghuman, T. Komatsu, E. Tsuchida, S. Curry, Crystal structural analysis of human serum albumin complexed with hemin and fatty acid, *BMC Struct. Biol.*, 3 (2003) 1-9.

15. A. Monzo, G.K. Bonn, A. Guttman, Lectin-immobilization strategies for affinity purification and separation of glycoconjugates, *Trends Anal. Chem.*, 26 (2007) 423-432.
16. Y.H. Wang, S.L. Wu, W.S. Hancock, Monitoring of glycoprotein products in cell culture lysates using lectin affinity chromatography and capillary HPLC coupled to electrospray linear ion trap-Fourier transform mass spectrometry (LTQ/FTMS), *Biotechnol. Progr.*, 22 (2006) 873-880.
17. M. Bedair, Z. El Rassi, Affinity chromatography with monolithic capillary columns - II. Polymethacrylate monoliths with immobilized lectins for the separation of glycoconjugates by nano-liquid affinity chromatography, *J. Chromatogr. A*, 1079 (2005) 236-245.
18. K. Yoshida, M. Honda, K. Arai, Y. Hosoya, H. Moriguchi, S. Sumi, Y. Ueda, S. Kitahara, Serial lectin affinity chromatography with concanavalin A and wheat germ agglutinin demonstrates altered asparagine-linked sugar-chain structures of prostatic acid phosphatase in human prostate carcinoma, *J. Chromatogr. B*, 695 (1997) 439-443.
19. E. Song, R. Zhu, Z.T. Hammond, Y. Mechref, LC-MS/MS Quantitation of esophagus disease blood serum glycoproteins by enrichment with hydrazide chemistry and lectin affinity chromatography, *J. Proteome Res.*, 13 (2014) 4808-4820.

20. J.W. Becker, G.N. Reeke, J.L. Wang, B.A. Cunningham, G.M. Edelman, Covalent and 3-dimensional structure of concanavalin A. 3. Structure of monomer and its interactions with metals and sacharides, *J. Biol. Chem.*, 250 (1975) 1513-1524.
21. W. Min, A.J. Dunn, D.H. Jones, Non-glycosilated recombinant pro-concanavalin A is active without polypeptide cleavage, *Embo J.*, 11 (1992) 1303-1307.
22. Z. Derewenda, J. Yariv, J.R. Helliwell, A.J. Kalb, E.J. Dodson, M.Z. Papiz, T. Wan, J. Campbell, The structure of the saccharide-binding site of concanavalin A, *EMBO J.*, 8 (1989) 2189-2193.
23. K.D. Hardman, C.F. Ainsworth, Structure of concanavalin A at 2.4-Angstrom resolution, *Biochemistry*, 11 (1972) 4910-4919.
24. S. Ng, E. Lin, P.I. Kitov, K.F. Tjhung, O.O. Gerlits, L. Deng, B. Kasper, A. Sood, B.M. Paschal, P. Zhang, C.-C. Ling, J.S. Klassen, C.J. Noren, L.K. Mahal, R.J. Woods, L. Coates, R. Derda, Genetically encoded fragment-based discovery of glycopeptide ligands for carbohydrate-binding proteins, *J. Am. Chem. Soc.*, 137 (2015) 5248-5251.
25. D.S. Hage, High-performance affinity chromatography: a powerful tool for studying serum protein binding, *J. Chromatogr. B*, 768 (2002) 3-30.
26. D.S. Hage, J. Anguizola, O. Barnaby, A. Jackson, M.J. Yoo, E. Papastavros, E. Pfaunmiller, M. Sobansky, Z.H. Tong, Characterization of drug interactions with serum proteins by using high-performance affinity chromatography, *Curr. Drug Metabol.*, 12 (2011) 313-328.

27. D.S. Hage, J. Austin, High-performance affinity chromatography and immobilized serum albumin as probes for drug- and hormone-protein binding, *J. Chromatogr. B*, 739 (2000) 39-54.
28. A.J. Jackson, H. Xuan, D.S. Hage, Entrapment of proteins in glycogen-capped and hydrazide-activated supports, *Anal. Biochem.*, 404 (2010) 106-108.
29. P.F. Ruhn, S. Garver, D.S. Hage, Development of dihydrazide-activated silica supports for high performance affinity chromatography, *J. Chromatogr. A*, 669 (1994) 9-19.
30. A.J. Jackson, J. Anguizola, E.L. Pfaunmiller, D.S. Hage, Use of entrapment and high-performance affinity chromatography to compare the binding of drugs and site-specific probes with normal and glycosylated human serum albumin, *Anal. Bioanal. Chem.*, 405 (2013) 5833-5841.
31. B. Loun, D.S. Hage, Chiral separation mechanisms in protein-based HPLC columns. 1. Thermodynamic studies of (R)-warfarin and (S)-warfarin binding to immobilized human serum albumin, *Anal. Chem.*, 66 (1994) 3814-3822.
32. H.S. Kim, Y.S. Kye, D.S. Hage, Development and evaluation of N-hydroxysuccinimide-activated silica for immobilizing human serum albumin in liquid chromatography columns, *J. Chromatogr. A*, 1049 (2004) 51-61.
33. H.S. Kim, D.S. Hage, Chromatographic analysis of carbamazepine binding to human serum albumin, *J. Chromatogr. B*, 816 (2005) 57-66.
34. H.S. Kim, R. Mallik, D.S. Hage, Chromatographic analysis of carbamazepine binding to human serum albumin. II. Comparison of the Schiff base and N-

- hydroxysuccinimide immobilization methods, *J. Chromatogr. B*, 837 (2006) 138-146.
35. R. Mallik, M.J. Yoo, C.J. Briscoe, D.S. Hage, Analysis of drug-protein binding by ultrafast affinity chromatography using immobilized human serum albumin, *J. Chromatogr. A*, 1217 (2010) 2796-2803.
36. H.S. Kim, I.W. Wainer, Rapid analysis of the interactions between drugs and human serum albumin (HSA) using high-performance affinity chromatography (HPAC), *J. Chromatogr. B*, 870 (2008) 22-26.
37. D.J. Anderson, R.R. Walters, Affinity chromatographic examination of a retention model for macromolecules, *J. Chromatogr.*, 331 (1985) 1-10.
38. D.J. Anderson, R.R. Walters, Equilibrium and rate constants of immobilized concanavalin a cetermined by high-performance affinity-chromatography, *J. Chromatogr.*, 376 (1986) 69-85.
39. M.J. Yoo, J.E. Schiel, D.S. Hage, Evaluation of affinity microcolumns containing human serum albumin for rapid analysis of drug-protein binding, *J. Chromatogr. B*, 878 (2010) 1707-1713.
40. B. Loun, D.S. Hage, Characterization of thyroxine albumin-binding using high-performance affinity chromatography. 2. Comparison of the binding of thyroxine, triiodothyronines and related-compounds at the warfarin and indole sites of human serum albumin, *J. Chromatogr. B*, 665 (1995) 303-314.

41. P.K. Smith, R.I. Krohn, G.T. Hermanson, A.K. Mallia, F.H. Gartner, M.D. Provenzano, E.K. Fujimoto, N.M. Goetze, B.J. Olson, D.C. Klenk, Measurement of protein using bicinchoninic acid, *Anal. Biochem.*, 150 (1985) 76-85.
42. K.J. Wiechelman, R.D. Braun, J.D. Fitzpatrick, Investigation of the bicinchoninic acid protein assay: identification of the groups responsible for color formation, *Anal. Biochem.*, 175 (1988) 231-237.
43. K. Kim, J. Yu, H. Min, H. Kim, B. Kim, H.G. Yu, Y. Kim, Online monitoring of immunoaffinity-based depletion of high-abundance blood proteins by UV spectrophotometry using enhanced green fluorescence protein and FITC-labeled human serum albumin, *Proteome Sci.*, 8 (2010) 62.
44. S.A.T. Bulletin, FluoroTag(TM) Conjugation Kit, in: S. Aldrich (Ed.), Sigma, St. Louis, MS, 2012.
45. D. Sheehan, *Physical biochemistry: principles and applications*, 2nd ed., 2nd ed., Wiley, Hoboken, NJ, 2010.
46. K. Can, M. Ozmen, M. Ersoz, Immobilization of albumin on aminosilane modified superparamagnetic magnetite nanoparticles and its characterization, *Colloids Surf. B Biointerf.*, 71 (2009) 154-159.
47. Y.H. Tan, J.A. Davis, K. Fujikawa, N.V. Ganesh, A.V. Demchenko, K.J. Stine, Surface area and pore size characteristics of nanoporous gold subjected to thermal, mechanical, or surface modification studied using gas adsorption isotherms, cyclic voltammetry, thermogravimetric analysis, and scanning electron microscopy, *J. Mater. Chem.*, 22 (2012) 6733-6745.

48. D.L. Nelson, M.M. Cox, *Lehninger Principles of Biochemistry*, 5th ed., Freeman, New York, NY, 2008.
49. F. Vilaplana, R.G. Gilbert, Analytical methodology for multidimensional size/branch-length distributions for branched glucose polymers using off-line 2-dimensional size-exclusion chromatography and enzymatic treatment, *J. Chromatogr. A*, 1218 (2011) 4434-4444.
50. C.R. Keener, C.A.C. Wolfe, D.S. Hage, Optimization of oxidized antibody labeling with Lucifer yellow CH, *Biotechniques*, 16 (1994) 894-897.
51. C.A.C. Wolfe, D.S. Hage, Studies on the rate and control of antibody oxidation by periodate, *Anal. Biochem.*, 231 (1995) 123-130.
52. H. Xuan, D.S. Hage, Immobilization of alpha(1)-acid glycoprotein for chromatographic studies of drug-protein binding, *Anal. Biochem.*, 346 (2005) 300-310.

CHAPTER 3.

OPTIMIZATION OF A FLOW-BASED FORMAT FOR ENTRAPMENT

3.1. INTRODUCTION

High-performance affinity chromatography (HPAC) combines the high specificity of affinity chromatography with the instrumentation of HPLC to provide a fast and high throughput approach for biochemical separations [1-5]. Several rigid supports with high mechanical stability and good mass transfer properties are available for use in HPAC, such as porous silica beads, perfusion supports, polymer-based monoliths, and silica monoliths [6-11]. Chromatographic columns that contain porous silica supports and immobilized proteins or antibodies as affinity ligands have all been used in the past for studying biological interactions [12-19].

One method that has been widely used for the immobilization of proteins to supports that are used in HPAC is covalent attachment. One disadvantage of this approach is that it suffers from effects such as multisite attachment and steric hindrance, which may lead to some loss in the apparent activity of an immobilized binding agent [20-22]. In the previous chapter, an alternative method to covalent immobilization based on entrapment was optimized to produce affinity supports with high protein contents. This technique offered the potential advantage of providing an immobilized protein or binding agent that was fully active and in a soluble form for interacting with drugs and other small analytes that may be applied later to the affinity column [23-26].

In this chapter, an alternative method for immobilizing proteins by entrapment within HPLC-grade porous silica is discussed. Ways to use this approach to further increase the protein content of affinity supports that are prepared through entrapment are also explored. The primary method that will be examined will be based on the entrapment of proteins by recirculating these and the other reagents through hydrazide-activated silica that has previously been packed in a column. This flow-based format should provide the smallest possible volume that can be occupied by the silica particles during the entrapment process. It is expected that this reduced volume should promote better contact of the proteins with the surface and pores of the particles while the active aldehyde groups on the capping agent (i.e., oxidized glycogen) are reacting with hydrazide groups on the particles. This, in turn, should result in larger amounts of protein that can be entrapped when compared to the slurry-based method that was described in the previous chapter. The on-column method of entrapment that will be examined in this chapter should also be more amenable for automation than the slurry-based method. Finally, this on-line format has the potential for reducing the amount of protein and reagents that are required for entrapment, which may make it possible to apply this technique to other types of affinity ligands.

3.2. EXPERIMENTAL SECTION

3.2.1. Reagents

The human serum albumin (HSA, essentially fatty acid free, purity $\geq 96\%$), concanavalin A (Con A, type V, lyophilized powder, purity $\geq 99\%$), glycogen (from bovine liver, type IX; total glucose $\geq 85\%$, dry basis), racemic warfarin (purity $\geq 98\%$), *R*-warfarin (purity $\geq 97\%$), carbamazepine (purity $\geq 98\%$), 4-methylumbelliperyl α -D-

mannopyranoside (MUM, purity \geq 96%), 4-methylumbelliperyl α -D-galactopyranoside (MUGA, purity \geq 98%), and periodic acid reagent (H_5IO_6 , purity 99%) were purchased from Sigma-Aldrich (St. Louis, MO, USA). The Nucleosil Si-300 silica (7 μm particle diameter, 300 \AA pore size, 100 m^2/g surface area) was obtained from Macherey-Nagel (Düren, Germany). All other chemicals were of the purest grades available. All buffers and aqueous solutions were prepared using water from a Nanopure system (Barnstead, Dubuque, IA, USA) or a MilliQ Advantage 10 system (EMD Millipore Corporation, Billerica, MA, USA). The buffers were filtered through 0.20 μm GNWP nylon membranes from Millipore (Billerica, MA, USA) and were degassed by sonication under vacuum for at least 20 min prior to use.

3.2.2. Apparatus

The chromatographic system consisted of two 1200 isocratic pumps from Agilent (Santa Clara, CA, USA), a Series 200 UV-Vis detector and a vacuum degasser from Perkin Elmer (Waltham, MA, USA), a Rheodyne LabPro valve (Cotati, CA, USA) equipped with a 5 μL or 20 μL sample loop, and a series 1200 autosampler from Agilent. An Isotemp 9100 circulating water bath (Fisher Scientific, Pittsburgh, PA, USA) and a water jacket from Alltech (Deerfield, IL, USA) were used for temperature control of the columns. The chromatographic data were collected and processed using LabView 8 software (National Instruments, Austin, TX, USA). The chromatograms were analyzed using PeakFit 4.12 (Systat Software, San Jose, CA, USA).

Two PHD Ultra syringe pumps (Harvard Apparatus, Holliston, MA, USA) were used for the on-column entrapment method. A Pack-in-a-Box system (ChromTech, Apple

Valley, MN, USA) was used for packing the supports into columns. A UV-160A spectrophotometer (Shimadzu, Kyoto, Japan) was used for the BCA protein assay.

3.2.3. Preparation of columns containing entrapped proteins

Diol silica was prepared from Nucleosil 300-7 silica by following a previous procedure [1]. This support was then dried at 60 °C and stored in a desiccator. Portions of this support (i.e., 50 mg batches of the diol silica) were further treated, as described previously, to produce hydrazide-activated silica [1]. Each batch of the hydrazide-activated silica was washed with pH 7.4, 0.067 M potassium phosphate buffer and downward slurry packed into a 1 cm × 2.1 mm i.d. stainless steel column with the same type of 7.4 buffer acting as the packing solution. In order to ensure homogeneous packing, a slurry of the support was made with 5 mL of the pH 7.4 buffer, which was added to the reservoir of the packing system after the column was attached to the bottom; this was followed by a step where an additional 15 mL of the 7.4 buffer was used to fill the rest of the reservoir. The packing was then begun by flowing the buffer and slurry at 3.0 mL/min. The packing pressure and the flow were gradually increased over 10-15 min until reaching a maximum pressure of 3400 psi (23.4 MPa). After 40 min, the pressure was gradually relieved for 10-15 min to avoid disturbing the chromatographic support in the column.

The columns packed with hydrazide-activated silica were used for the on-column entrapment of proteins in the presence of solutions of the desired protein and oxidized glycogen. The reagents that were used for preparing the entrapped protein supports, the proportions in which these reagents were combined, and the reaction times that were used were the same as described in Chapter 2 [25]. In this chapter, a flow-based and on-column entrapment approach was explored as an alternative to the previous method that was based

on a reaction slurry. The conditions that were used for this modified entrapment approach are described in the Results and Discussion section.

3.2.4. Chromatographic methods

The application and elution buffer that was used for the chromatographic studies with HSA was pH 7.4, 0.067 M potassium phosphate. This same buffer has been used in previous studies with HSA to provide physiological conditions for drug-protein binding studies [13,27-32]. In the work with Con A, the application/elution buffer was pH 5.0, 0.50 M sodium acetate that contained 1 mM calcium chloride and 1 mM manganese chloride to ensure optimum activity for the Con A, according to conditions reported in previous studies [33,34]. The equilibration conditions and temperature of the chromatographic studies were the same as described in Chapter 2. The wavelengths used for detection were 307 nm for warfarin, 285 nm for carbamazepine, 280 nm for L-tryptophan, 316 nm for MUM and MUGA, and 205 nm or 220 nm for sodium nitrate.

In the zonal elution studies, each analyte was dissolved in the desired application buffer and a sample volume of 5 μ L or 20 μ L was placed into the system by using an injection valve. The concentrations of the analytes that were used in these experiments were selected so that linear elution conditions were present. These conditions were determined and confirmed by making several injections at various sample concentrations to ensure that sample conditions were used over which the retention factor did not change (at the 95% confidence level) with the concentration of the injected analyte [29,32,35,36]. The final sample concentrations that were used were 10-40 μ M for each injected analyte or probe and 2.5-5 μ M for sodium nitrate. The flow rates that were used for measuring the retention factors of these compounds were between 0.2 and 0.5 mL/min, with no significant

difference been seen at the 95% confidence level in the results that were obtained over this range of flow rates.

The retention times for each injected solute were found by carrying out a non-linear fit with PeakFit 4.12 and by using an exponentially-modified Gaussian and half-Gaussian modified Gaussian (EMG+CMG) function. The retention time or elution time was estimated by using the first statistical moment of the fitted peak (i.e., the centroid). At least three injections were done under each set of conditions for each solute and column. A sodium nitrate solution was injected for determining the void time of each column. The average retention factor and standard deviation of each solute on each entrapment column were calculated. Injections of each solute on a control column were also made to correct for non-specific binding, as explained in Section 2.3.7. These non-specific interactions accounted for less than 1% of the overall retention for warfarin and less than 2% for MUGA.

3.3. RESULTS AND DISCUSSION

3.3.1. Optimization of the on-column entrapment method

The on-column entrapment method was initially carried out by using one syringe pump, where two 1 mL plastic syringes were placed and connected to columns that were packed with hydrazide-activated silica. Tubing was connected to each column and directed to 2 mL vials. This system is shown in Figure 3.1(a). One column was used for the entrapment reaction with the desired protein and the other was used to prepare a control column that did not contain the protein (e.g., HSA in the initial studies with this method). The reagents were dissolved in pH 5.0, 0.10 M potassium phosphate buffer and recirculated

through the columns at 50 $\mu\text{L}/\text{min}$. When making the entrapped protein column, 0.8 mL of 20 mg/mL HSA was recirculated through this column for 4 h, with the flow direction being changed every three minutes. The solutions in the syringes were changed to 0.8 mL of a mixture of 20 mg/mL HSA and 4.2 mg/mL oxidized glycogen, and the recirculation was continued for 16 h. Finally, 200 μL of a solution containing 1 mg/mL oxalic dihydrazide was mixed with the other reactants and the reaction was allowed to continue for another hour under the same recirculation conditions. For the control column, the HSA solutions were replaced with pH 5.0, 0.10 M potassium phosphate buffer.

The immobilization method with one syringe pump had some issues with bubble formation in the HSA solutions and the formation of a void region in the syringes, which was most noticeable in the syringe that was connected to the entrapped protein column. It was found that atmospheric pressure was not enough to keep the solutions going through columns when the syringes were used to draw the solutions from the collecting vials. The higher viscosity of the solution with HSA made this problem more noticeable for the entrapped protein column. As a result, bubbles formed in the syringe and created a situation in which sometimes little or no protein solution was withdrawn by the syringe. To achieve a better delivery of the reagents through the column, it was necessary to periodically stop the delivery and refill the syringe with the solution from a collection vial. When the retention factor for racemic warfarin was measured for such a column, the result was $19 (\pm 2)$, where the value in parentheses represents one standard deviation for three replicate injections that were made onto the same column.

A second column containing entrapped protein was made by using 40 mg/mL HSA, with most of the other conditions being kept the same as in the previous study. The flow

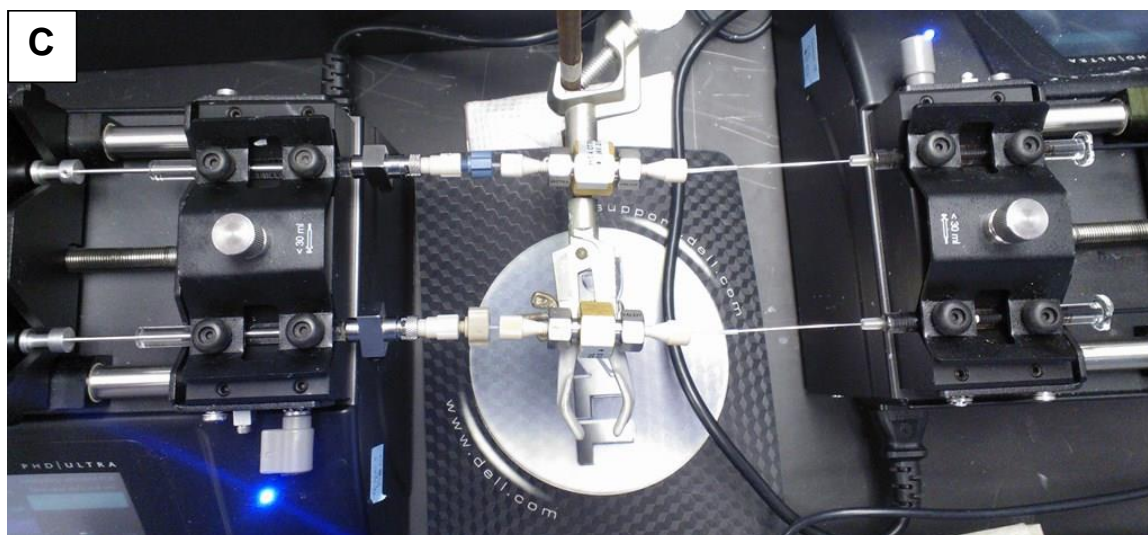
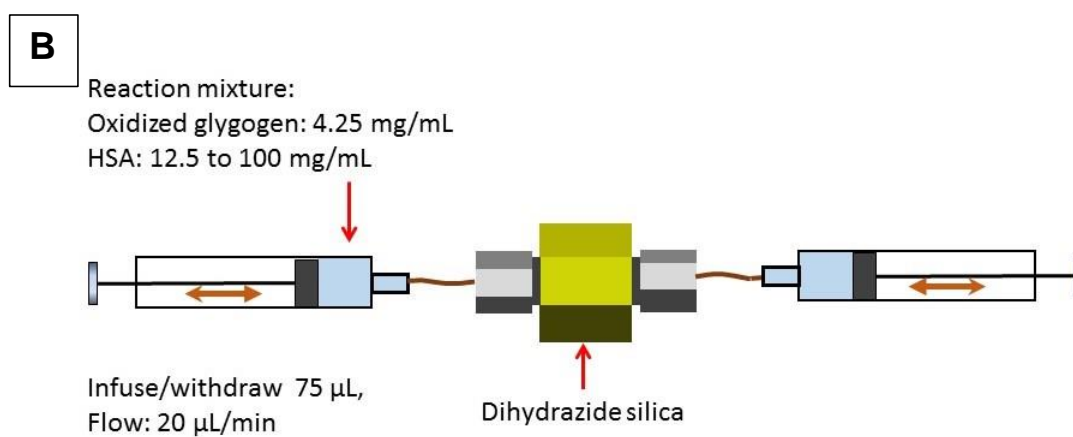
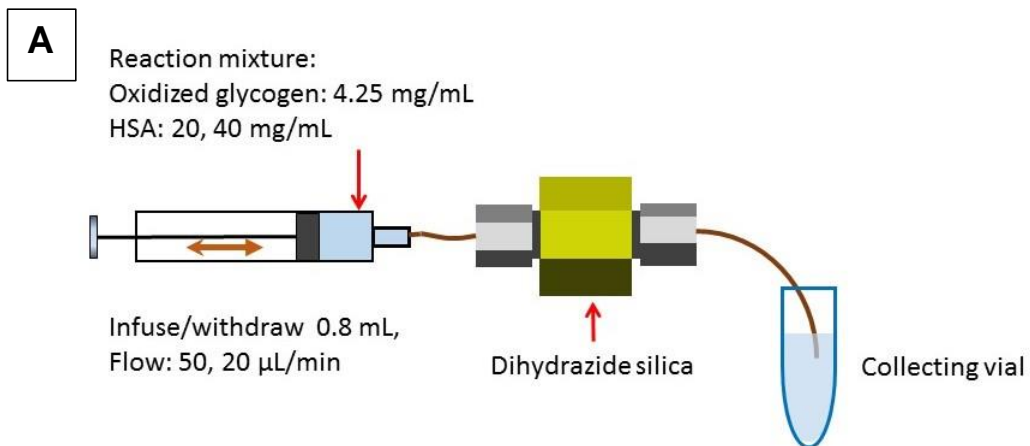
rate was reduced to 20 $\mu\text{L}/\text{min}$ in an attempt to reduce bubble formation during the entrapment process. A retention factor for warfarin of 82 (± 4) was achieved when this second type of column was compared with its control column. This experiment indicated that the use of a higher protein concentration during the entrapment process and the use of an improved reagent delivery system gave a significant increase in the amount of protein that was entrapped. However, it was still desirable to find a way to make the entrapment conditions easier to control and to make this process more fully automated.

In the next phase of this study, the columns were each connected to two syringe pumps that were equipped with 250 μL syringes. These pumps were synchronized to recirculate a solution through the columns, with one syringe infusing a solution while the other was used to withdraw the same solution. A diagram of such a system is given in Figure 3.1(b). A picture of the entrapped protein columns and control columns when they were attached to the syringe pumps in this system is provided in Figure 3.1(c). The volume of solution that was used in each syringe was 200 μL , and the syringes were used to infuse or withdraw 75 μL of this solution each cycle at a flow rate of 20 $\mu\text{L}/\text{min}$. A stop time of 1 min was included in this program between each change in direction of syringe movement to allow the solution to completely go through the column and relieve any pressure buildup before changing the direction of solution application. The solutions in this system could be circulated through the columns without the formation of bubbles or foam, and the system could be left unattended during the entrapment reaction. With this system, columns were prepared by using concentrations of HSA that ranged from 12.5 to 100 mg/mL , as were used to study the effect of protein concentration on the amount of protein that could be entrapped by this immobilization method.

The final entrapment procedure involved the use of the two-syringe system for 4 h to apply a solution that first contained only the protein dissolved in pH 5.0, 0.10 M potassium phosphate buffer; this was followed by the application of a mixture of the protein and 4.2 mg/mL of oxidized glycogen in the same buffer for 16 h. Finally, a portion of 200 μ L of 1 mg/mL oxalic dihydrazide in the same buffer was added to the reaction mixture and the solution delivery was continued for another 2 h at room temperature. A control column was made under the same conditions but with the solution of HSA being replaced with an equal volume of pH 5.0, 0.10 M potassium phosphate buffer.

Immediately after this reaction was finished, the column was connected to an HPLC pump and pH 7.4, 0.067 M potassium phosphate buffer was applied at 0.5 mL/min for 1 h to wash away the excess reactants (e.g., any unreacted oxidized glycogen or oxalic dihydrazide, and any remaining non-entrapped HSA).

Figure 3.1 (a) Diagram of the on-column entrapment method with one syringe pump or (b) two syringe pumps, and (c) an image of the on-column entrapment system with two syringe pumps. The concentrations of protein and oxidized glycogen in pH 5.0, 0.10 M phosphate buffer, the volume of the solutions that were used and the flow rate are all indicated. Other entrapment conditions are given in the text.



The dual-syringe entrapment system was used to make several columns that contained entrapped HSA or Con A to study the effects of the protein concentration in the reaction mixture on the protein content of the resulting support. Examples of some chromatograms and retention factors that were obtained for *R/S*-warfarin on columns that were made by entrapment and using various concentrations of HSA are shown in Figure 3.2. The results for a column that was made by using the slurry entrapment method and 100 mg/mL of HSA are also included in this figure for comparison. For these HSA columns, a 1.7-fold increase in the retention factor for *R/S*-warfarin occurred when going from conditions that used 12.5 to 25 mg/mL HSA during the entrapment process. An increase of 6.3% was seen in going from using 25 to 50 mg/mL HSA during entrapment. These results indicated that an on-column entrapment method using 25 mg/mL HSA was probably the most efficient and cost effective approach for entrapping this protein under this given set of conditions.

These data were also used to compare the results obtained with the slurry method vs. entrapment. In the slurry method, a 0.4 mL portion of 100 mg/mL HSA was used to make the column, or a total of 40 mg protein. The on-column method only needed 0.4 mL of 25 mg/mL HSA to make a column of the same size, or the equivalent of 10 mg protein, and the retention factor that was obtained for warfarin increased by 1.5-fold (or was about 50% higher). Thus, the on-column method based on 25 mg/mL HSA was also a more efficient and cost-effective approach for entrapment than the slurry method under this set of conditions.

Some chromatograms and retention results that were obtained for Con A columns that were prepared by the on-column method and slurry method are shown in Figure 3.3.

Figure 3.2 Chromatograms and retention factors obtained for *R/S*-warfarin on columns containing entrapped HSA and made by the slurry method or the on-column method and using various protein concentrations in the reaction mixture. Conditions: sample, 40 μ M *R/S*-warfarin; column size, 1.0 cm \times 2.1 mm i.d.; flow rate, 0.50 mL/min; temperature, 37 $^{\circ}$ C. The values in parentheses represent a range of \pm 1 S.D. ($n = 3-4$).

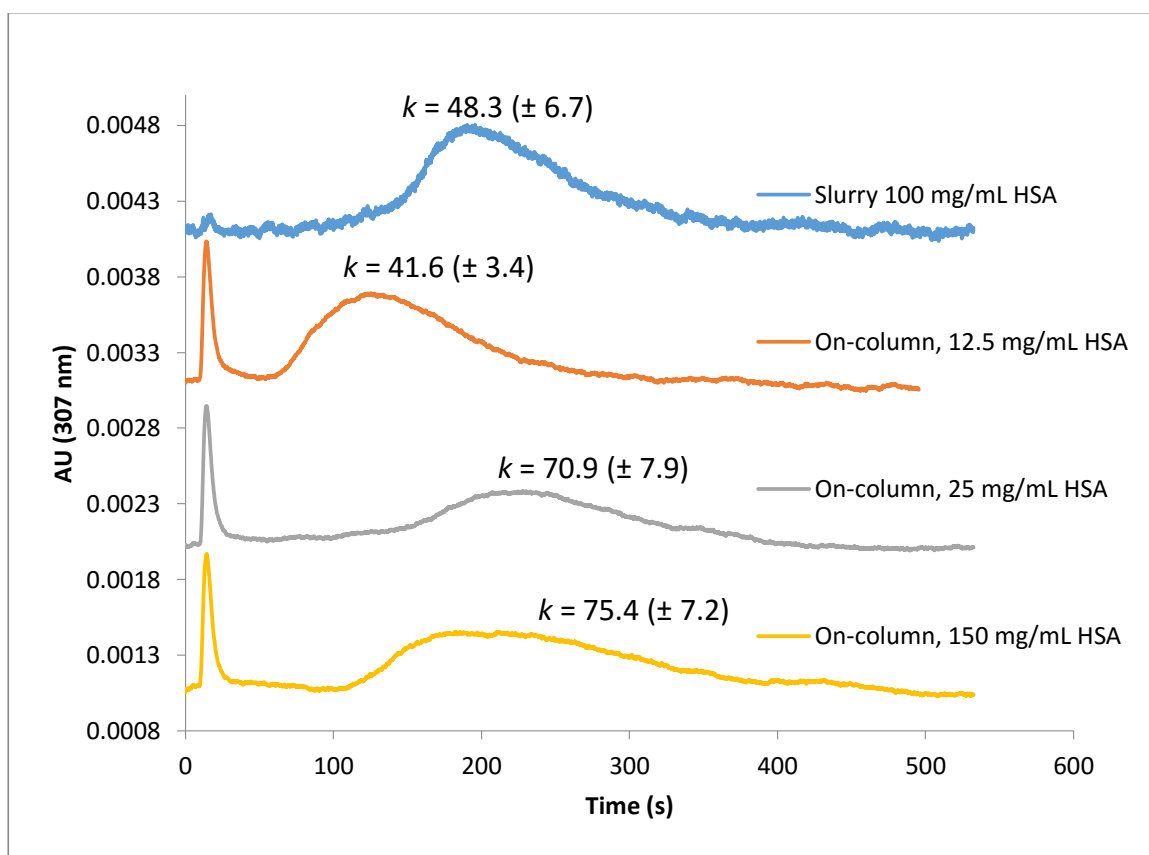
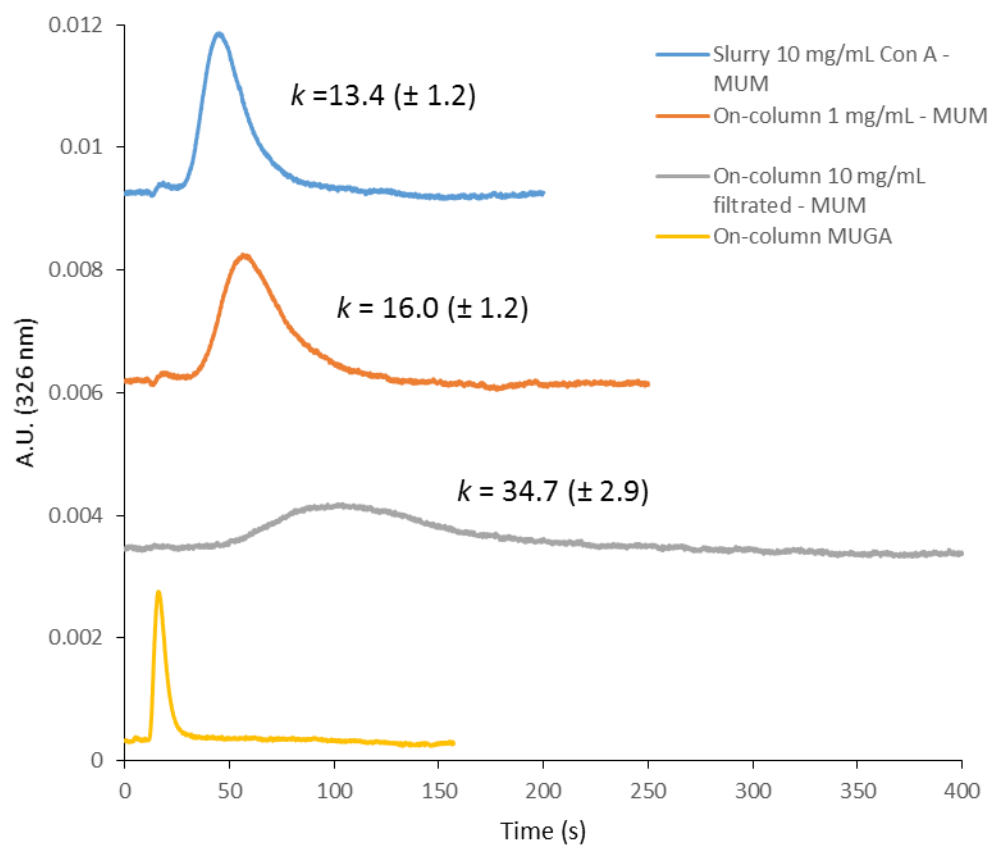


Figure 3.3 Chromatograms and retention factors obtained for MUM on columns containing entrapped Con A that were prepared by various methods and reaction conditions. The bottom chromatogram shows the results for MUGA, which does not bind to Con A, and which was used to measure the void time of the Con A columns. Conditions: samples, 10 μM MUM or 10 μM MUGA; column size, 1.0 cm \times 2.1 mm I.D.; flow rate, 0.50 mL/min; temperature, 20 $^{\circ}\text{C}$. The values in parentheses represent a range of ± 1 S.D. ($n = 3$).



The solubility of Con A limited the concentrations that could be used with the protein for the entrapment process, but an increase of over two-fold in the retention factor for MUM was seen when going from columns that were made using 1 mg/mL to 5 mg/mL Con A (Note: at this later concentration, some of the Con A started to precipitate, and it was necessary to filter this solution before using it for entrapment). The column that was prepared by using 1 mg/mL Con A in the on-column entrapment method gave a retention factor for MUM that was 1.2-fold higher than what was seen for the column that was made using the same concentration of Con A in the slurry entrapment method. The column that was made using 5 mg/mL Con A for on-column entrapment gave 2.6-fold higher retention for MUM than the column that was made by the slurry method and using 1 mg/mL Con A.

3.3.2. Estimation of protein content following on-column entrapment

In the on-column method, the entrapment is performed directly on the column and it is not possible to analyze the protein directly on the support by means such as absorbance, fluorescence or a standard protein assay. However, it could be possible to estimate the content of the active protein in the resulting column by conducting zonal elution experiments in which solutes are injected that have known interactions and association equilibrium constants (K_a) for these proteins. This latter approach was employed in this study.

One feature that makes the entrapment technique suitable to this type of assay is the fact that the protein is immobilized without covalent linkage to the support [16,25]. As a result, the active sites of the protein should be fully active and available to an injected probe that is able to enter the support and bind to these sites. Under these conditions, the retention factor that is measured for the injected probe (k) can be related to the strength of

the probe-protein interaction and the amount of protein in the column through the following relationship [16,24,37].

$$k = (n_1K_{a1} + n_2K_{a2} + \dots n_nK_{an})m_{Ltotal}/V_m \quad (3.1)$$

where m_{Ltotal} represents the total moles of binding sites for the probe in the column, and V_m is the column void volume. The term in parentheses is a number-weighted sum of the association equilibrium constants for all of the binding sites that are involved in the probe-protein interaction, where n_i is the relative number of moles of binding site i per mole of protein, and K_{ai} is the association equilibrium constant of the probe at binding site i . This equation also assumes that all the binding sites for the probe are independent of each other [16,24,37].

For the case of probe compounds that have only a single binding site on a protein (e.g., as is the case for warfarin and carbamazepine with HSA) [16,29], Equation 3.1 can be rewritten in the form shown in Equation 3.2 [16].

$$k = K_a \frac{m_{Ltotal}}{V_m} \quad (3.2)$$

In this case $n = 1$ for the probe (e.g., warfarin), and the ratio m_{Ltotal}/V_m represents the total concentration of protein that is immobilized or entrapped in the column [12,13,16]. If the retention factor is also corrected for any non-specific binding that may be occurring with the support, this corrected value can be used with Equation 3.2 to estimate the concentration or total moles of protein in the column.

The protein contents for columns containing entrapped HSA were estimated by using carbamazepine or warfarin as the injected probes. The following association equilibrium constants have been previously reported for the interactions of these drugs with

HSA at pH 7.4 and 37°C: carbamazepine, $5.4 (\pm 0.2) \times 10^3 \text{ M}^{-1}$; *R*-warfarin, $2.1 (\pm 0.2) \times 10^5 \text{ M}^{-1}$; and racemic warfarin, $2.3 (\pm 0.4) \times 10^5 \text{ M}^{-1}$, where this value is the average of the values for *R*- and *S*-warfarin [29,30,32]. The retention measurements that were made for all of these drugs were also carried out at pH 7.4 and 37°C, along with a flow rate of 0.2 or 0.5 mL/min. Table 3.1 shows the corrected retention factors that were obtained with these probes on columns that were made by using on-column entrapment method and various concentrations of HSA. The protein contents that were estimated from these results are shown in Table 3.2.

Table 3.1. Corrected retention factors measured for several probe compounds that were injected onto HSA columns that were prepared by the on-column entrapment method and using various concentrations of HSA in the reaction mixture¹

Type of entrapment method and HSA concentration	Corrected retention factor, <i>k</i>		
	Carbamazepine	<i>R</i> -Warfarin	<i>R/S</i> -Warfarin
Slurry method, 100 mg/mL HSA	0.95 (± 0.12)	39.5 (± 4.4)	37.6 (± 5.2)
On-column method, 12.5 mg/mL HSA	1.42 (± 0.20)	45.1 (± 7.0)	42.4 (± 1.0)
On-column method, 25 mg/mL HSA	1.65 (± 0.20)	61.1 (± 4.4)	68.2 (± 3.8)
On-column method, 40 mg/mL HSA ²	1.98 (± 0.24)	69.0 (± 5.7)	65.2 (± 2.9)
On-column method, 50 mg/mL HSA	1.91 (± 0.11)	73.9 (± 4.5)	75.6 (± 3.5)
On-column method, 100 mg/mL HSA	5.75 (± 1.01)	196.1 (± 5.4)	227.8 (± 5.4)

¹The results for an HSA column that was prepared by the slurry method and using 100 mg/mL HSA is included in this table for reference. All of the retention factors in this table were measured at 0.5 mL/min and 37 °C. The numbers in parentheses represent a range of ± 1 S.D., as obtained for at least two or three injections per column; the only exception was for *R/S*-warfarin, in which two or three columns were used and the value that is given is the combined average of the retention factors for these columns.

²This type of support was prepared by using only one syringe pump.

Table 3.2. Protein content measured by using the retention factors for several probe compounds that were injected onto HSA columns that were prepared by the on-column entrapment method and using various concentrations of HSA in the reaction mixture¹

Type of entrapment method and HSA concentration	Protein content (mg/g silica) ¹			
	Carbamazepine	<i>R</i> -Warfarin	<i>R/S</i> -Warfarin	Average
Slurry method, 100 mg/mL HSA	20.7 (± 5.7)	22.1 (± 6.3)	19.2 (± 6.3)	20.7 (± 3.5)
On-column method, 12.5 mg/mL HSA	23.5 (± 7.1)	19.2 (± 6.2)	20.9 (± 6.4)	21.2 (± 3.8)
On-column method, 25 mg/mL HSA	34.0 (± 8.9)	32.3 (± 8.4)	32.9 (± 9.7)	33.1 (± 5.2)
On-column method, 40 mg/mL HSA	39.3 (± 10.4)	35.2 (± 9.4)	30.4 (± 9.0)	35.0 (± 5.6)
On-column method, 50 mg/mL HSA	45.9 (± 10.7)	34.3 (± 8.8)	40.0 (± 11.5)	40.1 (± 6.0)
On-column method, 100 mg/mL HSA	126 (± 37)	114 (± 28)	121 (± 34)	120 (± 19)

¹The conditions are the same as in Table 3.1. The numbers in parentheses represent a range of ± 1 S.D., as obtained for at least three injections per column. The protein content was calculated by using molar mass of 66.4 kDa for HSA, the volume of the column, and a packing density for silica of 0.45 g/cm³. A 1:1 binding model was used along with the following association equilibrium constants: carbamazepine: $5.4 (\pm 0.2) \times 10^3 \text{ M}^{-1}$ [29], *R*-warfarin, $2.1 (\pm 0.2) \times 10^5 \text{ M}^{-1}$; racemic warfarin, $2.3 (\pm 0.4) \times 10^5 \text{ M}^{-1}$, where this last value is the average of the values for *R*- and *S*-warfarin) [32].

The protein content that was obtained through this process for the HSA column that was made by the slurry entrapment method was compared to the result that was estimated for the same type of support when using a protein assay. In this case, the protein content was also estimated by using fluorescence measurements and a support that had been prepared under the same conditions by using fluorescein-labeled HSA. The reference method gave a protein content for this support that was equal to 20.1 (\pm 1.1) mg/g of silica. This value was statistically equivalent to the values that were estimated in Table 3.2 when using the injected probes and their measured retention factors.

It can be observed in Tables 3.1 and 3.2 that the retention factors and calculated protein contents gave similar trends in the results that were obtained for carbamazepine, *R*-warfarin and *R/S*-warfarin. The use of even 12.5 mg/mL HSA in the on-column entrapment method gave a similar protein content to what was obtained when using 100 mg/mL HSA in the slurry entrapment method. Using a higher concentration of HSA in the on-column entrapment method tended to give an increase in the measured retention factors and estimated protein content of the final column. The column that was made using 100 mg/mL HSA for on-column entrapment gave the highest overall retention and protein content. The protein content of this column was about six-fold higher than the protein content that was obtained by the slurry entrapment method when using the same concentration of HSA for entrapment. Approximately the same increase was seen in going from the use of 12.5 to 100 mg/mL HSA for on-column entrapment.

Although the three types of probe compounds gave good agreement in the protein contents that they provided for these columns, there were advantages and disadvantages to the use of each type of probe. The analysis time for the elution of carbamazepine was

shorter than for warfarin because the affinity of this drug for HSA was also weaker. This made this probe useful for obtaining a fast estimate of the protein content; however, this feature also made this probe more difficult to use than warfarin for examining the protein content of small columns. *R*-Warfarin gave sharper elution profiles than racemic warfarin, since this peak was due to only a single enantiomer rather than the result of two overlapping peaks for two enantiomers. However, *R*-warfarin was also much more expensive than racemic warfarin and more difficult to obtain.

3.3.3. Column stability and comparison with previous HSA columns

Table 3.3 compares the retention factors that were measured in this study for warfarin on the columns that were prepared by entrapment vs. results obtained with previous HSA columns that have been used with this probe and that have been prepared by covalent immobilization methods. It can be seen that the retention factors obtained by the entrapment method were similar to or higher than the highest retention factors that have been obtained in prior work with HSA that has been covalently immobilized to silica by the Schiff base method. This difference was particularly true in the case where the retention factors were compared for the on-column entrapment method that used up to 100 mg/mL HSA for entrapment.

The data in Table 3.3 for the entrapment method also provide some information on the stability and reproducibility of the columns that were prepared by this approach. For instance, the two top entries in Table 3.3 provide the range of retention factors that were obtained over the course of about one and a half years for columns that were made by the slurry entrapment method and the on-column entrapment method. These results indicate that both entrapment methods were able to provide HSA supports that had good activity

for extended periods of time when used under the storage and application conditions that were employed in this study. These two types of columns were each stored at 4 °C when not in use and were used for multiple injections of various probes, with typical lifetimes of over 150 h of use at a flow rate of 0.5 mL/min.

Table 3.3. Comparison of retention factors measured for warfarin with columns containing immobilized HSA that were prepared by entrapment or through covalent immobilization

Experiment/ Type of warfarin	Retention factor, <i>k</i>	Method and conditions [Refs.]
1) <i>Racemic</i>	38-51 ¹	Slurry entrapment method using 100 mg/mL HSA and porous silica. Column size: 1 cm × 2.1 mm. Mobile phase: pH 7.4, 0.067 M potassium phosphate buffer. Temperature: 37 °C.
2) <i>Racemic</i>	70-82 ²	On-column entrapment method using 50 mg/mL of HSA and porous silica. Column size: 1 cm × 2.1 mm. Mobile phase: pH 7.4, 0.067 M potassium phosphate buffer. Temperature: 37 °C
3) <i>R-Warfarin</i>	74 (± 4) ³	Same conditions as the previous experiment
4) <i>Racemic</i>	191-236 ²	100 mg/mL of HSA, the other conditions were the same as the previous experiment
5) <i>R-Warfarin</i>	196-224 ²	Same conditions as the previous experiment

Table 3.3. (Continued)

Experiment/ Type of warfarin	Retention factor, k	Method and conditions [Refs.]
<i>R</i>-Warfarin	2.3 (\pm 0.2)	Schiff base method. Column size: 5 cm \times 2.1 mm. Mobile phase: pH 7.4, 0.067 M potassium phosphate buffer. Room temperature [15]
<i>S</i>-Warfarin	98 (\pm 1)	
<i>R</i>-Warfarin	39 ⁴	Schiff base method. Column size: 5 cm \times 2.1 or 4.6 mm. Mobile phase: pH 7.4, 0.067 M potassium phosphate buffer. Temperature: 37 °C [16]
<i>R</i>-Warfarin	12.8 (\pm 0.3) ⁵	Schiff base method. Column size: 5 cm \times 4.6 mm. Mobile phase: pH 7.4, 0.067 M potassium phosphate buffer, containing 5% 2-propanol and 1 mM octanoic acid. Temperature: 25 °C [31]
<i>S</i>-Warfarin	26.8 (\pm 0.4) ⁵	
<i>R</i>-Warfarin	82 (\pm 4) ⁶	Schiff base method. Column size: 2.0, 0.5 or 0.1 cm length, respectively, 2.1 mm I.D. Mobile phase: pH 7.4, 0.067 M potassium phosphate buffer. Temperature: 37 °C [31]
	57 (\pm 6) ⁶	
	38 (\pm 8) ⁶	

¹This range of results was obtained over 1.5 years using the same column.

²This range of results was obtained over 1.5 years from two columns.

³These results were obtained over three injections on the same day and on one column.

⁴The value was calculated from a point in a graph, so no standard error is available.

⁵2-Propanol and octanoic acid were used in this case as mobile phase modifiers or competing agents to adjust and lower the retention factors for the injected analytes.

⁶These are average retention factors at flow rates from 0.1 to 5 mL/min. All other experiments were performed at 0.5 mL/min.

3.4. CONCLUSIONS

Several factors were examined for maximizing the amount of HSA or Con A that could be immobilized within porous silica by the on-column entrapment method. These factors included the use of one or two syringe pumps, the flow rate that was used for the entrapment process, and the protein concentration that was employed. A technique for determining the protein content of HSA supports that were made by the on-column approach was also developed, which was based on the use of injected probes such as warfarin and carbamazepine. It was found in the use of on-column entrapment for HSA that the final protein content could be increased by at least six-fold versus what has been observed for columns that were made with the slurry method of entrapment. The entrapment of Con A also increased by almost three-fold with the use of the on-column method.

One reason for the higher levels of protein that were obtained in the on-column method is the reduced volume of the reaction slurry that was occupied by the packed support. In the on-column method, only the void volume of the column was available for the entrapment reaction, which probably led to an increased chance for the protein getting entrapped when the oxidized glycogen molecules reacted with hydrazide groups on the support. The use of flow to pass these reagents through the support may also have increased the contact of the protein with the pores during this process.

This on-column entrapment approach can be adapted for use with other proteins or supports. The protein content that can be obtained by this method should be advantageous in future work with microcolumns or microfluidic systems or for any application of HPAC

in which relative strong binding or good retention is needed in small devices or miniaturized systems.

REFERENCES

53. P.F. Ruhn, S. Garver, D.S. Hage, Development of dihydrazide-activated silica supports for high performance affinity chromatography, *J. Chromatogr. A*, 669 (1994) 9-19.
54. C. Wang, J. Ge, J. Zhang, T. Guo, L. Chi, Z. He, X. Xu, P. York, L. Sun, H. Li, Multianalyte determination of the kinetic rate constants of drug-cyclodextrin supermolecules by high performance affinity chromatography, *J. Chromatogr. A*, 1359 (2014) 287-295.
55. F.O. Gbormittah, B.B. Haab, K. Partyka, C. Garcia-Ott, M. Hancapie, W.S. Hancock, Characterization of glycoproteins in pancreatic cyst fluid using a high-performance multiple lectin affinity chromatography platform, *J. Proteome Res.*, 13 (2014) 289-299.
56. K. Vuignier, D. Guillarme, J.L. Veuthey, P.A. Carrupt, J. Schappler, High performance affinity chromatography (HPAC) as a high-throughput screening tool in drug discovery to study drug-plasma protein interactions, *J. Pharmaceut. Biomed. Anal.*, 74 (2013) 205-212.
57. Y.-F. Li, X.-Q. Zhang, W.-Y. Hu, Z. Li, P.-X. Liu, Z.-Q. Zhang, Rapid screening of drug-protein binding using high-performance affinity chromatography with columns containing immobilized human serum albumin, *J. Anal. Methods Chem.*, 2013 (2013) 439039.

58. P.-E. Gustavsson, P.-O. Larsson, Support materials for affinity chromatography, in: D.S. Hage (Ed.) Handbook of Affinity Chromatography, 2nd ed., CRC Press, Boca Raton, FL, 2006, pp. 16-33.
59. X. Yang, Y. Hu, G. Li, Online micro-solid-phase extraction based on boronate affinity monolithic column coupled with high-performance liquid chromatography for the determination of monoamine neurotransmitters in human urine, *J. Chromatogr. A*, 1342 (2014) 37-43.
60. P. Jandera, Advances in the development of organic polymer monolithic columns and their applications in food analysis – a review, *J. Chromatogr. A*, 1313 (2013) 37-53.
61. Z. He, C. Lv, X. Fan, Z. Zhou, A novel lipase-based stationary phase in liquid chromatography, *Anal. Chim. Acta*, 689 (2011) 143-148.
62. H. Wang, P. Jiang, M. Zhang, X. Dong, Synthesis of a novel restricted access chiral stationary phase based on atom transfer radical polymerization and click chemistry for the analysis of chiral drugs in biological matrices, *J. Chromatogr. A*, 1218 (2011) 1310-1313.
63. Y. Wu, D. Abraham, G. Carta, Particle size effects on protein and virus-like particle adsorption on perfusion chromatography media, *J. Chromatogr. A*, 1375 (2015) 92-100.
64. D.S. Hage, High-performance affinity chromatography: a powerful tool for studying serum protein binding, *J. Chromatogr. B*, 768 (2002) 3-30.

65. D.S. Hage, J. Anguizola, O. Barnaby, A. Jackson, M.J. Yoo, E. Papastavros, E. Pfaunmiller, M. Sobansky, Z.H. Tong, Characterization of drug interactions with serum proteins by using high-performance affinity chromatography, *Curr. Drug Metabol.*, 12 (2011) 313-328.
66. D.S. Hage, J.A. Anguizola, C. Bi, R. Li, R. Matsuda, E. Papastavros, E. Pfaunmiller, J. Vargas, X. Zheng, Pharmaceutical and biomedical applications of affinity chromatography: recent trends and developments, *J. Pharmaceut. Biomed. Anal.*, 69 (2012) 93-105.
67. D.S. Hage, J. Austin, High-performance affinity chromatography and immobilized serum albumin as probes for drug- and hormone-protein binding, *J. Chromatogr. B*, 739 (2000) 39-54.
68. D.S. Hage, A. Jackson, M.R. Sobansky, J.E. Schiel, M.J. Yoo, K.S. Joseph, Characterization of drug-protein interactions in blood using high-performance affinity chromatography, *J. Sep. Sci.*, 32 (2009) 835-853.
69. D.S. Hage, S.A. Tweed, Recent advances in chromatographic and electrophoretic methods for the study of drug-protein interactions, *J. Chromatogr. B*, 699 (1997) 499-525.
70. E. Pfaunmiller, A.C. Moser, D.S. Hage, Biointeraction analysis of immobilized antibodies and related agents by high-performance immunoaffinity chromatography, *Methods*, 56 (2012) 130-135.
71. X.F. Zhao, Q. Li, J.J. Huang, J.B. Zheng, X.H. Zheng, Z.J. Li, Y.Y. Zhang, Effects of temperature and mobile phase composition on the interaction between berberine

- and immobilized beta (2)-adenoreceptor by high performance affinity chromatography, *J. Liq. Chromatogr. Related Technol.*, 37 (2014) 88-98.
72. H.S. Kim, D. Hage, S., Immobilization methods for affinity chromatography, in: D.S. Hage (Ed.) *Handbook of Affinity Chromatography*, 2nd ed., CRC Press, Boca Raton, FL, 2006, pp. 36-78.
73. M.C. Millot, S. Servagent-Noinville, N.L. Taleb, M.H. Baron, M. Revault, B. Sebille, Structural changes of human serum albumin immobilized on chromatographic supports: a high-performance liquid chromatography and Fourier-transform infrared spectroscopy study, *J. Chromatogr. B*, 753 (2001) 101-113.
74. M.C. Millot, N.L. Taleb, B. Sebille, Binding of human serum albumin to silica particles by means of polymers: a liquid chromatographic study of the selectivity of resulting chiral stationary phases, *J. Chromatogr. B*, 768 (2002) 157.
75. R. Matsuda, S.H. Kye, J. Anguizola, D.S. Hage, Studies of drug interactions with glycated human serum albumin by high-performance affinity chromatography, *Rev. Anal. Chem.*, 33 (2014) 79-94.
76. A.J. Jackson, J. Anguizola, E.L. Pfaunmiller, D.S. Hage, Use of entrapment and high-performance affinity chromatography to compare the binding of drugs and site-specific probes with normal and glycated human serum albumin, *Anal. Bioanal. Chem.*, 405 (2013) 5833-5841.
77. A.J. Jackson, H. Xuan, D.S. Hage, Entrapment of proteins in glycogen-capped and hydrazide-activated supports, *Anal. Biochem.*, 404 (2010) 106-108.

78. R. Bakry, W.M. Stoeckl, E.O. Hochleitner, G. Stecher, C.W. Huck, G.K. Bonn, Silica particles encapsulated poly(styrene-divinylbenzene) monolithic stationary phases for mu-high performance liquid chromatography, *J. Chromatogr. A*, 1132 (2006) 183-189.
79. B. Loun, D.S. Hage, Chiral separation mechanisms in protein-based HPLC columns.1. Thermodynamic studies of (R)-warfarin and (S)-warfarin binding to immobilized human serum albumin, *Anal. Chem.*, 66 (1994) 3814-3822.
80. H.S. Kim, Y.S. Kye, D.S. Hage, Development and evaluation of N-hydroxysuccinimide-activated silica for immobilizing human serum albumin in liquid chromatography columns, *J. Chromatogr. A*, 1049 (2004) 51-61.
81. H.S. Kim, D.S. Hage, Chromatographic analysis of carbamazepine binding to human serum albumin, *J. Chromatogr. B*, 816 (2005) 57-66.
82. H.S. Kim, R. Mallik, D.S. Hage, Chromatographic analysis of carbamazepine binding to human serum albumin - II. Comparison of the Schiff base and N-hydroxysuccinimide immobilization methods, *J. Chromatogr. B*, 837 (2006) 138-146.
83. R. Mallik, M.J. Yoo, C.J. Briscoe, D.S. Hage, Analysis of drug-protein binding by ultrafast affinity chromatography using immobilized human serum albumin, *J. Chromatogr. A*, 1217 (2010) 2796-2803.
84. H.S. Kim, I.W. Wainer, Rapid analysis of the interactions between drugs and human serum albumin (HSA) using high-performance affinity chromatography (HPAC), *J. Chromatogr. B*, 870 (2008) 22-26.

85. D.J. Anderson, R.R. Walters, Equilibrium and rate constants of immobilized concanavalin A determined by high-performance affinity-chromatography, *J. Chromatogr.*, 376 (1986) 69-85.
86. D.J. Anderson, R.R. Walters, Affinity chromatographic examination of a retention model for macromolecules, *J. Chromatogr.*, 331 (1985) 1-10.
87. M.J. Yoo, J.E. Schiel, D.S. Hage, Evaluation of affinity microcolumns containing human serum albumin for rapid analysis of drug-protein binding, *J. Chromatogr. B*, 878 (2010) 1707-1713.
88. B. Loun, D.S. Hage, Characterization of thyroxine-albumin binding using high-performance affinity chromatography. 2. Comparison of the binding of thyroxine, triiodothyronines and related compounds at the warfarin and indole sites of human serum albumin, *J. Chromatogr. B*, 665 (1995) 303-314.
89. D.S. Hage, J. Chen, Quantitative affinity chromatography, in: D.S. Hage (Ed.) *Handbook of Affinity Chromatography*, 2nd ed., CRC Press, Boca Raton, FL, 2006, pp. 595-628.

CHAPTER 4.

RAPID ANALYSIS OF DRUG PROTEIN BINDING BASED ON COLUMNS PREPARED BY ENTRAPMENT

4.1. INTRODUCTION

It is important to know the activity and fate of pharmaceutical agents in the body. When a drug enters the circulatory system, it may undergo interactions with proteins that are found in blood, such as human serum albumin (HSA), α_1 -acid glycoprotein (AGP) and lipoproteins. These interactions can be described by using a parameter such as the association equilibrium constant (K_a) of the drug-protein complex. These drug-protein interactions are often strong and significant, with approximately 43% of the 1500 most common drugs having at least 90% binding to serum proteins. As a result, these interactions can have a large impact on the absorption, distribution, metabolism and excretion (ADME) of a drug in the human body [1].

Because of the potential impact of these interactions, it is important to conduct drug-protein binding studies on pharmaceutical agents to help determine their dosages and the frequency at which these drugs should be taken [2]. Binding studies that are conducted *in vitro* may give general information for a particular drug and its interactions, while *in vivo* studies can potentially provide specific information that is more tailored to an individual patient's needs, as can be used for personalized medicine [3].

Human serum albumin (HSA) is a transport protein in the circulatory system that can bind to many endogenous and exogenous compounds. HSA is the most abundant

protein in human plasma, where it is found at concentrations ranging from 30–50 g/L (0.53–0.75 mM). The high concentration of HSA accounts for approximately 60% of the total protein content in serum and gives this protein the ability to greatly influence the pharmacokinetics and activity of many common drugs [4–6]. HSA plays a key role in the reversible binding and transport of drugs, metabolites, and various endogenous ligands such as fatty acids. In addition, HSA can increase the solubility of lipophilic drugs, sequester toxins, and act as an important antioxidant in plasma [7,8].

There are two major binding sites for drugs on HSA, which are located in subdomains IIA and IIIA of this protein. These sites are often referred to as Sudlow sites I and II after Gillian Sudlow, who proposed their existence in 1975 [9,10]. Sudlow site I, which is also known as the warfarin-azapropazone site, binds to bulky heterocyclic anions such as warfarin and salicylate. Sudlow site II, or the indole-benzodiazepine site, binds primarily to aromatic carboxylic acids like ibuprofen and L-tryptophan. At least two minor binding sites for drugs HSA have also been proposed for compounds such as digitoxin and tamoxifen (i.e., the digitoxin site and tamoxifen site) [11,12].

Diabetes is a metabolic disease that can be described as a group of disorders that result from insulin deficiency and/or insulin resistance. Insulin is a hormone produced in the beta cells of the islets of Langerhans of the pancreas and is responsible for the regulation of glucose in the circulation. The presence of either insulin deficiency or insulin resistance in diabetes produces abnormally high levels of glucose in blood and results in a condition known as hyperglycemia [13,14]. Diabetes is a major cause of morbidity and mortality, and its global prevalence is growing rapidly [15]. The number of people worldwide who have diabetes is estimated to be around 366 million, and this figure is projected to rise to

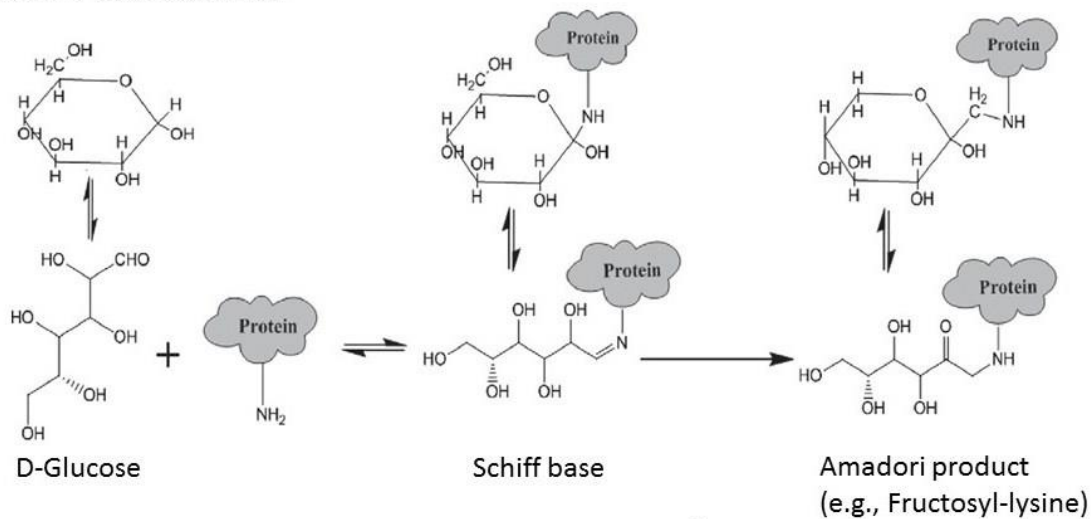
552 million by 2030. In the United States, it is estimated that 26 million people now live with this disease [3,16]. The high blood glucose concentrations that are seen in diabetes can lead to a number of detrimental health effects, ranging from an increased risk of heart disease and stroke to kidney disease, blindness, and lower limb amputations [13].

There are two types of diabetes: type 1 diabetes, which is also known as immune-mediated, insulin-dependent or juvenile-onset diabetes; and type 2 diabetes, which is also called non-insulin dependent or adult-onset diabetes. In type 1 diabetes, the body's immune system attacks the pancreatic beta cells that produce insulin. Type 2 diabetes is caused by an inadequate cellular response to insulin in organs or tissue (e.g., adipose cells). This later type of diabetes is the most common, accounting for 90 to 95% of the individuals with this disease, and is strongly related to obesity, age, and a family history of this disease [3,16].

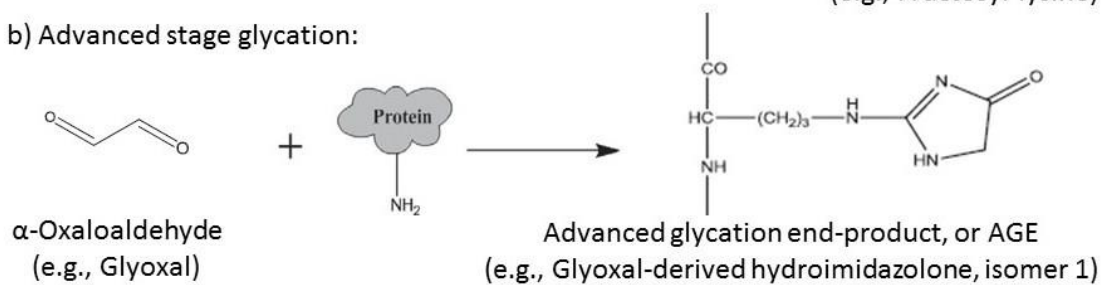
Many of the long term complications of diabetes, such as heart disease and nerve damage, are associated with the non-enzymatic glycation of proteins that occurs in the presence of sustained high levels of glucose in blood [14,17]. The process of protein glycation is shown in Figure 4.1. Glycation starts when a reducing sugar such as glucose undergoes a nucleophilic attack onto a primary amine group on a protein to form a reversible Schiff base. This intermediate can then slowly rearrange to form a more stable Amadori product [14,17,18]. Oxidation and rearrangement of the Amadori products or free sugars can also generate reactive α -oxoaldehydes that react with both lysines and arginines on proteins to form advanced glycation end-products (AGEs) [14,18].

Figure 4.1 General reactions involved in the glycation of a protein such as human serum albumin (HSA). This figure is adapted with permission from Ref. [14].

a) Early stage glycation:



b) Advanced stage glycation:



In recent years, it has been found that the glycation of HSA may affect its binding to solutes such as many drugs. Sulfonylureas, which are often used to treat type 2 diabetes, are one group of drugs that have been found to be affected by this glycation process. These drugs are highly bound to serum proteins, and especially to HSA [14,19-24]. Binding studies based on high-performance affinity chromatography (HPAC) have found that glycation can affect the equilibrium constants of sulfonylurea drugs with HSA and that the extent of this change is affected by both the degree of protein glycation and the specific drug that is being examined [3,14,19-23,25].

This chapter deals with the application of a new and rapid approach for performing drug-protein binding studies by using preparations of entrapped proteins and zonal elution experiments. The use of columns that contained entrapped proteins should allow the determination of binding constants from simple retention measurements because the immobilized protein in such a column remains in a soluble state and is fully active. This feature should allow for a simplification in the measurements that are needed for determining binding constants through chromatographic methods, because there is no need to perform additional independent experiments to obtain the amount of active ligand that is present in the column [19].

This technique will be tested and applied to studying the effects of glycation on HSA with regards to the binding of this protein with three sulfonylurea drugs: acetohexamide, tolbutamide and gliclazide. The results will be used to see how HPAC and columns made by entrapment can be used to study the effects of glycation on drug-protein binding and to determine the binding constants of a drug with a protein through a simple set of experiments and series of sample injections.

4.2. EXPERIMENTAL SECTION

4.2.1. Materials

The HSA (essentially fatty acid free, purity $\geq 96\%$), glycogen (bovine liver, type IX; total glucose $\geq 85\%$, dry basis), racemic warfarin (purity $\geq 98\%$), *R*-warfarin (purity $\geq 97\%$), L-tryptophan (purity $\geq 98\%$) and periodic acid reagent (H_5IO_6 , purity 99%) were purchased from Sigma-Aldrich (St. Louis, MO, USA). Nucleosil Si-300 silica (7 μm particle diameter, 300 \AA pore size, 100 m^2/g surface area) was obtained from Macherey-Nagel (Düren, Germany). The *in vitro* samples of glycated HSA were purified through the use of Econo-Pac 10DG desalting columns from Bio-Rad Laboratories (Hercules, CA, USA) and Slide-A-Lyzer digest 7K dialysis cassettes (7 kDa MW cutoff; 0.5-3, 3-12 or 12-30 mL sample volumes) from ThermoScientific (Rockford, IL, USA). All other chemicals were of the purest grades available. All buffers and aqueous solutions were prepared using water from a Milli-Q Advantage 10 system (EMD Millipore Corporation, Billerica, MA, USA). The buffers were filtered through 0.20 μm GNWP nylon membranes from Millipore (Billerica, MA, USA) and were degassed by sonication under vacuum for at least 20 min prior to use. A fructosamine assay kit, obtained from Diazyme Laboratories (San Diego, CA, USA), was used to measure the glycation levels of the *in vitro* glycated HSA.

4.2.2. Apparatus

The chromatographic system that was used in the zonal elution studies consisted of a DG-2080 degasser, two PU-2080 pumps, an AS-2057 autosampler, a CO-2060 column oven, and a UV-2075 absorbance detector from Jasco (Tokyo, Japan), plus a Rheodyne

LabPro six-port valve (Cotati, CA, USA). LC Net and ChromNav from Jasco (Tokyo, Japan) were used to control the chromatographic system and to collect the data.

For the frontal analysis studies, two 1200 isocratic pumps and a 1200 autosampler from Agilent (Santa Clara, CA, USA) were used, along with a Series 200 UV-Vis detector and a vacuum degasser from Perkin Elmer (Waltham, MA, USA). A Rheodyne LabPro valve and an Isotemp 9100 circulating water bath (Fisher Scientific, Pittsburgh, PA, USA) with a water jacket from Alltech (Deerfield, IL, USA) were used for temperature control of the columns. The chromatographic data in this case were collected and processed using LabView 8 software (National Instruments, Austin, TX, USA).

The results for the zonal elution and frontal analysis experiments were analyzed by using PeakFit 4.12 (Systat Software, San Jose, CA, USA). Regression analysis of the frontal analysis data was performed with Origin 2015 (OriginLab, Northampton, MA, USA). The calculation of retention factors and binding constants was performed with Microsoft Excel 2013 (Microsoft, Redmond, WA, USA).

A Pack-in-a-Box system (ChromTech, Apple Valley, MN, USA) was used for packing the supports into the columns. Two PHD Ultra syringe pumps (Harvard Apparatus, Holliston, MA, USA) were used for the on-column entrapment method. A Jasco V-630 UV/VIS spectrophotometer (Jasco, Kyoto, Japan) equipped with temperature control for the cuvette holder was used for taking absorbance readings during the fructosamine assay.

4.2.3. Preparation of *in vitro* glycated HSA

Three samples of *in vitro* glycated HSA were prepared at physiological concentrations of HSA and glucose, as described previously [26-28]. These samples were representative of glycation levels that are found in patients with prediabetes, confirmed diabetes, and advanced diabetes, and will be referred to in this chapter as “gHSA1”, “gHSA2” and “gHSA3”, respectively. To prevent bacterial growth during the glycation process, all materials (e.g., glassware and spatulas) were first sterilized in an autoclave. A pH 7.4, 0.20 M potassium phosphate buffer containing 1 mM sodium azide was prepared for use in this procedure. This buffer was also sterilized in an autoclave to prevent bacterial growth.

The *in vitro* glycated HSA was prepared by dissolving 840 mg of normal HSA into a solution that contained 5 mM, 15 mM or 30 mM glucose (i.e., for the preparation of gHSA1, gHSA2 or gHSA3, respectively) in sterile pH 7.4, 0.20 M phosphate buffer. The final concentration of HSA in these solutions was 42 mg/mL, or 0.63 mM. This concentration of HSA was within the typical range (35–50 g/L) that is found in human serum under normal physiological conditions. These protein/glucose mixtures were incubated for five weeks at 37 °C to produce glycated HSA. The proteins in these samples were later purified through the use of size exclusion columns and pH 7.4, 0.067 M potassium phosphate buffer to remove the excess glucose. The collected protein fractions were further dialyzed three times, using sterile dialysis cassettes and against a volume of water that was 200-500 times the volume of the protein solution [26]. The final protein solutions were lyophilized and stored at -80 °C until further use.

Portions of the *in vitro* glycated HSA samples were analyzed in triplicate by using a fructosamine assay to determine their glycation levels, as described previously [26,29,30]. The measured glycation levels were 0.27 (\pm 0.01), 2.01 (\pm 0.05) and 4.13 (\pm 0.08) mol hexose/mol HSA for gHSA1, gHSA2 and gHSA3, respectively. These levels of glycation were comparable to those obtained in prior studies that used a similar approach to prepare *in vitro* glycated HSA [26,30].

4.2.4. Support preparation

Diol-bonded silica was prepared from Nucleosil 300-7 silica, as described previously, followed by the drying of this support and its storage for future use. Hydrazide-activated silica was prepared from the diol-bonded silica also according to a procedure that has been described in the literature [31]. The support size of 7 μ m and the pore size of 300 Å that were chosen for these supports have previously been found to be optimal for the entrapment of HSA and proteins with comparable sizes [32].

An amount of hydrazide-activated silica that was equivalent to an initial amount of 50 mg of diol-bonded silica was washed with pH 7.4, 0.067 M potassium phosphate buffer and downward slurry packed into 1.0 cm \times 2.1 mm stainless steel columns by using pH 7.4, 0.067 M potassium phosphate buffer as the packing solution, as indicated in Section 3.2.3 of this dissertation. The columns that were packed with the hydrazide-activated silica were used for the on-column entrapment of normal HSA or HSA with various levels of glycation.

The conditions used for on-column entrapment were the same as the final conditions of on-column entrapment that were described in Section 3.3.1 of this

dissertation. A solution containing 50 mg/mL of the normal HSA or glycated HSA in pH 5.0, 0.10 M potassium phosphate buffer was circulated through the column at 20 μ L/min for 4 h. This was followed by the application of a solution over 16 h that contained a mixture of the normal HSA or glycated HSA at 50 mg/mL and oxidized glycogen at 4.2 mg/mL in the same phosphate buffer. Finally, 200 μ L of 1 mg/mL of oxalic dihydrazide in the same buffer was added to the reaction mixture, and the circulation of this solution through the column was continued for two more hours. A control column was made under the same conditions but with the solutions of HSA being replaced with an equal volume of pH 5.0, 0.10 M potassium phosphate buffer. All of the columns were washed by flowing pH 7.4, 0.067 M potassium phosphate buffer through them at 0.5 mL/min for 1 h or until a stable baseline response was reached for these columns.

4.2.5. Chromatographic studies

Stock solutions of the sulfonylurea drugs (i.e., acetohexamide, tolbutamide and gliclazide) were prepared in pH 7.4, 0.067 M potassium phosphate buffer at a typical concentration of 100 μ M. The stock solutions of the site-specific probes were also prepared in this buffer and had typical concentrations of 100 μ M for warfarin and 1.3 mM for L-tryptophan. The acetohexamide, tolbutamide and gliclazide solutions were used within one week of preparation. The warfarin solutions were used within one week, and L-tryptophan solutions were used within two days of preparation. It has been demonstrated in previous studies that similar solutions of these drugs and solutes are stable over for these given periods of time.

The mobile phases that were used in the competition studies with the site-specific probes were prepared at concentrations that were typically 1 mM for L-tryptophan and 40

μM for warfarin, as made by diluting the stock solutions for these probes with pH 7.4, 0.067 M potassium phosphate buffer. The injected samples for these experiments were prepared by using the stock solutions for the sulfonyleurea drugs, warfarin or L-tryptophan and the pH 7.4, 0.067 M potassium phosphate buffer. The concentrations of the sulfonyleurea drugs ranged from 20 μM to 40 μM . Additional experiments were performed by using 10 μM L-tryptophan or 20 μM warfarin in the same pH 7.4 buffer, as used for determining the retention factors and protein content of the normal HSA and glycated HSA columns. It has been shown in previous work that the sample concentrations that were used in this study provide linear elution conditions for the given drugs on HSA columns. The chromatographic experiments were carried out at a typical flow rate of 0.50 mL/min and at a temperature of 37 °C. All of the injected solutions and mobile phases that were used in the experiments were passed through 0.2 μm filters and degassed for 10-15 min prior to use.

In the frontal analysis experiments with warfarin and L-tryptophan, the columns were first equilibrated with pH 7.4, 0.067 M potassium phosphate buffer. Using a six-port valve, a switch was made from this pH 7.4 buffer to a solution containing a known concentration of the desired probe compound in the same buffer. After a breakthrough curve had been formed and a stable plateau had been reached, a switch was made back to pH 7.4, 0.067 M potassium phosphate buffer to elute the retained drug or solute. These frontal analysis experiments were carried out by using seven solutions that contained 1-40 μM warfarin, with the elution of warfarin being monitored at 307 nm, and seven solutions containing 1-1000 μM of L-tryptophan, with elution of L-tryptophan being monitored at 280 nm. All these experiments were performed in triplicate or quadruplicate. The

midpoint of each breakthrough curve was determined with Peak Fit 4.12 by using the centroid of the first derivative for the curve, following smoothing by the Savitsky-Golay method [33]. A correction for the system void time and for non-specific binding was made by subtracting the results for the control column from the results that were obtained on each entrapped protein column, using an approach described in previous studies [20,22].

4.3. THEORY

4.3.1. Zonal elution

The global affinity of a target compound for a binding agent with several independent sites (e.g., as often occurs for the binding of drugs with HSA) can be described as the addition of the affinities for all the sites on the binding agent. For a column that is made by entrapment, essentially all the binding agent will be active and the overall retention factor (k) of a drug or solute due to binding at these sites can be described by the relationship in Equation 4.1 [19],

$$k = (n_1K_{a1} + n_2K_{a2} + \dots + n_nK_{an})m_{Ltot}/V_m \quad (4.1)$$

where n_i is the relative moles of binding site i for a given drug or solute per mole of protein, K_{ai} is the association equilibrium constant for the same site and drug/solute, m_{Ltot} is the total moles of all binding sites for the solute in the column, and V_m is the column void volume. The global affinity in this equation is the term in parentheses and can also be represented by the sum of these terms, nK_a' . This is a number-weighted sum of the equilibrium constants for all the binding sites for the drug or solute on the immobilized binding agent [19].

When a probe interacts with a single type of site on an entrapped binding agent, Equation 4.1 can be reduced to the following expression,

$$k = K_a \frac{m_{Ltot}}{V_m} \quad (4.2)$$

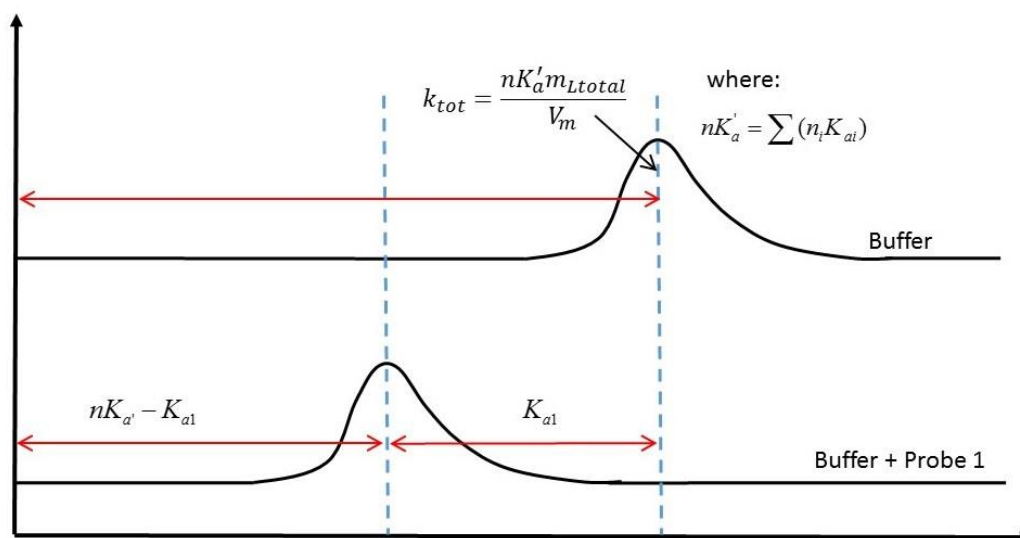
where K_a is the association equilibrium constant for the probe with the specific binding site [19].

Equations 4.1 and 4.2 indicate that the measured retention factor for a solute on a column that contains an entrapped binding agent can allow a direct determination of the global binding constant or site-specific binding constant for this solute. This can be accomplished by using experiments like those shown in Figure 4.2. First, an injection of a drug or solute that is dissolved in the buffer alone can be made onto a column containing the entrapped binding agent, making it possible to determine the total retention factor, k_{tot} . This parameter, along with a previous measurement of the column void volume and m_{Ltot} , makes it possible to obtain the global affinity, as is shown in the following reduced form of Equation 4.1 [19],

$$k_{tot} = \frac{nK'_a m_{Ltot}}{V_m} \quad (4.3)$$

where $nK'_a = \sum(n_i K_{ai})$.

Figure 4.2 Use of zonal elution experiments for estimating the global affinity (nK_a') or site-selective affinity (K_{a1}) for a solute on a column that contains an entrapped protein or binding agent. Other terms in this figure are described in the text.



The same drug or solute can then be injected in the presence of a mobile phase that contains a site-selective probe (e.g., warfarin for Sudlow site I or L-tryptophan for Sudlow site II of HSA). The agent added to the mobile phase is present at a level that saturates a known fraction of the given site in the column. During this second injection, the retention for the solute will be lower because the probe in the mobile phase is binding to one of the sites on the entrapped agent. The shift in retention can make it possible to find the association equilibrium constant for this specific binding site (K_{a1}), as is indicated in Equation 4.4.

$$k = \frac{(nK'_a - K_{a1})m_{Ltot}}{V_m} \quad (4.4)$$

The value of m_{Ltot} in Equations 4.3 and 4.4 can be obtained through independent frontal analysis measurements or by making a retention factor measurement with a probe that has a known value for its association equilibrium constant with the same binding agent. Repeating the experiment in Figure 4.2 with probes for other binding sites should make it possible to also find the solute's affinity for each of the other binding regions [19].

The following equations are used to obtain the experimental values of the retention factors that are used to estimate the overall and site-specific affinities.

$$k_{tot} = \frac{t_{rt} - t_m}{t_m - t_v} \quad (4.5) \quad k = \frac{t_r - t_m}{t_m - t_v} \quad (4.6)$$

$$k_1 = k_{tot} - k = \frac{t_{rt} - t_r}{t_m - t_v} \quad (4.7)$$

where t_{rt} and t_r are the retention times for the injected solute in the presence of only buffer or the buffer plus the site-specific probe; and t_m and t_v are the void times of the column and the system (e.g., as obtained for a non-retained solute with or without a column being

placed in the system); and other terms are the same as defined previously. Substituting the relationship for k_1 that is given in Equation 4.7 and placing this into Equation 4.2 to solve for K_{a1} gives the following combined expression.

$$K_{a1} = \frac{k_1 V_m}{m_{Ltotal}} = \frac{(t_{rt}-t_r)}{(t_m-t_v)} \frac{V_m}{m_{Ltot}} \quad (4.8)$$

This equation shows how a site-specific binding constant for a drug with a binding agent can be obtained from retention time measurements that are performed on both a column that contains the entrapped binding agent and a control column.

The concentration of a site-specific probe (e.g., warfarin and L-tryptophan for HSA) that is needed in the mobile phase to obtain a given level of saturation for the entrapped binding agent can be found by using the following relationship,

$$\frac{k-k_{min}}{k_{max}-k_{min}} = \frac{1}{1+K_I [I]} \quad (4.9)$$

where I represents the probe, K_I is the association equilibrium constant for this probe at its binding site, and $[I]$ is the concentration of the probe in the mobile phase [33]. The terms k , k_{min} and k_{max} are the retention factor that should result for the injected solute at a given concentration of the probe, the minimum possible retention factor for this solute (i.e., when all the given binding sites are saturated), and the maximum possible retention factor for the solute (i.e., when all these sites are available for binding).

The ratio on the left of Equation 4.9 represents the relative retention that is observed for the solute in the presence of the competing agent. This ratio is also related to the fraction of binding sites that are available to interact with the solute. When the value of $[I]$ is 0, the value of k will be equal to k_{max} and the ratio on the left of Equation 4.9 will be equal to 1.0 (or 0% site saturation). As the value of $[I]$ approaches infinity, the value of k

approaches k_{min} and the fraction on the left of Equation 4.9 approaches 0 (or 100% site saturation) [33]. It is also possible to use intermediate concentrations of the competing agent to produce a given shift in retention. For instance, the concentration of the competing agent that is needed to reach 90% saturation at the given site on the binding agent can be found by setting the left side of Equation 4.9 equal to 0.1 and using the remaining terms to find the value of $[I]$ that is needed to obtain this condition.

4.3.2. Frontal analysis

For a column with a single type of binding site for an analyte (A), Equation 4.10 describes the relationship between the apparent moles of the applied analyte (m_{Lapp}) that are required to reach the mean position of the breakthrough curve [33].

$$m_{Lapp} = \frac{m_{Ltot}K_a[A]}{(1+K_a[A])} \quad (4.10)$$

In this equation, m_{Ltot} is the total moles of active binding sites for the analyte in the column, and K_a is the association equilibrium constant for the analyte at these binding sites. This equation can be rearranged into the following form, which is useful for obtaining the moles of active binding sites through the use of a double-reciprocal plot of $1/m_{Lapp}$ vs $1/[A]$.

$$\frac{1}{m_{Lapp}} = \frac{1}{K_a m_{Ltot}[A]} + \frac{1}{m_{Ltot}} \quad (4.11)$$

The frontal analysis experiments involve applying analyte solutions of various concentrations to the entrapped protein columns, and measuring the values of m_{Lapp} that were needed to reach the central point of each breakthrough curve. Then, using equation 4.11, it is possible to find the total moles of binding sites for A in the column, m_{Ltot} . The

value of the association equilibrium constant K_a can be obtained from the same plot, by using the ratio of the intercept over the slope for the best-fit line [33].

The range of analyte concentrations to be used in a frontal analysis experiment in order to cover the range of signal variation, is calculated by employing a modified version of Equation 4.10 [33],

$$\frac{m_{Lapp}}{m_{Ltot}} = \frac{K_a[A]}{(1+K_a[A])} \quad (4.12)$$

where all the terms are the same as defined earlier. The left side of this equation is the fraction of the binding sites in the column that are bound to the analyte at a given concentration. The fraction is equal to zero when no analyte is applied, and approaches one when the analyte concentration goes to infinity. For achieving measurable shifts in the central point of the breakthrough curve, it is advisable to choose concentrations for A that will produce a degree of saturation for the column that is between 10% and 90%, or conditions that will give a value for the ratio on the left-hand side of Equation 4.12 that is between 0.10 and 0.90 [33].

4.4. RESULTS AND DISCUSSION

4.4.1. Estimation of the amount of an entrapped protein in a column

The amount of HSA that was entrapped in a column was determined by using both frontal analysis and zonal elution experiments with warfarin and L-tryptophan. The frontal analysis experiments were carried out by using a 1.0 cm \times 2.1 mm i.d. column that contained the entrapped HSA. The application of either warfarin or L-tryptophan to this column gave frontal analysis results that provided a good fit to Equation 4.11 and a single-

site binding model. Figure 4.3 shows some examples of breakthrough curves that were obtained in the frontal analysis experiments with L-tryptophan. Figures 4.4 and 4.5 show the double-reciprocal plots that were obtained for warfarin and L-tryptophan, respectively, when their data were analyzed according to Equation 4.11. The concentrations of the analyte solutions that were used in these frontal analysis experiments were selected to provide between 10% and 90% saturation of the total binding sites, as calculated by using Equation 4.12.

The total moles of protein were also estimated by using zonal elution experiments that were carried out with the same column and using the same analyte or probes as were used in the frontal analysis experiments. The values for the moles of entrapped protein that were obtained by both of these methods are provided in Table 4.1. There was good agreement between the two methods, with no significant difference being present at the 95% confidence level. This indicated that it was possible to measure the total moles of binding sites and protein by either method, with the zonal elution technique being preferred in later studies because it required much less time and reagents than the frontal analysis experiments.

The value of K_a that was obtained from the double-reciprocal plot for warfarin was $2.6 (\pm 0.3) \times 10^5 \text{ M}^{-1}$, which was in good agreement with an average value of $2.4 (\pm 0.4) \times 10^5 \text{ M}^{-1}$ that has been previously determined for the R- and S-enantiomers of warfarin with HSA. The value of K_a that was obtained from the double-reciprocal plot for L-tryptophan was $0.93 (\pm 0.23) \times 10^4 \text{ M}^{-1}$, which was also in good agreement with a value of $1.1 (\pm 0.3) \times 10^4 \text{ M}^{-1}$ that has been reported in previous studies with HSA [26,33].

Figure 4.3 Frontal analysis experiments conducted with L-tryptophan being applied to a 1.0 cm × 2.1 mm i.d. column that contained entrapped HSA. The temperature of this column was 37 °C and the flow rate was 0.5 mL/min.

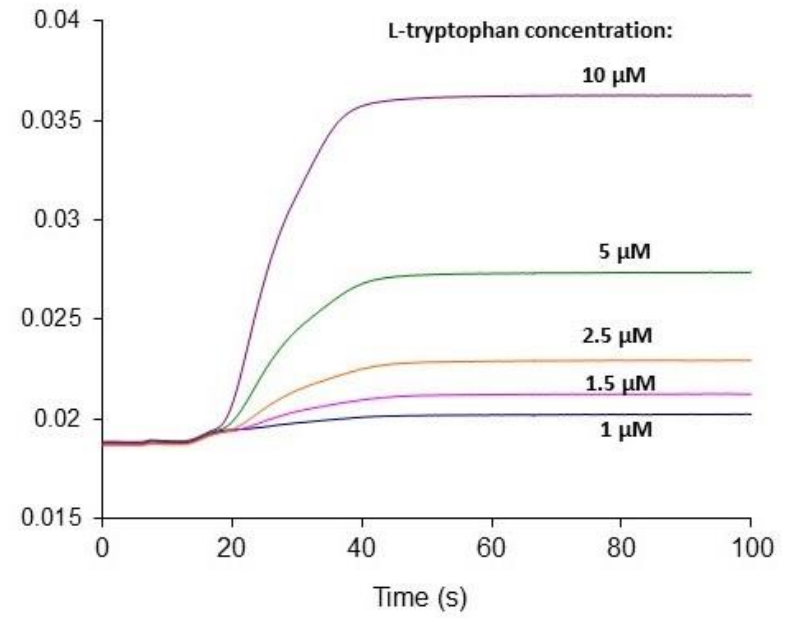
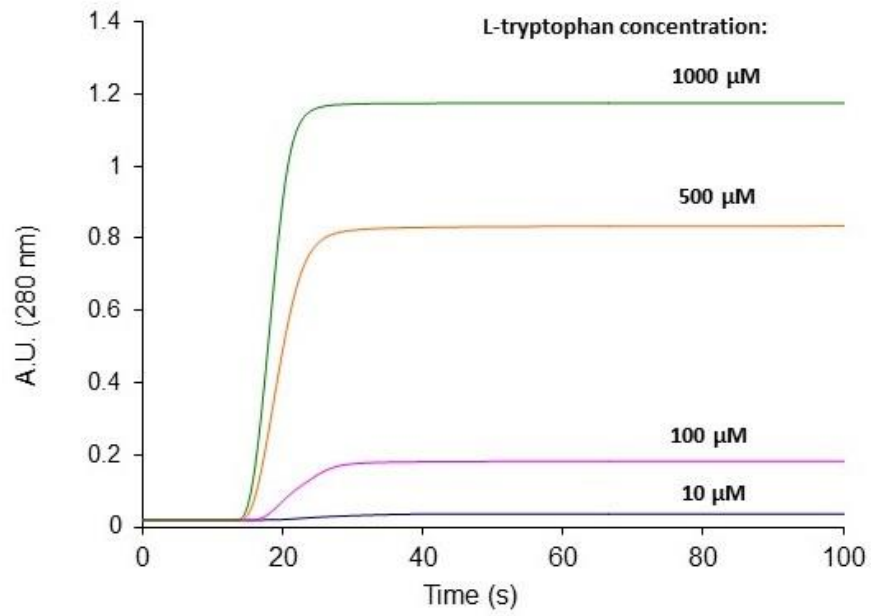


Figure 4.4 Double-reciprocal plot obtained for frontal analysis studies with warfarin on a $1.0 \text{ cm} \times 2.1 \text{ mm}$ i.d. column containing entrapped HSA, as measured at 37°C and 0.5 mL/min . The best-fit line was obtained by applying Equation 4.11 to these data. The inset shows the residual plot for the distribution of the data about the best-fit line.

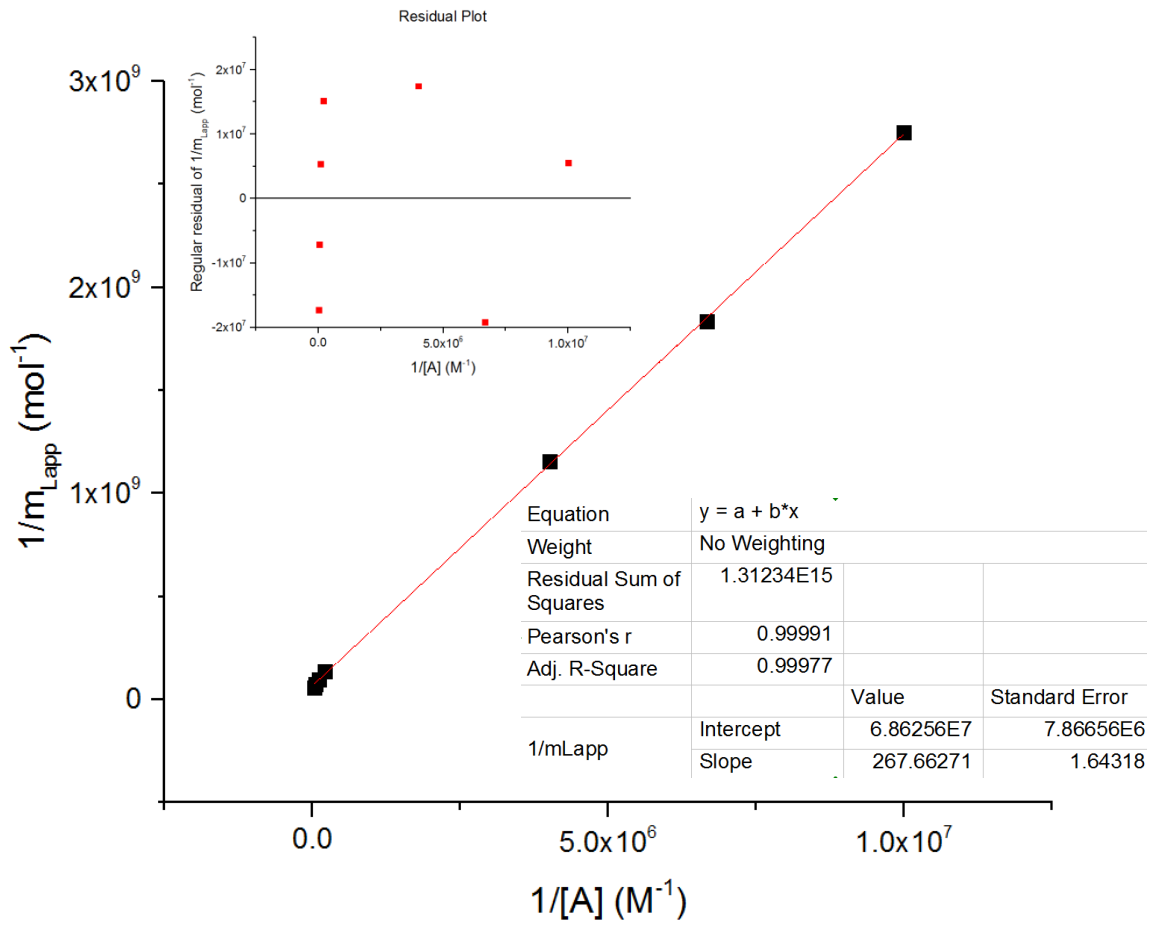


Figure 4.5 Double-reciprocal plot obtained for frontal analysis studies with L-tryptophan on a 1.0 cm × 2.1 mm i.d. column containing entrapped HSA, as measured at 37 °C and 0.5 mL/min. The best-fit line was obtained by applying Equation 4.11 to these data. The inset shows the residual plot for the distribution of the data about the best-fit line.

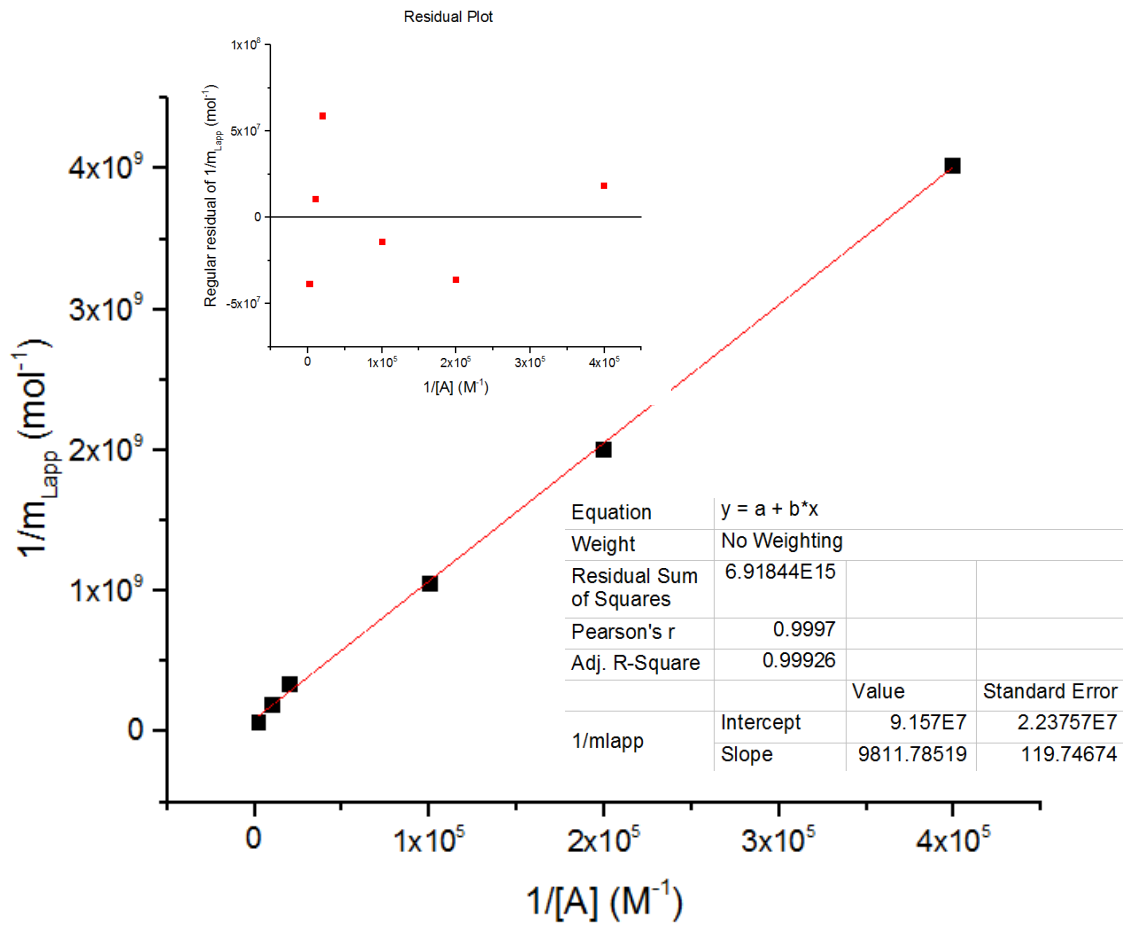


Table 4.1. Estimates of the amount of entrapped normal HSA, as determined by zonal elution and frontal analysis

Probe or analyte	Column void volume, V_m ($L \times 10^{-5}$)	Moles of entrapped protein ¹ ($\text{mol} \times 10^{-8}$)	
		Zonal elution	Frontal analysis
Warfarin	3.35 (± 0.07)	1.83 (± 0.31)	1.46 (± 0.17)
L-Tryptophan		1.26 (± 0.35)	1.09 (± 0.27)

¹These values were measured at 37 °C in pH 7.4, 0.067 M phosphate buffer. The values in parentheses represent a range of ± 1 S.D.

4.4.2. Estimation of global affinity constant and site-specific binding constants for acetohexamide with entrapped normal HSA

Once the total moles of entrapped normal HSA had been determined, the global affinity constant for acetohexamide with the entrapped HSA was determined by making injections of acetohexamide on both the entrapped HSA column and a control column. A second set of injections were then made for acetohexamide in the presence of a site-selective probe for HSA (e.g., warfarin for Sudlow site I or L-tryptophan for Sudlow site II) to determine the binding constants of acetohexamide at specific sites on HSA.

Equation 4.9 was used to determine the concentrations of the site-specific probes that were needed in these experiments to achieve near complete saturation of the binding sites. This was done by setting the left side of Equation 4.9 equal to a relative retention of 0.05 (representing 95% site saturation) for calculating the concentration that would produce a 95% shift in retention from its maximum possible value. The known association equilibrium constants for HSA with warfarin and L-tryptophan (i.e., the probes that were used as site-selective additives in this work) were also used in these calculations. The conditions needed for 95% site saturation were estimated to occur when the mobile phase contained 79 μM warfarin or 1.7 mM L-tryptophan. Experiments that were also done at 90% site saturation, which corresponded to the use of 40 μM warfarin or 850 μM L-tryptophan in the mobile phase.

Table 4.2 shows the association equilibrium constants that were measured by zonal elution for acetohexamide in the presence of various amounts of the mobile phase additives.

Table 4.2. Site-specific association equilibrium constants measured for acetohexamide in zonal elution experiments and using various concentrations of site-selective probes in the mobile phase

Probe ¹	Mobile phase concentration	Site-specific association equilibrium constant, K_a ($M^{-1} \times 10^4$) ²	
		Sudlow site I	Sudlow site II
Warfarin/L-tryptophan	101.6 μ M/1.7 mM	10.9 (\pm 1.9)	6.9 (\pm 2.0)
Warfarin/L-tryptophan	40 μ M/850 μ M	9.9 (\pm 0.18)	6.8 (\pm 2.0)
Warfarin (racemate)	40 μ M	8.3 (\pm 1.4)	N.A.
R-Warfarin	40 μ M	8.9 (\pm 0.9)	N.A.

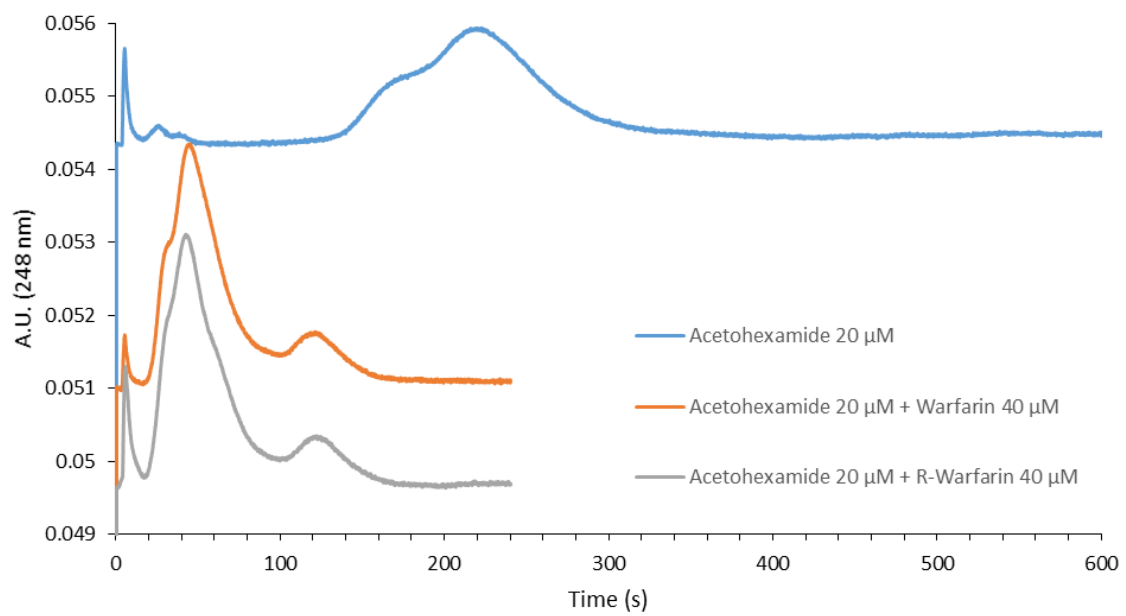
¹Warfarin was used as a probe for measuring the binding constant for Sudlow site I and L-tryptophan was used for Sudlow site II. These probes were used in separate sample solutions for each experiment. Physiological conditions were also used in these measurements (i.e., pH 7.4, 0.067 M potassium phosphate buffer and a column temperature of 37 °C).

²The values in parentheses represent a range of \pm 1 S.D.

One observation made was that there was no significant difference at the 95% confidence level in the association equilibrium constants that were obtained when using mobile phase additives that corresponded to 95% or 90% site saturation. Given the fact that lower concentrations of these additives also resulted in a decrease in reagent costs and a lower background signal for the detector, mobile phase concentrations of 40 μM warfarin or 1000 μM L-tryptophan were selected for use in all subsequent zonal elution studies. The global affinity constant that was obtained in these experiments and from the retention factor for acetohexamide was $1.96 (\pm 0.33) \times 10^5 \text{ M}^{-1}$, which was in good agreement with values of $1.2\text{-}2.0 \times 10^5 \text{ M}^{-1}$ that have been previously obtained for this drug with HSA [19-21].

The impact of using racemic warfarin versus a single warfarin enantiomer as a mobile phase additive for probing Sudlow site I was also considered in this study. Examples of some chromatograms that were obtained in these experiments are shown in Figure 4.6 and the results are included in Table 4.2. The association equilibrium constants that were obtained for acetohexamide at Sudlow site I when using either type of probe were statistically equivalent at the 95% confidence level. From this result, it was decided that racemic warfarin would be used as the probe for Sudlow site I in all later experiments with other sulfonylurea drugs.

Figure 4.6 Chromatograms obtained for the injection of acetohexamide onto a column containing entrapped HSA and in the absence or presence of *R*-warfarin or racemic warfarin in the mobile phase.



4.4.3. Estimation of global affinity constants and site-specific binding constants for sulfonylurea drugs with entrapped samples of normal or glycated HSA

The use of on-column entrapment and zonal elution was next used to examine the global affinities and site-specific binding constants for various sulfonylurea drugs with either normal HSA or glycated HSA. As was demonstrated previously, the total moles of HSA in such a column could be obtained from retention measurements that were made using a well-characterized probe for such a protein. For these experiments, warfarin was selected as the probe for measuring m_{Tot} because this solute has been shown in previous studies to have no significant change in its affinity in the presence of low-to-moderate levels of glycation for HSA [19,26].

In this section, injections of racemic warfarin were first made onto columns containing entrapped samples of normal HSA or glycated HSA, and onto a control column, to provide an estimate of the total protein content of each column. The same columns were then used for the injection of samples that contained the sulfonylurea drugs acetohexamide, tolbutamide or gliclazide. These injections were initially made in the presence of only buffer to obtain the global affinity constants for each drug with normal HSA or the samples of glycated HSA. The same drugs were then injected in the presence of a mobile phase that contained a site-selective probe for HSA. To examine the binding of these drugs at Sudlow site I, 40 μM warfarin was added to the mobile phase. To examine the binding of these drugs at Sudlow site II, 1000 μM L-tryptophan was added. The differences in the retention times that were seen for each drug in the presence of only buffer or in the presence of a known concentration of a site-specific probe were then used to calculate the site-specific association equilibrium constants for each drug at Sudlow sites I and II. The global

affinity constants and site-specific association equilibrium constants that were measured for these drugs at Sudlow sites I and II are summarized in Tables 4.3 through 4.5.

Table 4.3 shows the global affinity constants that were measured for the sulfonylurea drugs with normal HSA or HSA with three levels of glycation: gHSA1, which had a modification level that was typical of that seen in prediabetes; gHSA2, which had a modification level corresponding to controlled diabetes; and gHSA3, which corresponded to advanced/uncontrolled diabetes. For all sulfonylurea drugs, there was an increase in the global affinity constant when going from normal HSA to gHSA1 and a further increase when going to gHSA2. However, the global affinity constant decreased when going to gHSA3. The highest increase that was observed was 1.3-fold, as noted for acetohexamide and gliclazide with the gHSA2 sample. However, none of these apparent differences were statistically significant when the standard deviations (in parentheses) were considered. The global affinity constants for these drugs with normal HSA were in good agreement with those reported in previous studies: $16 (\pm 1) \times 10^4$ for acetohexamide, $10 (\pm 1) \times 10^4$ for tolbutamide, and $5.8 (\pm 0.2) \times 10^4$ for gliclazide [14,19,22,24].

Table 4.3. Global affinity constants obtained for various sulfonylurea drugs with columns containing entrapped samples of normal HSA or HSA with various levels of glycation

Drug	Global affinity constant ($M^{-1} \times 10^4$) and type of HSA ¹			
	Normal HSA	gHSA1	gHSA2	gHSA3
Acetohexamide	18.7 (\pm 3.4)	20.9 (\pm 3.9)	25.5 (\pm 4.7)	22.8 (\pm 4.4)
Tolbutamide	9.9 (\pm 1.8)	11.2 (\pm 2.1)	13.5 (\pm 2.5)	12.6 (\pm 2.4)
Gliclazide	4.2 (\pm 0.8)	5.0 (\pm 0.9)	6.3 (\pm 1.2)	5.9 (\pm 1.1)

¹These values were measured at 37 °C in pH 7.4, 0.067 M phosphate buffer. The values in parentheses represent a range of \pm 1 S.D.

Table 4.4. Association equilibrium affinity constants obtained at Sudlow site I for various sulfonylurea drugs with columns containing entrapped samples of normal HSA or HSA with various levels of glycation

Drug	Association equilibrium constant ($M^{-1} \times 10^4$) and type of HSA ¹			
	Normal HSA	gHSA1	gHSA2	gHSA3
Acetohexamide	10.6 (± 2.0)	10.9 (± 2.0)	13.4 (± 2.7)	11.3 (± 2.2)
Tolbutamide	6.7 (± 1.2)	7.2 (± 1.3)	7.9 (± 1.6)	7.0 (± 1.3)
Gliclazide	2.5 (± 0.5)	2.47 (± 0.5)	3.1 (± 0.6)	2.9 (± 0.5)

¹These values were corrected for the fact that only 90% site saturation was used. These results were measured at 37 °C in pH 7.4, 0.067 M potassium phosphate buffer. The values in parentheses represent a range of ± 1 S.D.

Table 4.5. Association equilibrium affinity constants obtained at Sudlow site II for various sulfonylurea drugs with columns containing entrapped samples of normal HSA or HSA with various levels of glycation.

Drug	Association equilibrium constant ($M^{-1} \times 10^4$) and type of HSA ¹			
	Normal HSA	gHSA1	gHSA2	gHSA3
Acetohexamide	6.4 (± 1.2)	6.7 (± 1.2)	9.9 (± 2.0)	7.9 (± 1.6)
Tolbutamide	5.2 (± 0.9)	3.3 (± 0.7)	4.5 (± 0.9)	5.0 (± 0.9)
Gliclazide	1.7 (± 0.3)	2.1 (± 0.4)	3.4 (± 0.7)	3.0 (± 0.6)

¹These values were corrected for the fact that only 90% site saturation was used. These results were measured at 37 °C in pH 7.4, 0.067 M potassium phosphate buffer. The values in parentheses represent a range of ± 1 S.D.

Tables 4.4 and 4.5 compare the sulfonylurea drugs in terms of their association equilibrium constants for the two main drug binding sites on HSA: Sudlow sites I and II. In general, an increase in these site-specific binding site constants was observed for the three drugs when going from normal HSA to gHSA2. The affinity then tended to decrease with further glycation, as was typical of uncontrolled diabetes (gHSA3). The binding constant for Sudlow site I increased by 1.3-fold for acetohexamide, 1.2-fold for tolbutamide and 1.3-fold for gliclazide for gHSA2 relative to normal HSA. The binding constant for Sudlow site II increased by 1.5-fold for acetohexamide and 2-fold for gliclazide for gHSA2 relative to normal HSA. No increase was observed in the binding constant at Sudlow site II for tolbutamide as a result of glycation.

The association equilibrium constants at Sudlow site I and II were also compared between the various drugs. For instance, the binding constant at Sudlow site I was higher than the value at Sudlow site II for acetohexamide in normal HSA as well as in all of the samples of glycated HSA. The same trend was true for tolbutamide. For gliclazide, there was no statistically significant difference between the values that were measured at Sudlow sites I and II.

4.5. CONCLUSIONS

In this study, a novel approach was developed and tested for measuring global affinity constants and site-specific binding constants for drug-protein interactions. This method made use of columns containing entrapped proteins. With these columns, it was possible to estimate drug-protein binding constants by using relatively simple retention measurements for a drug in the presence of only a buffer or in the presence of a probe for each specific binding site that was to be studied.

The system was applied to the sulfonylurea drugs acetohexamide, tolbutamide and gliclazide, which are known to bind tightly to HSA and to have interactions at both Sudlow sites I and II of this protein [14,19-24]. A sample of normal HSA and three samples of HSA with various levels of glycation were immobilized by on-column entrapment using the conditions that were optimized in Chapters 2 and 3 of this dissertation.

In order to calculate the binding constants for these drugs with normal HSA or glycated HSA, it was necessary to also have an estimate of the total moles of active protein that were in each column. This estimate was made by using both zonal elution and frontal analysis experiments with a probe compound (i.e., warfarin) that had known interactions with these proteins. It was found that the values obtained by zonal elution were statistically equivalent to those measured with the more time-consuming method of frontal analysis. Racemic warfarin was used for this type of measurement in the later work with the normal HSA and glycated HSA, because it has been shown in previous studies that the affinity of this drug for HSA is not affected significantly by the glycation of HSA at the modification levels that are normally seen in diabetes [19,26].

The global affinity constants for several sulfonylurea drugs were measured by this new approach. Good agreement was seen between these values and those that have been previously estimated for these drugs with HSA. It was also shown how site-specific association equilibrium constants for these drugs could be measured with either normal HSA or glycated HSA. Good agreement was seen between the global affinity constants that were found in this study and values that have been calculated previously for the same drugs with HSA.

The change in binding affinity of sulfonylurea drugs to HSA as a function of glycation has profound biological implications in terms of changes in efficacy and side-effects of the diabetes drugs. The rapid approach addressed in this chapter for studying protein-drug interactions by using entrapped proteins in HPAC columns can be applied for screening the binding of drugs with proteins isolated from serum of patients with some pathological condition in order to tailor the treatment to each individual.

REFERENCES

1. D.S. Hage, J.A. Anguizola, A.J. Jackson, R. Matsuda, E. Papastavros, E. Pfaunmiller, Z.H. Tong, J. Vargas-Badilla, M.J. Yoo, X.W. Zheng, Chromatographic analysis of drug interactions in the serum proteome, *Anal. Methods*, 3 (2011) 1449-1460.
2. L. Hood, J.R. Heath, M.E. Phelps, B.Y. Lin, Systems biology and new technologies enable predictive and preventative medicine, *Science*, 306 (2004) 640-643.
3. J. Anguizola, K.S. Joseph, O.S. Barnaby, R. Matsuda, G. Alvarado, W. Clarke, R.L. Cerny, D.S. Hage, Development of affinity microcolumns for drug-protein binding studies in personalized medicine: interactions of sulfonylurea drugs with in vivo glycosylated human serum albumin, *Anal. Chem.*, 85 (2013) 4453-4460.
4. G.A. Ascoli, E. Domenici, C. Bertucci, Drug binding to human serum albumin: abridged review of results obtained with high-performance liquid chromatography and circular dichroism, *Chirality*, 18 (2006) 667-679.
5. X.M. He, D.C. Carter, Atomic structure and chemistry of human serum albumin, *Nature*, 358 (1992) 209-215.
6. G. Fanali, A. di Masi, V. Trezza, M. Marino, M. Fasano, P. Ascenzi, Human serum albumin: From bench to bedside, *Mol. Aspects Med.*, 33 (2012) 209-290.
7. T. Peters, Jr. All About albumin: Biochemistry, Genetics, and Medical Applications, 1996.

8. C. Bertucci, E. Domenici, Reversible and covalent binding of drugs to human serum albumin: methodological approaches and physiological relevance, *Curr. Med. Chem.*, 9 (2002) 1463-1481.
9. G. Sudlow, D.J. Birkett, D.N. Wade, Characterization of two specific drug binding sites on human serum albumin, *Mol. Pharmacol.*, 11 (1975) 824-832.
10. G. Sudlow, D.J. Birkett, D.N. Wade, Further characterization of specific drug binding-sites on human serum albumin, *Mol. Pharmacol.*, 12 (1976) 1052-1061.
11. A. Sengupta, D.S. Hage, Characterization of minor site probes for human serum albumin by high-performance affinity chromatography, *Anal. Chem.*, 71 (1999) 3821-3827.
12. D.S. Hage, A. Sengupta, Characterization of the binding of digitoxin and acetyldigitoxin to human serum albumin by high-performance affinity chromatography, *J. Chromatogr. B*, 724 (1999) 91-100.
13. D.L. Nelson, M.M. Cox, *Lehninger Principles of Biochemistry*, 5th ed., W.H. Freeman, New York, 2008.
14. J. Anguizola, R. Matsuda, O.S. Barnaby, K.S. Hoy, C.L. Wa, E. DeBolt, M. Koke, D.S. Hage, Review: glycation of human serum albumin, *Clin. Chim. Acta*, 425 (2013) 64-76.
15. L. Guariguata, D. Whiting, C. Weil, N. Unwin, The International Diabetes Federation Diabetes Atlas methodology for estimating global and national prevalence of diabetes in adults, *Diabetes Res. Clin. Practice*, 94 (2011) 322-332.

16. B.M. Kozak, M.Y. Tjota, K.L. Close, *Journal of Diabetes NEWS*, *J. Diabetes*, 4 (2012) 8-17.
17. J.W.L. Hartog, A.A. Voors, C.G. Schalkwijk, J. Scheijen, T.D.J. Smilde, K. Damman, S.J.L. Bakker, A.J. Smit, D.J. van Veldhuisen, Clinical and prognostic value of advanced glycation end-products in chronic heart failure, *Eur. Heart J.*, 28 (2007) 2879-2885.
18. P.J. Thornalley, A. Langborg, H.S. Minhas, Formation of glyoxal, methylglyoxal and 3-deoxyglucosone in the glycation of proteins by glucose, *Biochem. J.*, 344 (1999) 109-116.
19. A.J. Jackson, J. Anguizola, E.L. Pfaunmiller, D.S. Hage, Use of entrapment and high-performance affinity chromatography to compare the binding of drugs and site-specific probes with normal and glycated human serum albumin, *Anal. Bioanal. Chem.*, 405 (2013) 5833-5841.
20. K.S. Joseph, J. Anguizola, A.J. Jackson, D.S. Hage, Chromatographic analysis of acetohexamide binding to glycated human serum albumin, *J. Chromatogr. B*, 878 (2010) 2775-2781.
21. K.S. Joseph, D.S. Hage, Characterization of the binding of sulfonylurea drugs to HSA by high-performance affinity chromatography, *J. Chromatogr. B*, 878 (2010) 1590-1598.
22. R. Matsuda, J. Anguizola, K.S. Joseph, D.S. Hage, High-performance affinity chromatography and the analysis of drug interactions with modified proteins:

- binding of gliclazide with glycated human serum albumin, *Anal. Bioanal. Chem.*, 401 (2011) 2811-2819.
23. K.S. Joseph, J. Anguizola, D.S. Hage, Binding of tolbutamide to glycated human serum albumin, *J. Pharmaceut. Biomed. Anal.*, 54 (2011) 426-432.
24. R. Matsuda, S.H. Kye, J. Anguizola, D.S. Hage, Studies of drug interactions with glycated human serum albumin by high-performance affinity chromatography, *Rev. Anal. Chem.*, 33 (2014) 79-94.
25. R. Matsuda, J. Anguizola, K.S. Joseph, D.S. Hage, Analysis of drug interactions with modified proteins by high-performance affinity chromatography: binding of glibenclamide to normal and glycated human serum albumin, *J. Chromatogr. A*, 1265 (2012) 114-122.
26. K.S. Joseph, D.S. Hage, The effects of glycation on the binding of human serum albumin to warfarin and L-tryptophan, *J. Pharmaceut. Biomed. Anal.*, 53 (2010) 811-818.
27. K.A. Ney, K.J. Colley, S.V. Pizzo, The standardization of the thiobarbituric acid assay for nonenzymatic glycosylation of human serum albumin, *Anal. Biochem.*, 118 (1981) 294-300.
28. A. Lapolla, D. Fedele, R. Reitano, N.C. Arico, R. Seraglia, P. Traldi, E. Marotta, R. Tonani, Enzymatic digestion and mass spectrometry in the study of advanced glycation end products/peptides, *J. Am. Soc. Mass Spectrom.*, 15 (2004) 496-509.
29. D. Abidin, L. Liu, C. Dou, A. Datta, C. Yuan, An improved enzymatic assay for glycated serum protein, *Anal. Methods*, 5 (2013) 2461-2469.

30. T. Kouzuma, Y. Uemastu, T. Usami, S. Imamura, Study of glycated amino acid elimination reaction for an improved enzymatic glycated albumin measurement method, *Clin. Chim. Acta*, 346 (2004) 135-143.
31. P.F. Ruhn, S. Garver, D.S. Hage, Development of dihydrazide-activated silica supports for high-performance affinity chromatography, *J. Chromatogr. A*, 669 (1994) 9-19.
32. A.J. Jackson, H. Xuan, D.S. Hage, Entrapment of proteins in glycogen-capped and hydrazide-activated supports, *Anal. Biochem.*, 404 (2010) 106-108.
33. D.S. Hage, High-performance affinity chromatography: a powerful tool for studying serum protein binding, *J. Chromatogr. B*, 768 (2002) 3-30.

CHAPTER 5.

MICROFLUIDIC DEVICES WITH ENHANCED FLUORESCENCE DETECTION WITH MONOLITH SUPPORTS AND SILVER NANOPARTICLES

5.1. INTRODUCTION

The systems involved in the studies addressed in the first four chapters of this dissertation can be classified within the normal analytical scale. However, nanotechnology has opened up a new frontier for analytical sciences, leading to the development of microfabricated devices. These systems can be fabricated from glass, silicon, or polymer-based materials and fulfill the requirements for the creation of a complete “laboratory-on-a-chip” [1]. Affinity and immunoaffinity separation techniques are well suited to integration into these microsystems due to the specificity and fast reaction times that can occur in these systems for the analytes of interest. Affinity and immunoaffinity devices can be static, such as protein arrays, or can be based on microfluidics, as can occur when using capillary electrophoresis and chromatographic microfluidic systems [1,2].

One of the most appealing advantages of these microfluidics devices is the low limits of detection that can be attained with them, even when they are used with very small samples and small amounts of reagents. This is especially true when these devices are combined with fluorescence detection or mass spectrometry. This makes microfluidic devices attractive for use in biointeraction systems or for biomedical analysis [1,3]. The

development of nanomaterials (including carbon nanotubes, silica nanoparticles, gold or silver nanoparticles, magnetic beads, quantum dots and multifunctional core-shell systems) has led to approaches that may provide even greater signal intensities and higher stabilities in these signals at low detection limits [3-5]. For example, the increased surface areas for many of these materials can allow for an increase in sensitivity by providing more reaction centers, with some devices using nanomaterials allowing for detection in the nM or pM range [2,6-8].

Fluorescence-based detection has intrinsically high sensitivity due to the large extinction coefficients and quantum yields of the fluorescent labels that are in common use [9,10]. However, in the visible range of the electromagnetic spectrum, fluorescence detection suffers from interferences and frequently has a high background signal that is produced by autofluorescence and light scattering from biological components, membranes or plastics that are used in the construction of sensors or microfabricated platforms [7].

An alternative to overcome this problem is to use near-infrared (NIR) fluorescent labels for detection. NIR fluorescence involves the absorption and emission of light in the range of 700–900 nm. NIR fluorescent dyes can offer better sensitivity and higher signal-to-noise ratios than traditional fluorescent labels because the autofluorescence from common biological components such as proteins and cells is greatly reduced in the NIR region [10]. Plastics that are commonly used in detection or microfluidic systems, such as nitrocellulose, polyvinylidene difluoride (PVDF), poly(methylmethacrylate) (PMMA), and polydimethylsiloxane (PDMS), also have reduced light scattering and autofluorescence in the NIR region [7]. For this reason, NIR fluorescent labels have been of great interest for use in analyzing trace substances in biological environments [11,12].

Despite their drastic reduction in interferences and background signals, NIR fluorophores still suffer from lower signal intensities than fluorophores in the visible range of the spectrum, which is caused by their low intrinsic quantum yield [13]. Thus, there remains a need for improved sensitivity for these dyes, in order to expand the use of NIR fluorescence in the biomedical and bioanalytical fields. An approach to overcome the low intrinsic quantum yields of these fluorophores, and to improve the signal from NIR fluorescent probes, is to use plasmon-active nanostructures (e.g., made from gold or silver) located near but not in direct contact with the fluorophore. The close proximity of the nanoparticles and NIR fluorescent probe produces an effect known as surface-enhanced fluorescence (SEF).

SEF occurs because metal nanoparticles (mNPs) have conduction band electrons. When these free electrons are subjected to an electromagnetic field at a certain frequency, they are forced to oscillate within the particle volume and slightly into the surrounding material [14]. The oscillating electron clouds, which are referred to as surface plasmons, act as energy collectors that can concentrate energy from a large volume (e.g., the volume occupied by the light beam or laser used to illuminate a NIR fluorescent probe) to the much smaller volume that is occupied by the nanoparticles [15]. This causes electromagnetic fields to be greatly increased in the regions where the mNPs are concentrated and between joints and clusters of mNPs. Consequently, the excitation and emission rates of the fluorophore are greatly increased [16]. mNPs have been referred to as nanoantennas because of their ability to concentrate energy from a large space into a smaller region [17-20]. In areas of the material where the mNPs form clusters or junctions, known as “hot-spots”, the fluorescence intensity can be dramatically improved by SEF [21-25]. By

combining NIR fluorescent dyes and SEF, it is possible to improve the limits of detection for these dyes in fluorescence-based assays by simultaneously increasing the signal and reducing the background noise of the signal [26,27].

5.2. EXPERIMENTAL SECTION

5.2.1. Materials

The glycidyl methacrylate (GMA, 97% pure), ethylene dimethacrylate (EDMA, 98%), 1-dodecanol (98%) and cyclohexanol (99%) were purchased from Sigma-Aldrich (St. Louis, MO, USA). The PDMS prepolymer and curing agent were also obtained from Sigma-Aldrich. Camphorquinone (99%) and ethyl-4-dimethylaminobenzoate (99%) were purchased from Alfa Aesar (Ward Hill, MA, USA). All other reagents were of the purest grades available. A citrate-stabilized solution of silver nanoparticles (AgNPs; 18 nM with an average particle diameter of 18 Å) was a gift from LI-COR Biosciences (Lincoln, NE, USA). The AgNP solution was swirled and filtered through 0.20 µm nylon Acrodisc syringe filters (Pall, Washington, NY, USA) before use to eliminate any aggregates that may have formed in this preparation. A Vivaspin ultrafiltration spin column (300 kDa MW cutoff; Sartorius, Göttingen, Germany) was used for isolating the AgNPs from their original solution. The IRDye 800 CW carboxylate dye was obtained from LI-COR Biosciences. All buffers and aqueous solutions were prepared using water from a Milli-Q Advantage 10 system (EMD Millipore Corporation, Billerica, MA, USA). The buffers were filtered through 0.20 µm GNWP nylon membranes from EMD Millipore prior to their use.

5.2.2. Solution preparation

A solution containing the IRDye 800 CW carboxylate dye was prepared by combining the contents of a vial that contained 20 nmol of this dye with 0.5 mL of pH 7.4, 0.067 M potassium phosphate buffer. This gave a 40 μ M solution of this dye that was kept in the freezer at -20 °C. From this solution a diluted stock solution containing 1000 nM of the same dye was prepared by dilution with pH 7.4, 0.067 M potassium phosphate buffer. This diluted stock solution was stored at 4 °C and used within one month of preparation. The working standards were made from the 1000 nM dye solution by diluting them with pH 7.4, 0.067 M potassium phosphate buffer. These standards were used within two days of their preparation. All of these solutions were protected from the light by covering their vials with aluminum foil and storing the solutions in the dark.

5.2.3. Apparatus

Measurements of the IRDye 800 CW carboxylate dye were carried out by using the optical components of a 4200 near-infrared (NIR) fluorescence microscope that were provided by LI-COR. This type of microscope was equipped with 680 and 780 nm diode laser sources that were focused into a 200 μ m electron beam at a short distance from the detection objective lens. When one of these lasers (modulated at 9.2 kHz) illuminates a sample containing an appropriate NIR fluorescent dye, some of this dye may be excited and its fluorescent signal is converted into an electrical signal by an avalanche photodiode detector. The signal is preamplified in the detector and sent to a 4000M microscope controller, which was also from LI-COR. The controller demodulates the signal and provides a DC analog output that is proportional to the concentration of the dye in the sample.

This optical system was mounted onto a programmable platform from National Aperture (Salem, NH, USA) that could be moved in the x , y and z directions. This platform allowed travel up to 138 cm in any direction, with speeds up to 7.6 mm/s at a repeatability of 0.2 μm and with an accuracy of 0.7 μm . This combined system was used in this research to scan samples that contained the NIR fluorescent dye, to measure this dye, and to examine the signal of this dye as a function of position in a sample or in a device that contained the dye's solution (see Figure 5.1). LabView 8.0 and a data acquisition board from National Instruments (Austin, TX, USA), along with programs written in-house, were used for recording the signal from the NIR fluorescent microscope and for controlling the movable platform. A PHD Ultra syringe pump (Harvard Apparatus, Holliston, MA, USA) and a 0.5 μL Rheodyne valve (Rohnert Park, CA, USA) were used for the delivery of samples and solutions to the microfluidic devices that were placed onto the movable platform.

5.2.4. Construction of microfluidic devices

The microfluidic chips were made by employing a PDMS prepolymer and curing agent, which were mixed at a ratio of 10:1 and degassed under vacuum for 1 h [28]. This PDMS polymerization mixture was then cast onto a master mold made of polyethylene through 3D printing and containing the desired form of the microchannel (e.g., 2.5 cm length \times 200 μm width \times 50 μm depth). Next, the PDMS was thermally cured at 60 $^{\circ}\text{C}$ for 1 h. This combination of time and temperature was determined in this study to produce a stiff PDMS slab that still had enough elasticity to allow for cutting. The slab was then gently peeled off of the mold, to avoid damaging the microchannel, and the excess material was cut away [28,29]. The PDMS surface with the microchannel and a glass slide were treated separately with an oxygen plasma for 30 s. Immediately after this plasma treatment,

the PDMS and glass slide surfaces were aligned onto each other. This combined device was then placed into an oven at 80 °C for 15 min to finalize the bonding of the PDMS to the glass slide [29,30]. The inlet and outlet of the resulting device were punched by using a 0.048 inch o.d. biopsy tool, and type PE-60 polyethylene tubing (0.048 inch o.d., 0.036 inch i.d.) was inserted into the device after the holes had been made with the biopsy tool [31].

5.2.5. Monolith preparation

Monoliths based on poly(glycidyl methacrylate-co-ethylene dimethacrylate) (GMA/EDMA) were prepared by photopolymerization [32]. This was begun by mixing all of the components shown in Table 5.1 except for the photoinitiators (i.e., camphorquinone and ethyl-4-dimethylaminobenzoate). Before these components were mixed, the cyclohexanol and 1-dodecanol were heated in a water bath at 40 °C to get them into the liquid state. The monomer ratio and the proportion of the porogenic solvents that were used have been previously found to be appropriate for making monoliths that can be used for immobilizing proteins or antibodies and for use in affinity-based columns [32,33]. All of the components in Table 5.1 were then pipeted into a vial except the photoinitiators. The contents of this vial were placed onto a vortex mixer for 5 min in the dark. The photoinitiators were then added and mixing was continued for another 2 min. This mixture was poured onto a glass slide to form monolith layers or injected with a syringe into a microfluidic device. A light source was used to irradiate this mixture with intense blue light (472 nm) for a total 3 min, which was divided in 30 s intervals over which a different section of the mixture was irradiated. The light source was held at a distance of 1–2 cm from the mixture during this process. The glass slide or microfluidic chip was then placed

into an UV-curing oven, where it was exposed to blue light for 10 min to complete photopolymerization of the monolith. The protocol produced monoliths with enough mechanical stability for use in flow-based devices [30,33].

When curing was finished for the microfluidic devices, the tubing was taken off the PDMS slab and new PE-60 tubing was inserted through the inlet holes. In the microfluidic devices that were made later in this chapter, more of the PDMS polymerization mixture was applied around the entrance points of the inlet tubes, followed by heating at 60 °C for 1 h in an oven to cure this PDMS and to provide a good seal around the tubing. These devices were then mounted onto the microscope stage, as shown in Figures 5.1 and 5.5, and connected with PEEK tubing to a syringe pump for the application of sample and solutions to the system.

Figure 5.1 (Top) Microfluidics chip containing a $2.2\text{ cm} \times 250\text{ }\mu\text{m} \times 500\text{ }\mu\text{m}$ channel filled with a GMA/EDMA monolith. (Bottom left) An x - y - z scanning platform that contains a mounted microfluidic chip. (Bottom right) General components of the NIR fluorescence microscope stage. In this work, the platform containing the microfluidic chip was located in front of the microscope's objective lens.

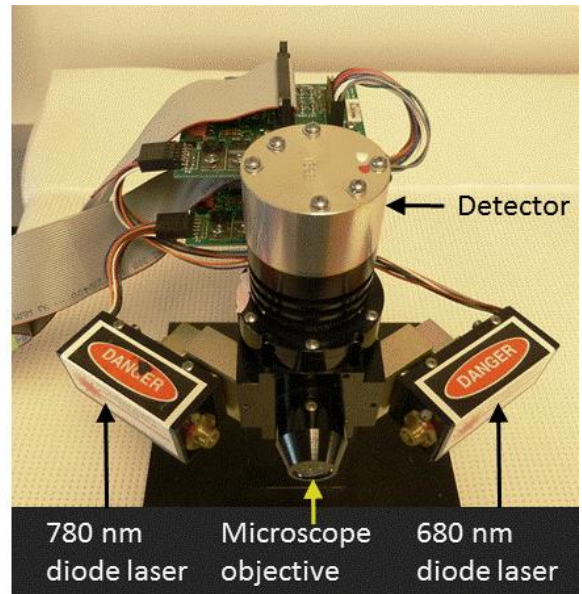
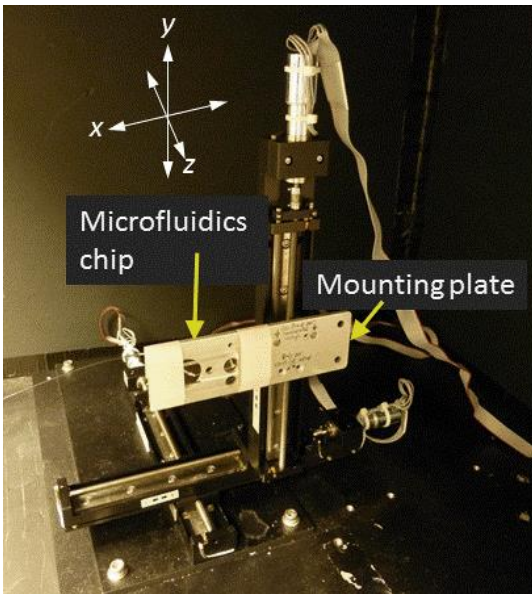
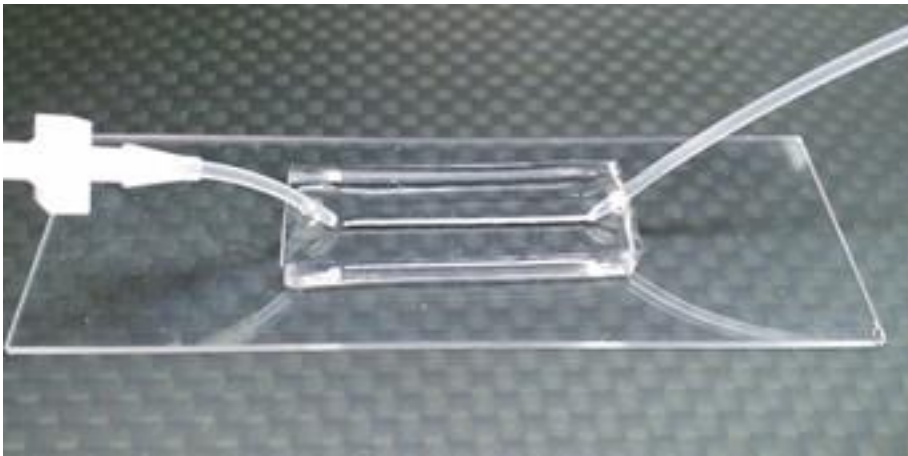


Table 5.1. Composition of the polymerization mixture that was used with photoinitiation to make EDMA/GMA monoliths.

Component	(% w/w)	mass (g)	Volume (mL)
GMA ¹	20	0.2	0.1860
EDMA ¹	20	0.2	0.1902
1-Dodecanol	48	0.48	0.5853
Cyclohexanol	12	0.12	0.126
Camphorquinone		0.004 ²	
Ethyl-4-dimethylaminobenzoate		0.004 ²	

¹Monomers: GMA, glycidyl methacrylate; EDMA, ethylene dimethacrylate.

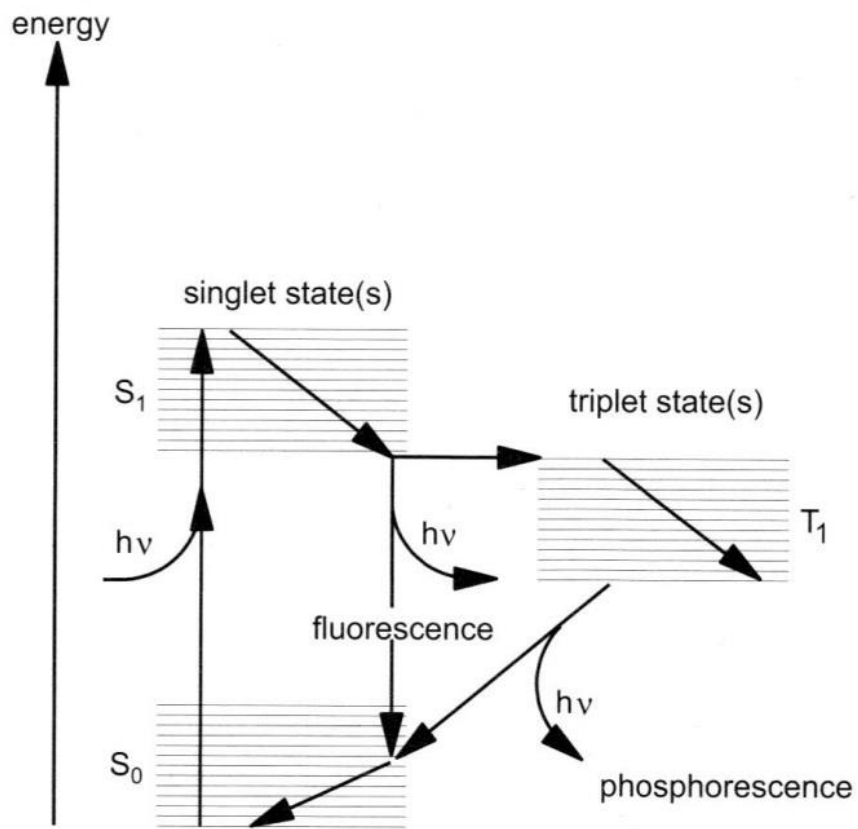
²These photoinitiators were added in a 1% (w/w) amount versus the monomers.

5.3. THEORY

5.3.1. Fluorescence spectroscopy

The energy absorbed by a molecule when irradiated by light must be released to the environment either 1) as heat through molecular vibrations and collisions or 2) as light by the processes of fluorescence or phosphorescence, which occur on two very different timescales. Figure 5.2 shows a Jablonski diagram [34] that illustrates the mechanisms of fluorescence and phosphorescence. Upon the absorption of a photon with an appropriate amount of energy, a molecule is initially excited from an electronic ground state (S_0) to its first excited state (S_1) over a short period of time (about 10^{-15} s) [34,35]. Over a time scale of about 10^{-12} s, the molecule relaxes to the ground vibrational state of its first excited electronic state. As the system relaxes, energy is released in the form of heat to the environment. The molecule stays a time period of a few nanoseconds in the first excited state, which corresponds to the fluorescence lifetime. Then, a photon is emitted in a process that again only lasts about 10^{-15} s [35]. Finally, the molecule releases more vibrational energy as heat, eventually returning to the lowest vibrational state of its ground electronic state. Because of the two vibrational relaxation steps that occur during this process, the emitted light will have less energy (or have a longer wavelength) than the absorbed light. Aromatic molecules with delocalized electrons can undergo relaxation by fluorescence or phosphorescence. These fluorophores may be from a natural source (e.g., tryptophan and naturally fluorescent proteins such as green fluorescent protein, GFP) or they can be synthetic in origin (e.g., Cyanine, Alexa, and Atto) [11].

Figure 5.2 General scheme showing the energy states that are associated with fluorescence and phosphorescence. A photon with energy $h\nu$ is first absorbed by a molecule, causing an electron to move from a ground state (S_0) to an excited singlet electronic state (S_1). The molecule loses some energy as heat as it moves to the lowest excited vibrational state in this electronic level. In fluorescence, a photon is then emitted, allowing the electron to move back to its ground electronic state. In phosphorescence, the excited electron instead first passes from the singlet state (S_1) to a triplet state (T_1) by means of intersystem crossing. The lifetime of this T_1 state can be quite long (i.e., 1 ms to hours). Reproduced with permission from reference [34].

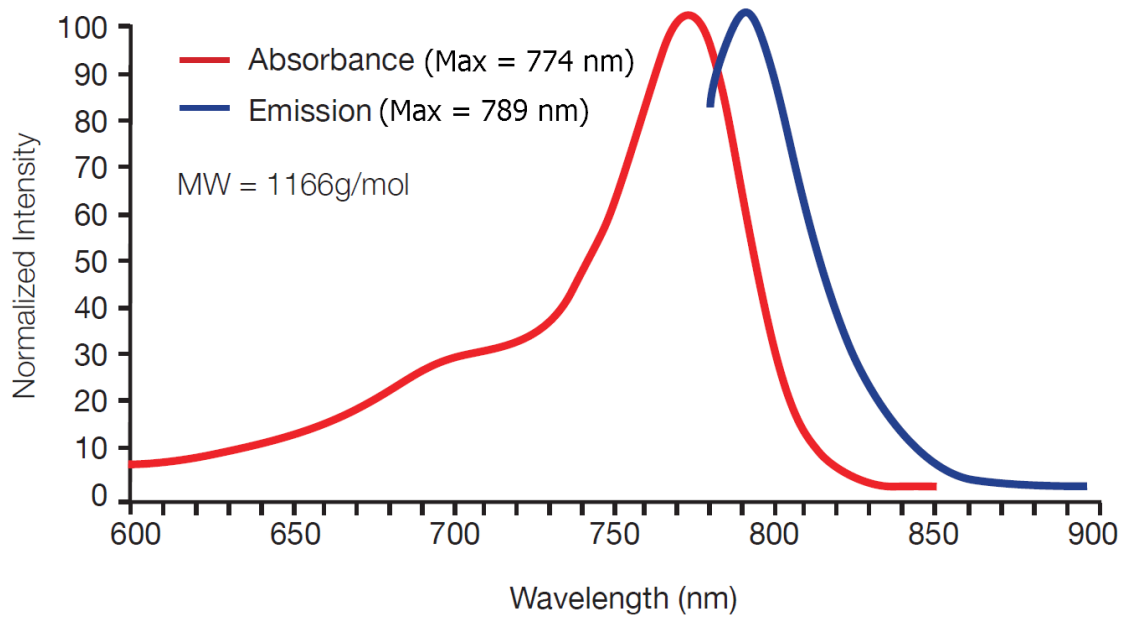


Fluorescence spectroscopy is conducted by exciting a fluorescent compound with light source at an appropriate wavelength and collecting the light that is emitted at a longer wavelength. The excitation source can be a laser, a light-emitting diode, or a broadband filament bulb that is equipped with a filter. The wavelength difference between the absorption and emission maxima is known as the Stokes' shift, and is usually 10-20 nm for organic-based fluorescent compounds. This is illustrated in Figure 5.3 by using the absorption and emission spectra for the NIR fluorescent dye IRDye 800CW, which was used for the studies reported in this chapter [10,12,34,35].

5.3.2. Surface-enhanced fluorescence

Surface-enhanced fluorescence (SEF) has been known for decades but only recently has it gained popularity within the scientific community. This technology makes it possible to significantly improve the quantum yield for a fluorophore by increasing the excitation rate of the fluorophore as well as improving its photostability [3]. The use of nanoparticles to enhance optical detection started to grow more rapidly when the related phenomenon of surface-enhanced Raman scattering (SERS) became popular in the research community [36,37]. Raman scattering is important because every molecule has a unique scattering spectrum. Unfortunately, Raman intensities are extremely low and, even with an enhancement in sensitivity, detecting this type of scattering remains an issue that limits the application of SERS in bioanalysis [36].

Figure 5.3 Absorption (red) and emission (blue) spectra for the dye IRDye 800CW in phosphate buffered saline. Copyright LI-COR, Inc. by permission.



The fluorescence enhancement of NIR dyes has been demonstrated with gold nanoparticles (AuNPs) and silver nanoparticles (AgNPs) in solution and on surfaces [4,5,13,38]. Gold nanostructures [39-45] and silver nanostructures [24,36,37,45] have been used for sensors that use light in NIR region [13], as well as in SERS detectors that have increased sensitivity [43]. Common examples of nanostructures that are used in fluorescence sensors with SEF are silver and gold nanoparticles. Plasmon resonance can produce fluorescence quenching or fluorescence enhancement for organic fluorophores, which will depend on the emission wavelength, the distance of the fluorophores to the metal nanoparticles, and the size of the nanoparticles [6,46-48]. Quenching usually dominates when the fluorophore is located at a short distance from the surface (i.e., typically within 5 Å) [44,49]. The plasmonic enhancement of fluorescence dominates when using gold and silver at greater distances [49].

The intrinsic fluorescence yield can be represented by the following expression [10,34],

$$\gamma_{em}^0 = \gamma_{ex}^0 \Phi^0 \quad (5.1)$$

where γ_{em}^0 and γ_{ex}^0 are the fluorescence emission rate and excitation rate, respectively.

The term Φ^0 is the quantum yield, which can be expressed as the ratio of the radiative decay rate to the total decay rate. In this case, Equation 5.1 turns into Equation 5.2 [49,50],

$$\gamma_{em}^0 = \gamma_{ex}^0 \cdot \frac{\gamma_r^0}{\gamma_r^0 + \gamma_{nr}^0} \quad (5.2)$$

where γ_r^0 and γ_{nr}^0 are the radiative and non-radiative intrinsic decay rates, respectively.

In the presence of surface plasmons, the excitation decay rate and the radiative decay rate are increased to γ_{em} and γ_{ex} respectively, and a new term appears for the non-radiative decay. This gives the following enhanced emission rate.

$$\gamma_{em} = \gamma_{ex} \cdot \frac{\gamma_r}{\gamma_r + \gamma_{nr} + \gamma_{nr}^0} \quad (5.3)$$

The second term in this expression is the enhanced quantum yield, Φ . SEF can then be described as a combination of enhanced excitation rate and quantum yield [51].

$$SEF = \frac{\gamma_{ex}}{\gamma_{ex}^0} \cdot \frac{\Phi}{\Phi^0} \quad (5.4.)$$

According to these equations, the fluorescence of a probe can be enhanced by increasing the excitation rate or the quantum yield [52]. The quantum yield cannot exceed unity, so there is a limit as to how much the fluorescence can be increased by this factor, especially for fluorophores that already have high intrinsic quantum yields. A local increase in field intensity can improve the excitation rate as well as the quantum yield, and is dependent on the optical properties of the material that forms the nanostructure, the geometry of the nanostructure, the orientation of the emitter dipole, and distance between the emitter and the nanostructure [53].

5.4. RESULTS AND DISCUSSION

5.4.1. Initial alignment of NIR fluorescence microscope stage

To align the stage of the scanning platform with the optics of the NIR fluorescence microscope, a piece of graph paper was glued to a glass slide that was fixed to the

microscope stage by using double sided tape. The graph paper served as a guide for finding the optimum distance between the objective of the microscope and the surface to be analyzed. The microscope stage was moved in the x - y - z planes with three servo motors that were controlled through a program written in LabView.

The initial signal adjustment was carried out by moving the platform in the z -axis until the red laser dot from the light source reflected on the surface of the paper and was centered in front of the objective. The final adjustment was achieved by moving the stage small distances along the z -axis (i.e., between 1000 and 200 counts, with 1 mm equaling 2800 counts) while observing the variation in the detector's signal until a maximum output was achieved.

It was observed that the background signal resulting from the light that was reflected and scattered by the paper's surface reached a maximum when the objective was located 13.2 mm from the paper. In the following experiments, a piece of heavyweight paper cut with a 13 mm width was used as a guide for setting the initial distance between the microscope objective and the surface of the sample. The final distance adjustment was made by moving the stage along the z -axis in small increments, as described in the previous paragraph.

Working solutions were prepared by taking a stock solution containing 1000 nM of the IR800 CW carboxylate dye and diluting it with pH 7.4, 0.067 M potassium phosphate buffer. The following dye concentrations were used for the initial studies in this chapter: 10 nM, 100 nM, 500 nM, and 1000 nM. Five drops of each solution were applied to EDMA/GMA monoliths that were formed in PEEK rings that had a 0.5 cm i.d. and a 1 mm depth. These monoliths were then placed onto on a glass slide. The slide was mounted on

the microscope stage with double sided tape, and the signal intensity for each dye solution was measured with the NIR fluorescence microscope by scanning along the x -axis and moving the stage in front of the microscope objective. It was found that the signal barely increased from the background level when looking at the 10 nM dye solution and reached almost the maximum level attainable by the microscope for 100 nM solution. The 500 nM and 1000 nM solutions gave the maximum possible response, indicating saturation of the microscope amplifier. Based on these results, the range of dye concentrations that were used in the following experiments was selected to be between 10 to 100 nM.

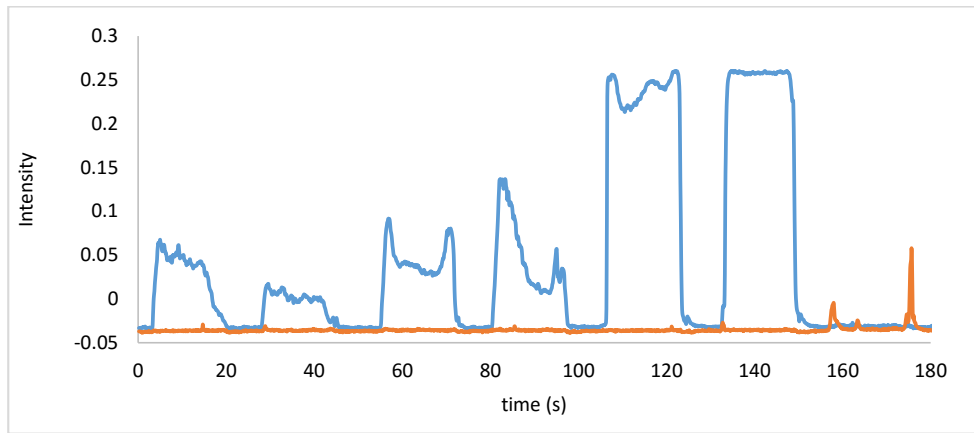
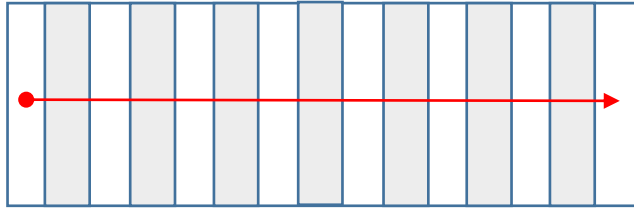
A plastic sheet of silica gel, as is used in thin layer chromatography, was cut in 0.5 cm wide strips and glued to a glass slide. The slide was mounted on the microscope stage, and the distance between this slide and the microscope objective was adjusted to provide the maximum fluorescence signal. Two drops of IR CW800 dye standards were applied over the top of each strip before scanning the strip along the x -axis. The results, as presented in Figure 5.4, show an increasing intensity when going from the left to the right (i.e., from 10 nM to 100 nM dye). The result obtained when no dye solution was present is shown in red and included for comparison. These results show an observable range between 10 and 100 nM of the IRDye 800CW dye on such a surface, with a limit of detection of around 10 nM. It was also observed that the signal decreased when the scan was repeated for the same strip if no fresh NIR fluorescent dye solution was added. This signal reduction was believed to be due to quenching by oxygen or photobleaching of the fluorophore [10,34].

The response of this system was compared with that of a benchtop spectrofluorometer when the same dye solutions were measured on a Cary Eclipse

fluorometer that was equipped with a 96-well plate reader. No signal was detected on the benchtop system at dye concentrations ranging from 10 nM to 100 nM, although a signal was clearly seen for the 1000 nM stock solution.

A citrate-stabilized solution of AgNPs (18 nM) was mixed with the 10 nM and 20 nM dye standards in proportions ranging from 10 to 50% to see if the addition of these nanoparticles gave any change in the dye's fluorescent signal. However, no significant increase in the signal was observed under these conditions.

Figure 5.4 (Top) Diagram showing the scan direction along the x -axis that was used for silica strips that were mounted on a glass slide. (Bottom) Scan of silica strips at 1000 revolutions/min (0.38 mm/s; the motor velocity, in revolutions per min, was converted to mm/s by using the fact that 1 revolution is 64 counts and 1 mm is 2800 counts) with the IRDye 800CW dye being present at the following concentrations (from left-to-right): 10 nM, 20 nM, 40 nM, 60 nM, 80 nM and 100 nM. The last position on the right is for a blank that contained no dye. The red tracing shows the results that were obtained for the same strip when no dye was present throughout the strip.

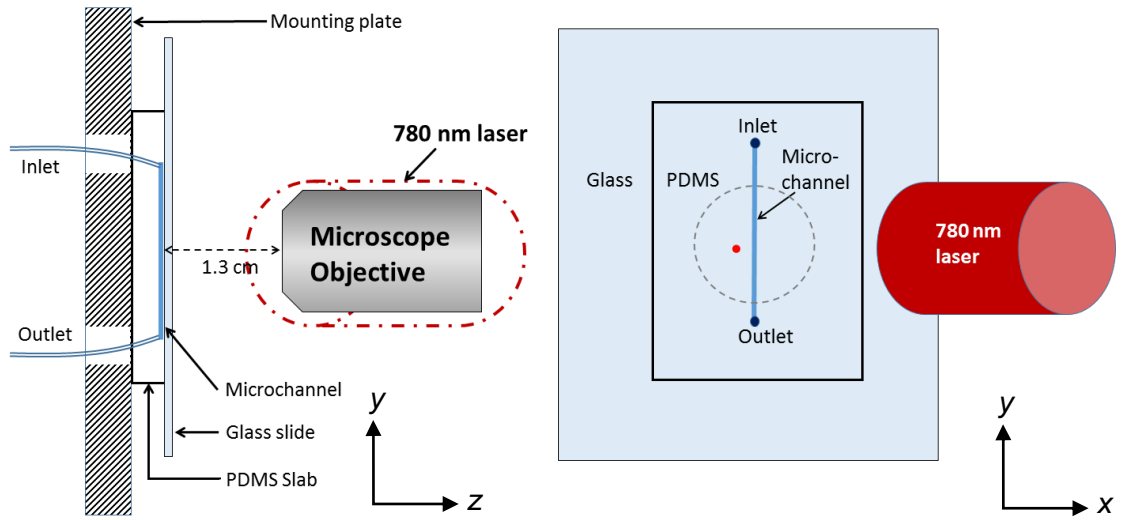


5.4.2. Fluorescence measurements of IR 800CW in microchannels and monoliths

The detection of the IR 800CW dyes in microchannels was studied by using a microfluidic device that was made of PDMS, as prepared in collaboration with Dr. Stephen Gross (Creighton University, Omaha, NE). This type of device had a straight microchannel with a length of 2.2 cm and a cross section of $250\ \mu\text{m} \times 50\ \mu\text{m}$. The microchannel was molded in a PDMS slab that was fixed to a glass slide. Teflon tubing was introduced through holes made in the PDMS at 90° versus the glass slide and in contact with the ends of the microchannel. An aluminum mounting plate with holes for directing the tubing was attached with screws to the microscope stage. The microfluidic chip was fixed with tape to the mounting plate, with the glass slide facing towards the microscope. The inlet tube was directed through a hole in the mounting plate and connected with PEEK tubing and adaptors to a syringe. The outlet was connected to a vial through another hole in the mounting plate. The location of the microfluidic chip in this system is illustrated in Figure 5.5.

The distance of the microscope from the surface of the chip was initially set at 1.3 cm. A 100 nM solution of IRDye 800CW dye was applied to the microfluidic chip at $20\ \mu\text{L}/\text{min}$. The signal from the microscope was monitored while the chip was scanned in the x - y plane to locate the microchannel. A camera with led illumination was used to assist in locating the microchannel. In this way, the position of the laser dot could be seen on the computer screen, avoiding the need to look directly into the enclosure that contained the microscope and the stage.

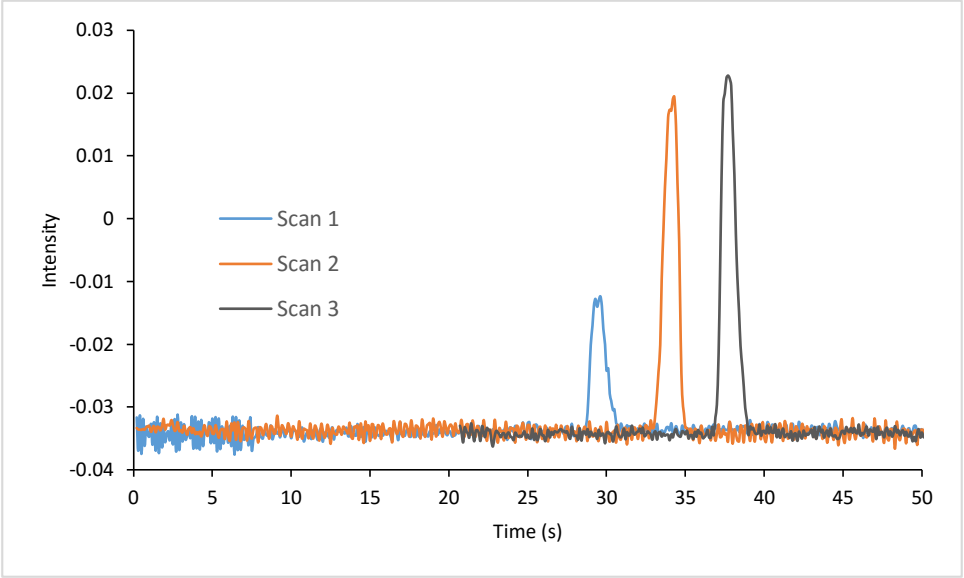
Figure 5.5 Schematic showing the position of the microfluidic chip relative to the microscope objective and the laser source. (Left) Lateral view showing the location of the laser source behind the microscope objective. (Right) Front view of the microfluidics chip, showing the position of the laser source and the reflection of the laser dot when it was crossing the microchannel. The microscope objective was centered in front of the microchannel (see dotted circle). The scans were made on the x -axis and crossed the microchannel.



Once a position for the laser beam had been located in the middle of the chip and next to the microchannel, scans were made along the x-axis, as is shown in Figure 5.4. These scans were made with the objective located at various different distances from the microscope (i.e., by varying the distance along the z-axis) until a peak was observed when the laser crossed the monolith containing the dye solution. The peak height became larger as this distance was optimized until a maximum in the response was attained. This is illustrated in Figure 5.6, which shows the variation in the signal intensity that was seen when scanning was carried out at three slightly different distances between the objective and the surface along the z-axis. In these results, the distance from the objective lens was smaller than the distance obtained in the previous section due to the presence of the glass slide that the laser has to cross before reaching the flowing dye solution. The apparent reflection point of the laser on the aluminum mounting plate appeared to be shifted to the left of the microchannel during detection because the laser source was located to the right of the microscope lens at an angle of 45° versus the glass surface, as can be seen in Figure 5.5.

Different positions along the length of the microchannel were scanned, giving similar results at the same scan velocities. These results indicated that the method of measuring the fluorescence of the IRDye 800CW dye while it was flowing through a microchannel with a $250 \times 50 \mu\text{m}$ cross section and molded into a PDMA microfluidic chip was reproducible and independent of the position along the channel's length. Small irregularities in the microchannel that may have been present did not appear to affect this result.

Figure 5.6 Signals obtained at scans of 1000 revolutions/min (or 0.38 mm/s) that were made at three distances, separated by 200 counts (or 0.071 mm), along the z-plane from the microscope objective to the microfluidic chip surface.



The effect of the scan velocity was studied by repeating the same type of scan at 0.038 mm/s (i.e., 1/10 the velocity used in the previous scans). The width of the peak for the signal as well as the height of this peak increased, with the peak height going from about 0.02 V to 0.06 V. The same level in the signal was reached when the laser was fixed at one point over the microchannel and the flow was stopped; but there was also an exponential decrease in the signal over time when dye was no longer flowing through the microchannel. These experiments showed that the signal increased when the scan velocity decreased and approached a maximum initial signal when the dye solution was not flowing. However, this last situation also lead to a decrease in the signal over time, which probably occurred due to photobleaching of the fluorophore [10,54].

The following experiments where performed for measuring the fluorescence of the IR 800CW dye when it was flowing through the system. The microfluidic device was fixed to the mounting stage with clamps or tape. The position of the device was adjusted while a solution of 100 nM or 500 nM of the dye was passed at 20 $\mu\text{L}/\text{min}$ through the microchannel. The signal was scanned at a distance of 1.3 cm or less between the microscope objective and the microchannel to find the position of the microchannel that gave a maximum response. Another distance adjustment was then made by moving the stage along the z -axis in increments going from 1000 counts and down 200 counts until a final maximum signal was reached.

A manual injection of 0.5 μL of the dye solution was used for these experiments. Solutions of the dye with concentrations of 500 nM, 50 nM, 20 nM or 10 nM were injected. Figure 5.7 shows the results that were obtained for a 500 nM solution of the dye that was

injected at 5 or 20 $\mu\text{L}/\text{min}$. At least three injections were made at each concentration of the dye and at each of these two flow rates.

As can be seen in Figure 5.7, decreasing the flow rate resulted in a larger peak in a manner similar to what occurred from decreasing the scan rate. The same trend was observed with the other concentrations of the dye that were studied. For the 10 nM dye solution, the signal was only slightly distinguishable from the background noise at the lowest flow rate that was tested (see Figure 5.8). By decreasing the flow rate, the time needed for the dye to enter and pass through the microchannel was also increased. This time could be decreased further by lowering the void time of the system (e.g., by decreasing the length and internal diameter of the connecting tubing), which would help provide less band broadening when this type of device is used in chromatographic separations or experiments.

The 10 nM and 20 nM solutions of the dye were mixed with the AgNP stock solution at various ratios to study the effect of these nanoparticles on the fluorescence intensity of the NIR fluorescent dye. No fluorescence enhancement was observed under these conditions.

The fluorescence of the dye was also measured in a $2\text{ cm} \times 250\text{ }\mu\text{m} \times 500\text{ }\mu\text{m}$ microchannel that contained a GMA/EDMA monolith, which was prepared as described in Sections 5.2.4 and 5.2.5. Injections of a $0.5\text{ }\mu\text{L}$ portion of solutions with dye concentrations ranging from 20 nM to 500 nM were made at $20\text{ }\mu\text{L}/\text{min}$. The peaks that were obtained showed some tailing, indicating that the dye may have been interacting with the monolith, as can be seen in Figure 5.9. The calibration curve for these results gave a linear response with a correlation coefficient of 0.9992 (r^2 , 0.9984).

Figure 5.7 Injections of a 500 nM solution of the IR CW 800 carboxylate dye in pH 7.4, 0.067 M potassium phosphate buffer at several flow rates and onto a microchannel with following dimensions: 2.5 cm × 250 μm × 50 μm.

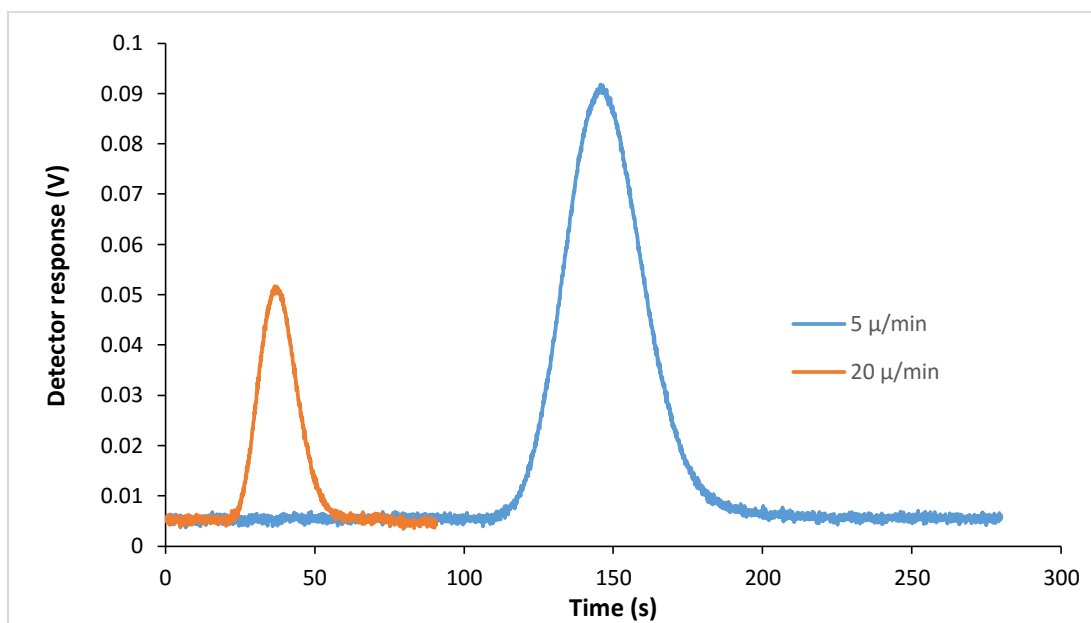


Figure 5.8 Injections of the IR CW 800 carboxylate dye at several concentrations in pH 7.4, 0.067 M potassium phosphate buffer. Conditions: injection volume, 0.5 μL ; microchannel dimension, 2.2 cm \times 250 \times 50 μm ; flow rate, (left) 20 $\mu\text{L}/\text{min}$ and (right) 5 $\mu\text{L}/\text{min}$.

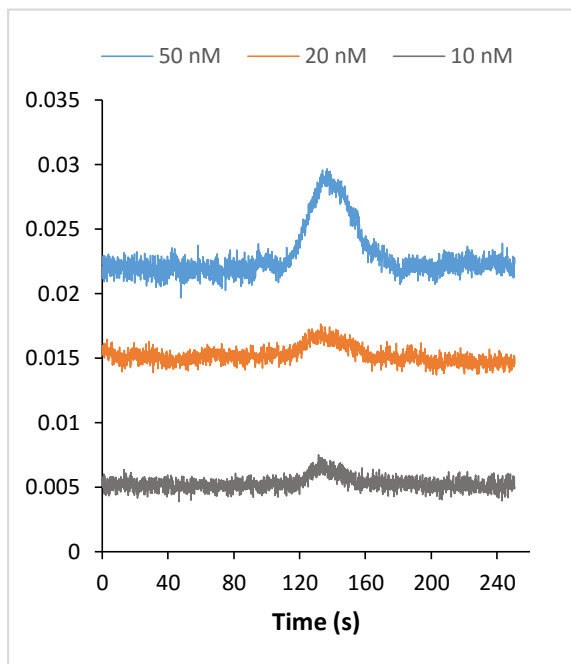
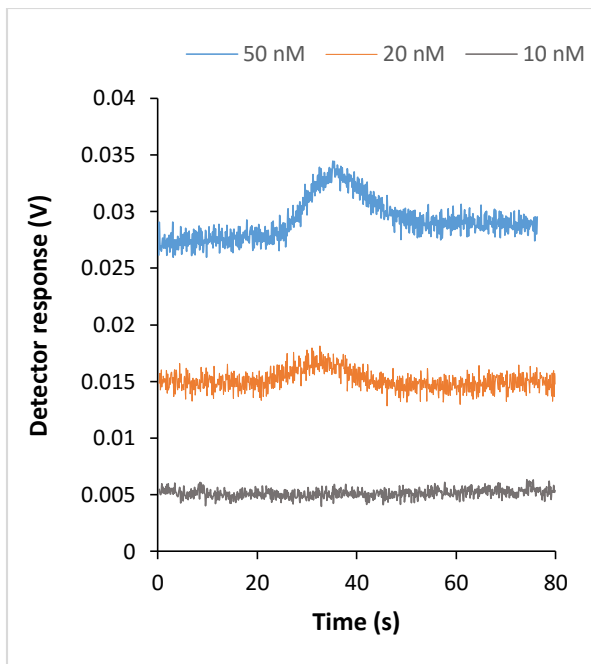
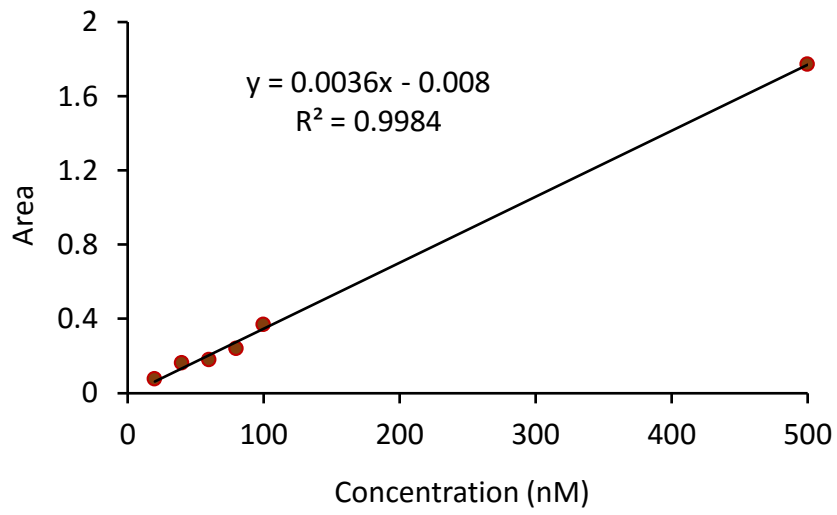
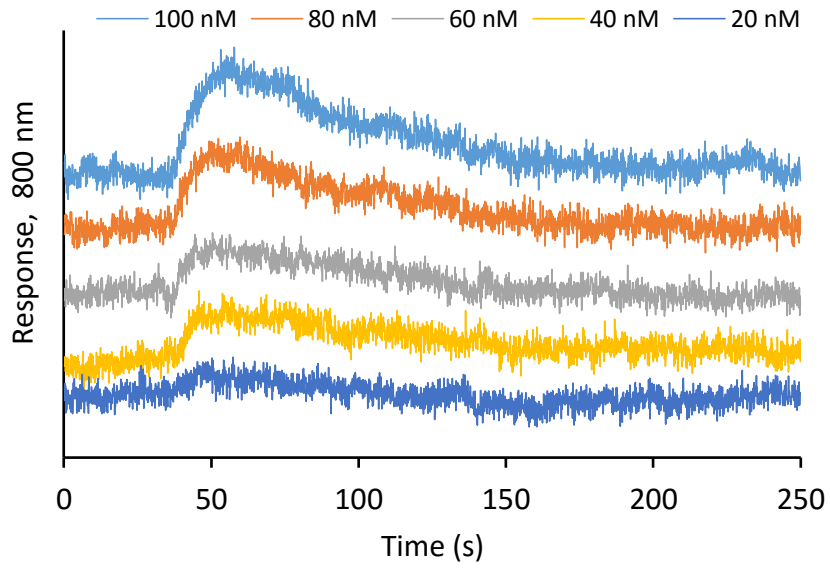


Figure 5.9 (Top) Injections of 0.5 μL for several concentrations of the IR CW 800 carboxylate dye onto a $2\text{ cm} \times 500\ \mu\text{m} \times 250\ \mu\text{m}$ microchannel that was filled a GMA/EDMA monolith and in the presence of pH 7.4, 0.067 potassium phosphate buffer at $20\ \mu\text{L}/\text{min}$. (Bottom) Calibration plot obtained for these same results.

Concentration:



5.4.3. Fluorescence enhancement in EDMA/GMA monoliths

5.4.3.1. Adjustment of the fluorescence microscope controller

To achieve an appropriate dynamic range for measuring the signal from the NIR fluorescence microscope, the optimum settings for the gain and offset in the microscope controller were varied when using the 800 nm detection channel of this system. The settings were optimized while the signal was used to monitor a 20 nM solution of the IRDye 800CW dye in pH 7.4, 0.067 M potassium phosphate buffer, which was applied at 25 $\mu\text{L}/\text{min}$ through an empty glass capillary that was mounted on the stage and over a card with a non-reflective black surface. The gain and the offset settings were adjusted so that the output was about -0.034 V for the dye solution and -0.043 V for the background signal that was present when looking at the black card. A similar background signal was obtained when using a capillary that contained a flowing blank solution of pH 7.4, 0.067 M phosphate buffer. This approach made it possible to ensure that the signal that was being optimized was due to the fluorescence of the IRDye 800CW and was not due to reflected or scattered light.

The voltages that were listed in the previous paragraph were located at the lower end of the total possible voltage range (-0.06 to 0.06 V) of the detection system, which allowed enough room for signals due to higher dye concentrations without being too close to the minimum voltage. The gain of the controller was increased for detecting dye concentrations at lower levels or decreased for the analysis of higher dye concentrations while still keeping the voltage signal within the measurable range.

5.4.3.2. Preparation of monoliths with AgNP

Several attempts were carried out to incorporate AgNPs into GMA/EDMA mixtures before they were polymerized for form monoliths by photoinitiation. Because the aqueous solution of the citrate-stabilized AgNPs was immiscible with the other polymerization components, aliquots of the AgNP solution were first dried at 60 °C; however, it was not possible to later resuspend the AgNPs in either the polymerization mixture or in one of the porogens (i.e., cyclohexanol).

In a second approach, a 18 nM solution of the AgNPs was placed into a Vivaspin ultrafiltration column with a 300 kDa MW cutoff and a 6 mL capacity. The filtrating element in this column was a double polyethersulfone membrane, which should have been capable of retaining the AgNPs because their average diameter (i.e., 20 nm) was much larger than the sizes of molecules that are able to pass through this type of filtration membrane.

The spin time that was used for ultrafiltration was found to be critical. The use of a time that was too long resulted in all the AgNPs sticking to the membrane; it was not possible to the resuspend these particles. The use of too little time for ultrafiltration resulted in some of the original aqueous solution remaining in the tube, which caused problems when attempts were made to later place the AgNPs into an organic solvent (i.e., giving two phases and poor dispersion). After several trials, it was found that the best approach was to spin the AgNP solution for 30 to 60 s, followed by the careful addition of a non-aqueous solvent (e.g., cyclohexanol) over the AgNP solution (i.e., without disturbing the solution) and followed by centrifugation. The second centrifugation step of 1 min, expelled the remaining water and allowed to obtain a pellet of AgNPs on the bottom of the

tube. Too much time yielded the AgNPs stuck to the membrane. Finally, the tube was inverted twice to remove the AgNP pellet and the contents were poured into another tube. After this new suspension had been mixed by vortexing at a high speed for 20 s, the resulting suspension of AgNPs in cyclohexanol appeared to be homogeneous and, when mixed with the rest of the components, gave a polymerization mixture that was stable for several days.

Three preparations were made by using 1 mL, 3 mL or 5 mL of the original AgNP solution and 1 mL of cyclohexanol. The final conditions that were used are listed in Table 5.2. Although it was not possible to recover all the AgNPs from the ultrafiltration tubes, this method was fast and did produce a suspension of AgNPs in cyclohexanol that would settle down very slowly and could easily be resuspended by vortex mixing.

Pictures of the AgNP suspensions in cyclohexanol are provided in Figure 5.10 as well as UV/Vis spectra for the AgNPs in a 1:10 aqueous solution and for the AgNP/cyclohexanol suspension. The aqueous solution spectrum shows a characteristic maximum for AgNPs near 460 nm [5,24]. The spectrum of the AgNP/cyclohexanol suspension was dominated by the background after 300 nm but had a small peak at 336 nm.

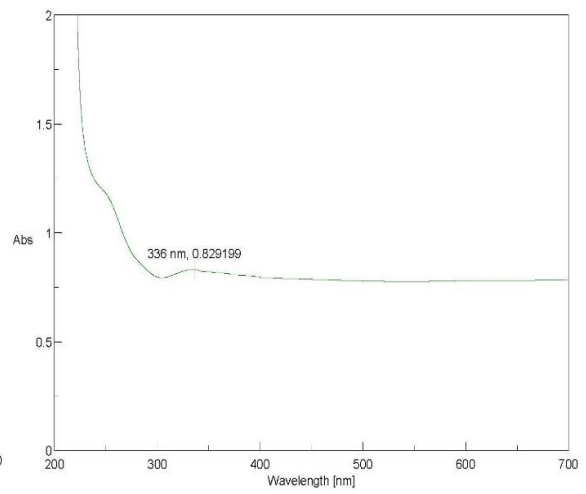
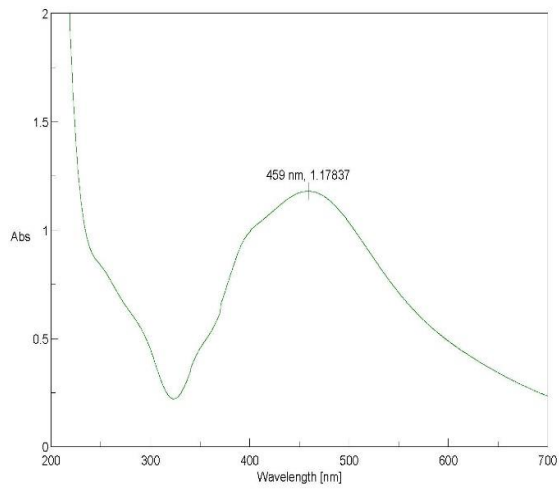
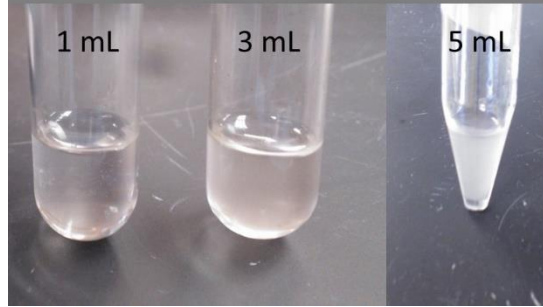
Table 5.2. Final conditions for dispersing AgNP in cyclohexanol (CyOH)

Condition	Volume of AgNP solution		
	1 mL	3mL	5 mL
Spin time before adding CyOH (min)	0.5	1.5	2.5
Spin time after adding CyOH (min)	0.5	0.75	1.0
Conditions used for spinning (g $\times 10^{-3}$) ¹	2.0	2.0	2.0

¹The centrifugation temperature was 25 °C.

Figure 5.10 (Top) Suspensions of AgNPs in cyclohexanol (CyOH) that were made by combining various volumes of a citrate-stabilized 18 nM AgNP solution with 1 mL of cyclohexanol. (Bottom left) UV/Vis spectrum for a citrate stabilized 2 nM AgNP solution in water. (Bottom right) UV/Vis spectrum for a AgNP/cyclohexanol suspension made under the conditions shown in Table 5.2 for a 3 mL of AgNP solution.

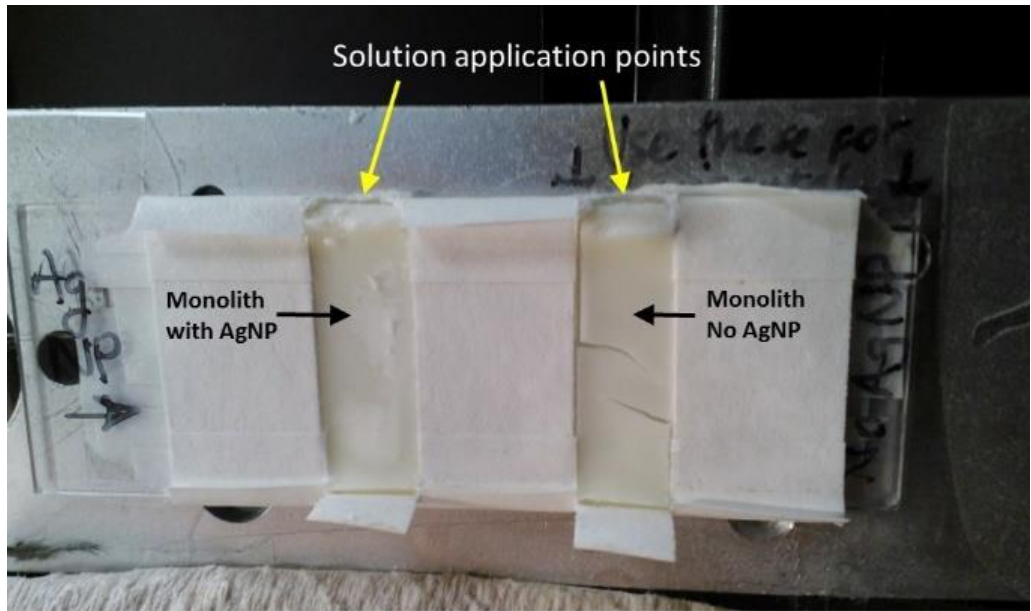
Volume of AgNP solution used for preparing the suspension:



Monoliths based on the conditions that are listed in Table 5.1 were prepared with cyclohexanol that contained AgNPs. The AgNP/cyclohexanol suspension was made according to the conditions that are given in Table 5.2 when starting with 3 or 5 mL of AgNP aqueous solutions. Another monolith preparation was made as a control that used cyclohexanol but had no AgNPs present. Sections of glass slides were covered with layers of adhesive tape for creating two pockets where the monolith mixtures containing AgNPs or no AgNPs could be cast and polymerized through photoinitiation, as described previously. After this process was completed, the slide now had a monolith layer that was 0.7 cm wide and about 1 mm thick, as shown in Figure 5.11.

Two types of monoliths were made on each glass slide: one containing a monolith layer with AgNPs and the other without AgNPs. The system that was used to conduct NIR fluorescent experiments with these slides was the same as depicted earlier in Figure 5.5. Each glass slide was fixed to the mounting stage of the system with double sided tape. A piece of adsorbent paper was attached to the mounting plate for collecting excess solution. The initial position for the microscope objective was set at 1.3 cm from the surface of the monoliths.

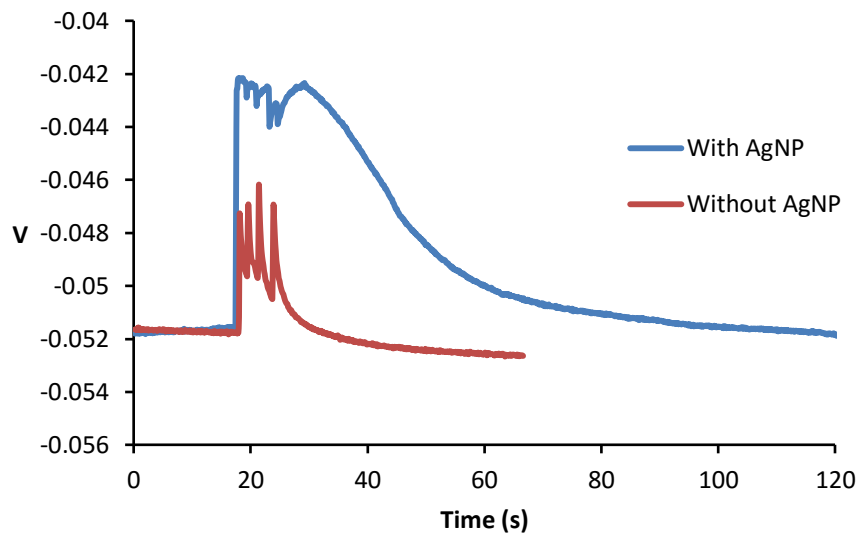
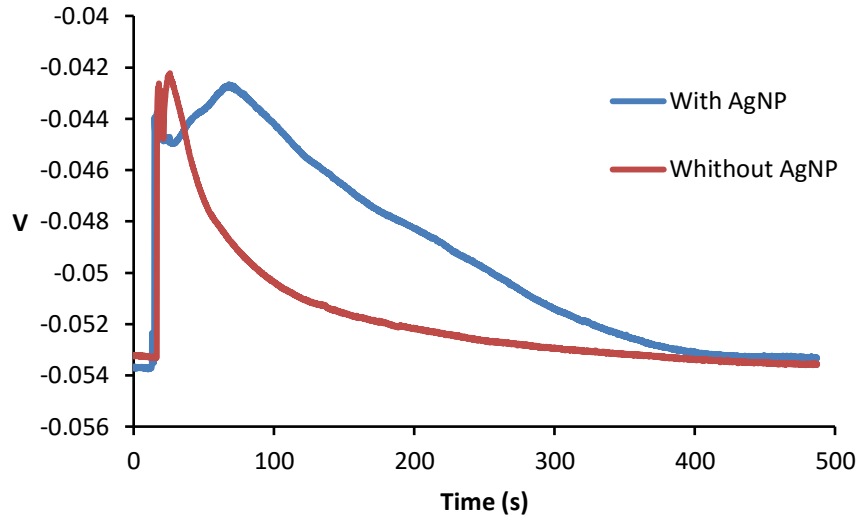
Figure 5.11 Glass slide with monolith layers containing or lacking AgNPs. A solution of the NIR fluorescent dye was applied to the top of each monolith with a dropper and allowed to flow downward across the monolith. Other conditions are given in the text.



A solution of the NIR fluorescent dye was applied with a dropper (e.g., four drops of 100 nM dye) to the top of each monolith and allowed to flow across the monolith through gravity. The fluorescence signal was recorded and the final distance between the monolith and the microscope objective was adjusted by using small movements along the z-axis, as described earlier. The signal was then recorded again while the dye solution was added to the monolith. After making these measurements for one of the monoliths (e.g., the one containing AgNPs), the microscope stage was moved to the other monolith and the process was repeated. The signal intensity was then compared for the monoliths with or without the AgNPs.

The results of the monolith made with 3 mL of the AgNP solution can be seen in Figure 5.12. After the dye solution was added to the top of each monolith and the laser was fixed at one spot on the monolith's surface, there was an initial increase in the signal, followed by a decrease as the dye solution moved across the monolith. The signal was allowed to return to the background level before adding more solution and doing the next measurement. Four measurements of this type were made at different spots on each monolith. For a 100 nM solution of the dye, an initial increase in signal to about 0.01 V was obtained on both types of monoliths. However, in the monolith with the AgNPs the fluorescence signal increased further after the addition of the dye and was followed by a much more gradual decrease. The overall result was that the signal after the addition of the dye was about two-fold larger for this monolith than for the control monolith that contained no AgNPs. When the concentration of the dye was decreased to 50 nM, an even greater change in the initial signal and an overall increase in signal was seen for the monolith with AgNPs versus the control monolith, as can be seen in Figure 5.12.

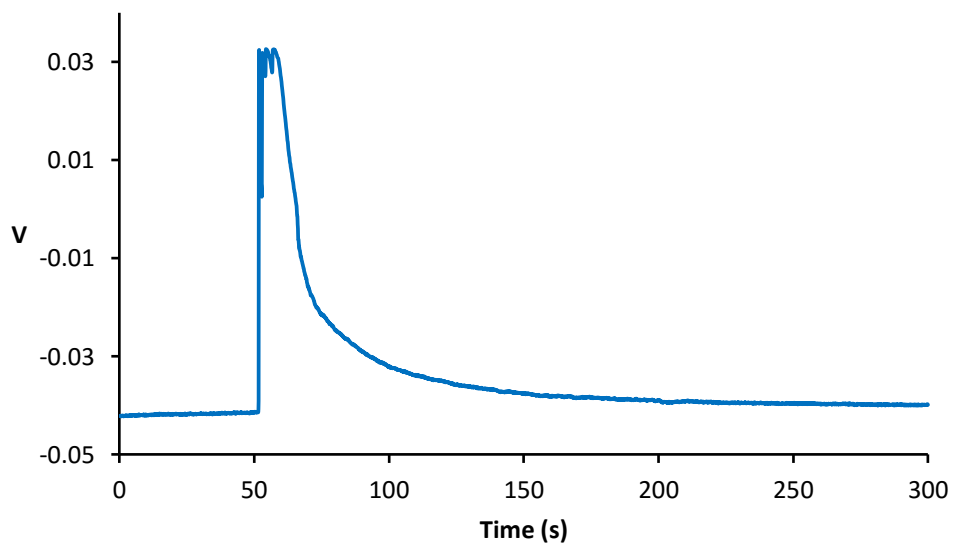
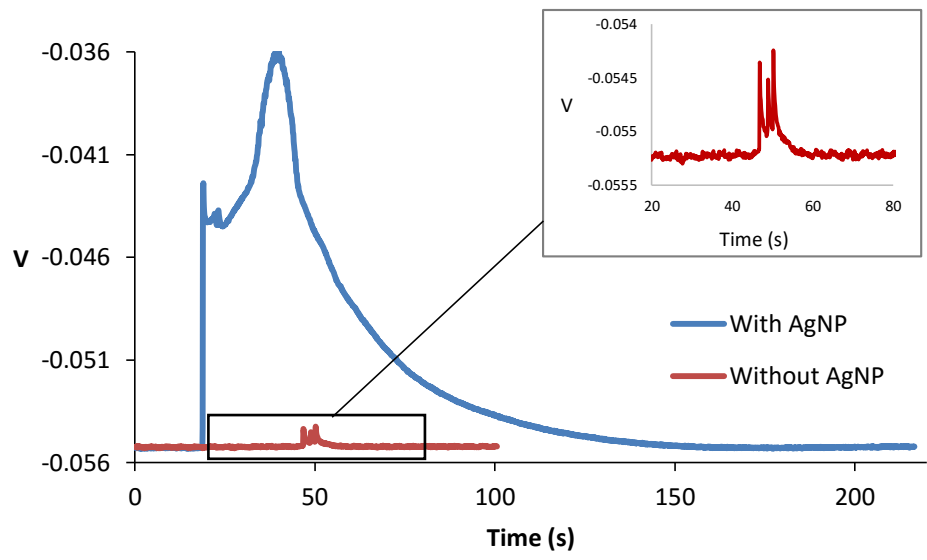
Figure 5.12 Fluorescence signals for solutions of the IR800CW dye that were applied to monolith layers containing AgNPs or no AgNPs. The dye concentrations were 100 nM (Top) or 50 nM (Bottom). The volume of the 18 nM AgNP stock solution that was used to make the first monolith was 3 mL.



The effect of increasing the AgNP concentration in the monolith was studied with a glass slide that contained a monolith layer made using the conditions that are listed in Table 5.2 for a 5 mL AgNP solution. The results were obtained at four different locations of monoliths that contained AgNPs or no AgNPs. Some typical results are shown for a 50 nM dye solution in Figure 5.13. An initial increase of 0.010–0.014 V in the signal was obtained when the dye solution was added to the top of the monolith with AgNPs. This signal increased after addition of the dye and then decreased exponentially. On the other hand, the monolith with no AgNPs showed an increase of only 0.001 to 0.0015 V when the dye solution was added to the top of the monolith. In this case, there was a ten- to 18-fold enhancement in signal on the monoliths that contained AgNPs. It should be noted that the graphs of the second glass plate were obtained by using a lower gain setting in order to bring the signal within the measurable range.

The fluorescence enhancement of the IRDye 800CW carboxylate dye was studied with a 5 nM solution and by increasing the gain of the microscope controller. As is demonstrated in Figure 5.13, the signal was easily seen in the monolith with AgNPs, but it was not detectable in the monolith with no AgNPs. The gain of the system for these experiments was close to the maximum that could be used with the instrument, but the results show that it was possible under these conditions to detect dye concentrations well below 1 nM on the GMA/EDMA monolith layer that contained AgNPs.

Figure 5.13 Fluorescent signal of IR800 CW dye solutions that were applied to monolith layers containing AgNPs or no AgNPs. The monolith with the AgNPs was made according to the conditions shown in Table 5.2 when using 5 mL of the original AgNP solution. The dye concentrations were 50 nM (top) or 5 nM (bottom). A signal due to the 5 nM dye solution was not detectable on the monoliths that did not contain AgNPs.



5.4.4. Fluorescence enhancement by AgNPs for monoliths in microfluidic chips

The fluorescence enhancement in EDMA/GMA monoliths containing AgNPs was next examined by using these monoliths in microfluidic devices. PDMS microfluidic devices were designed and produced for this work, as described in Section 5.2.4. These microfluidic devices were placed onto the microscope mounting stage, according to the procedures given in Section 5.4.2. Polymerization mixtures for the monoliths were made according to the conditions in Table 5.2 that used 5 mL of the original AgNP solution. A control monolith was made under the same conditions but without AgNPs. These mixtures were injected into the microchannel of each microchip by using a syringe, and polymerization was conducted as described previously.

When the dye solutions were first applied to these microfluidic channels, leaking occurred at cracks that were next to the inlet holes or over the body of the PDMS chip. These problems were caused by the backpressure that was generated by the monolith in the microchannel, and were exaggerated by the fact that the flow stream approached the monolith at a 90 ° angle. In an attempt to minimize or eliminate this issue, the cross section of the microchannel was increased to 250 × 500 μm and the inlet tube was placed at an angle of approximately 45° to the channel. These modifications reduced the problems with leaking but did not eliminate them completely.

As a result, a new design for the microfluidic chips, as inspired by the experiments with the monolith layers in the previous section, was next devised. These microchips were made in collaboration with Dr. Stephen Morin's lab and contained two micro-chambers with dimensions of 2 mm length × 1 mm width × 100 μm depth. These two chambers were connected to PE-60 tubing at the inlets. Monolith polymerization mixtures containing

AgNPs (made according to the conditions in Table 5.2 for a 5 mL AgNP solution) or without AgNPs were injected into these chambers with a syringe and through the inlet tubing. Photoinitiated polymerization was then carried out, and the inlets were connected to a syringe pump, as described previously. The design of this device, as shown in Figure 5.14, allowed for lower back pressures to be obtained because the flow path was straight from the inlet to the outlet and the monolith had a larger cross section. After their preparation, the monolith chambers were washed for 15 min with pH 7.4, 0.067 M potassium phosphate buffer at 50 $\mu\text{L}/\text{min}$. The optimum distance for detecting a flowing 100 nM IR 800CW dye solution was then determined by moving the stage versus the microscope objective along the z-axis. Next, 0.5 μL injections were made for solutions containing 0.5 to 100 nM of the IR 800CW NIR dye at 50 $\mu\text{L}/\text{min}$. This design allowed for a rapid adjustment of the relative position of detection for comparing the response between the monoliths with and without AgNPs.

Figure 5.14 PDMS microfluidic chip containing monoliths with or without AgNPs and for use in the detection of IRDye 800CW in a flowing stream. (Top) Side view showing the entrance of the polyethylene tubes next to the glass slide, and the thickness of the PDMS plate. (Bottom) Front view showing the monolith filled with AgNPs and the control monolith with no AgNPs present. The size of monoliths were 2 mm long \times 1 mm wide \times 100 μ m thick.

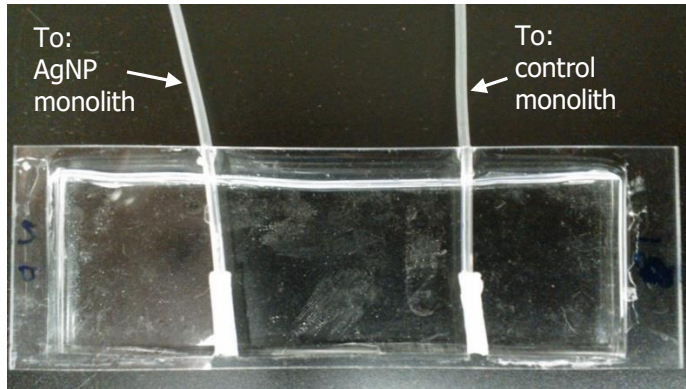
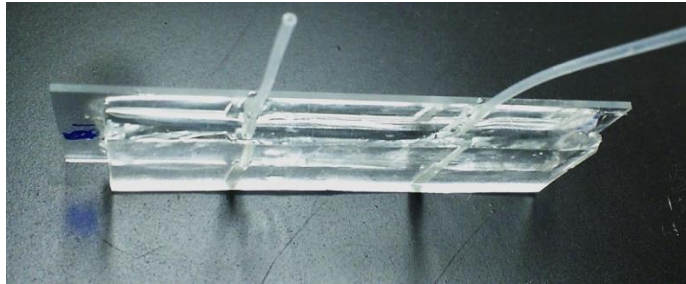
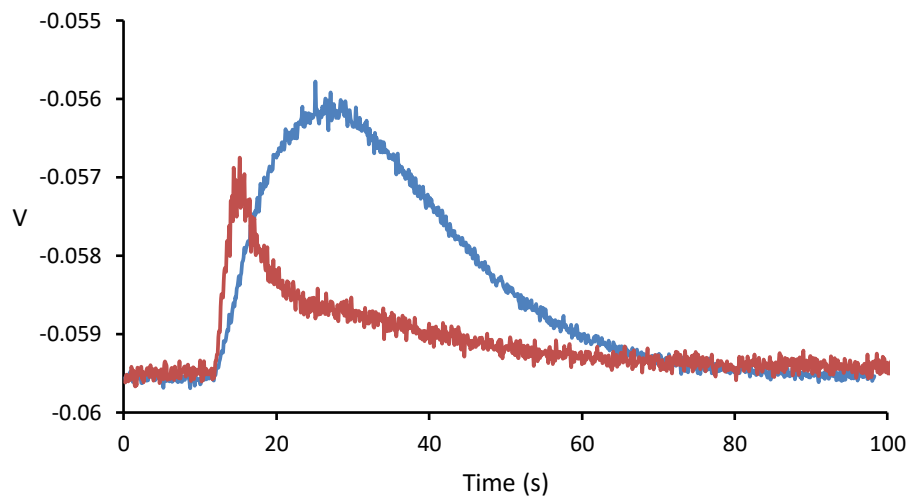
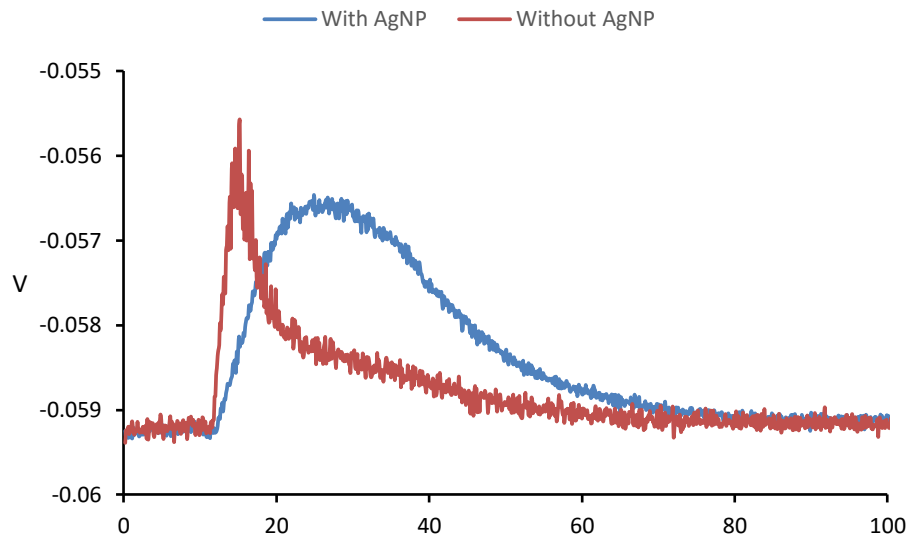


Figure 5.15 Comparison of the response versus time that was obtained by injecting IRDye 800CW solutions at various concentrations into the monoliths that were made with AgNPs or without AgNPs. Conditions: dye concentrations, (top) 60 nM or (bottom) 80 nM; injection volume, 0.5 μ L; flow rate, 0.5 μ L/min.



These results showed an effective fluorescence enhancement for the detection of the NIR fluorescent dye by using the AgNPs. This enhancement was most noticeable when comparing the peak areas that were obtained (see Figure 5.15). The observed trends were similar to those obtained for monolith layers (see Section 5.4.3). The fluorescence enhancement made it easier to detect the dye at low concentrations. For instance, the minimum concentration that could be detected for the NIR fluorescent dye in the presence of the AgNPs was 1 nM, whereas it was 5 nM without the use of AgNPs.

To estimate the amount of fluorescence enhancement that was obtained, the average peak areas for three injections were determined for each monolith and at each dye concentration. The peak area ratios that were measured both with and without the use of AgNPs were next determined at each dye concentration. The resulting enhancements in the fluorescence were between 1.5- and 2.5-fold. Calibration plots of area vs. concentration were also obtained for both types of monoliths. The correlation factors for these plots were high ($r^2 > 0.95$). The ratio between the slopes of the best-fit lines for the monoliths with and without AgNPs was 1.9, which again indicated a two-fold fluorescence enhancement with the monolith that contained AgNPs.

5.5. CONCLUSIONS

Detection of a model dye was achieved by using a NIR fluorescence microscope that was equipped with a laser light source and an x-y-z movable platform. This system was used for scanning and detecting fluorescence of the dye IR 800CW in microchannels, capillaries, monoliths, and monolith layers. This platform could be used in the future for biointeraction systems based on microfluidic chips or affinity microcolumns that contain monoliths based on GMA/EDMA, as has been previously demonstrated for the immobilization of proteins such as HSA and AGP [32,33,55]. With the scanning capabilities of this system, it was found that on-line detection could be carried out at several points along a microchannel, which makes this method useful for on-column or post-column detection.

The addition of AgNPs to the GMA/EDMA monoliths, by mixing the AgNPs with the porogen before polymerization, allowed for fluorescence enhancement of the IRDye 800CW. The results obtained in monolith layers that contained AgNPs showed at least a ten-fold enhancement in signal at the highest concentration of AgNPs that was tested. The signal was also more stable with the monoliths that had AgNPs than without AgNPs. The minimum concentration of the fluorophore that could be detected was improved from 10 nM without AgNPs to less than 1 nM with the highest concentration of AgNPs used. Even lower detection limits may be achieved by further increasing the AgNP content in the monoliths and by further optimizing the detection parameters for the microscope system.

The fluorescence enhancement in a flow-based system was studied by injecting a plug of NIR fluorescent dye into a microfluidic chip that contained microlayers of

GMA/EDMA. The results showed the same trend as with the dye solutions that were applied directly to the monolith layers. The AgNPs had the effect of increasing the fluorescence and producing a more stable signal. As a result of having a more stable signal, a better correlation between peak areas and the dye's concentration was also achieved. The detection limit was reduced from 5 nM to 1 nM in the presence of the AgNPs, with about a two-fold fluorescence enhancement being achieved when using monolith that contained AgNPs.

REFERENCES

1. T.M. Phillips, Microanalytical methods based on affinity chromatography, in: Handbook of Affinity Chromatography, 2nd ed., CRC Press, 2005, pp. 763-787.
2. H. Ju, X. Zhang, J. Wang, NanoBiosensing: Principles, Development and Application, Springer, New York, USA, 2011.
3. M.D. Furtaw, D. Lin, L. Wu, J.P. Anderson, Near-infrared metal-enhanced fluorescence using a liquid-liquid droplet micromixer in a disposable poly(methyl methacrylate) microchip, Plasmonics, 4 (2009) 273-280.
4. M.D. Furtaw, J.P. Anderson, L.R. Middendorf, G.R. Bashford, Near-infrared, surface-enhanced fluorescence using silver nanoparticle aggregates in solution, Plasmonics, 9 (2014) 27-34.
5. M.D. Furtaw, D.L. Steffens, T.M. Urlacher, J.P. Anderson, A near-infrared, surface-enhanced, fluorophore-linked immunosorbent assay, Anal. Chem., 85 (2013) 7102-7108.
6. S.M. Borisov, I. Klimant, Optical nanosensors - smart tools in bioanalytics, Analyst, 133 (2008) 1302-1307.
7. J.T. Cao, Z.X. Chen, X.Y. Hao, P.H. Zhang, J.J. Zhu, Quantum dots-based immunofluorescent microfluidic chip for the analysis of glycan expression at single-cells, Anal. Chem., 84 (2012) 10097-10104.
8. InTech, Advances in Immunoassay Technology, 1st ed., Rijeka, Croatia, 2012.

9. J.B. Grimm, L.M. Heckman, L.D. Lavis, The chemistry of small-molecule fluorogenic probes, in: M.C. Morris (Ed.) Fluorescence Based Biosensors: From Concepts to Applications, Academic Press, San Diego, CA, USA, 2013, pp. 1-34.
10. W.W. Parson, Modern Optical Spectroscopy, Springer, New York, NY, 2007.
11. S. Deshayes, G. Divita, Fluorescence technologies for monitoring interactions between biological molecules in vitro, in: M.C. Morris (Ed.) Fluorescence Based Biosensors: From Concepts to Applications, Academic Press, San Diego, CA, USA, 2013, pp. 109-144.
12. T. Nhu, N. Van, M.C. Morris, Fluorescent sensors of protein kinases: from basics to biomedical applications, in: M.C. Morris (Ed.) Fluorescence Based Biosensors: From Concepts to Applications, Academic Press, San Diego, CA, USA, 2013, pp. 217-2474.
13. G. Hong, S.M. Tabakman, K. Welsher, Z. Chen, J.T. Robinson, H. Wang, B. Zhang, H. Dai, Near-infrared-fluorescence-enhanced molecular imaging of live cells on gold substrates, *Angew Chem. Int. Ed.*, 50 (2011) 4644-4648.
14. A. Vial, A.S. Grimault, D. Macias, D. Barchiesi, M.L. de la Chapelle, Improved analytical fit of gold dispersion: application to the modeling of extinction spectra with a finite-difference time-domain method, *Phys. Rev. B*, 71 (2005).
15. D. Schebarchov, B. Auguie, E.C. Le Ru, Simple accurate approximations for the optical properties of metallic nanospheres and nanoshells, *Phys. Chem. Chem. Physics*, 15 (2013) 4233-4242.
16. L. Novotny, N. van Hulst, Antennas for light, *Nature Photonics*, 5 (2011) 83-90.

17. V. Giannini, A.I. Fernandez-Dominguez, S.C. Heck, S.A. Maier, Plasmonic nanoantennas: fundamentals and their use in controlling the radiative properties of nanoemitters, *Chem. Rev.*, 111 (2011) 3888-3912.
18. S.V. Boriskina, L. Dal Negro, Multiple-wavelength plasmonic nanoantennas, *Optics Lett.*, 35 (2010) 538-540.
19. M.P. Busson, B. Rolly, B. Stout, N. Bonod, S. Bidault, Accelerated single photon emission from dye molecule-driven nanoantennas assembled on DNA, *Nature Comm.*, 3 (2012).
20. D. Punj, M. Mivelle, S.B. Moparthy, T.S. van Zanten, H. Rigneault, N.F. van Hulst, M.F. Garcia-Parajo, J. Wenger, A plasmonic 'antenna-in-box' platform for enhanced single-molecule analysis at micromolar concentrations, *Nature Nanotechnol.*, 8 (2013) 512-516.
21. L. Qin, S. Zou, C. Xue, A. Atkinson, G.C. Schatz, C.A. Mirkin, Designing, fabricating, and imaging Raman hot spots, *Proc. Nat. Acad. Sci. U.S.A.*, 103 (2006) 13300-13303.
22. N.J. Borys, E. Shafran, J.M. Lupton, Surface plasmon delocalization in silver nanoparticle aggregates revealed by subdiffraction supercontinuum hot spots, *Sci. Reports*, 3 (2013).
23. E.M. Perassi, E.A. Coronado, The structure, energy, confinement, and enhancement of hot spots between two nanoparticles, *J. Phys. Chem. C*, 117 (2013) 7744-7750.

24. X. Wang, Y. Du, Q. Li, T. Wu, H. Hu, Y. Xu, H. Zhang, Y. Pan, Fabrication of uniform substrate based on silver nanoparticles decorated glycidyl methacrylate-ethylene dimethacrylate porous material for ultrasensitive surface-enhanced Raman scattering detection, *J. Raman Spectrosc.*, 45 (2014) 47-53.
25. F. Tam, G.P. Goodrich, B.R. Johnson, N.J. Halas, Plasmonic enhancement of molecular fluorescence, *Nano Lett.*, 7 (2007) 496-501.
26. L. Middendorf, J. Amen, R. Bruce, D. Draney, D. Degraff, J. Gewecke, D. Grone, P. Humphrey, G. Little, A. Lugade, N. Narayanan, A. Oommen, H. Osterman, R. Peterson, J. Rada, R. Raghavachari, S. Roemer, Near-infrared fluorescence instrumentation for DNA analysis, in: S. Daehne, U. Resch-Genger, O.S. Wolfbeis (Eds.) *NATO ASI Series 3 High Technology; Near-Infrared Dyes for High Technology Applications*, 1998, pp. 21-53.
27. Y. Ohba, Y. Fujioka, S. Nakada, M. Tsuda, Fluorescent protein-based biosensors and their clinical applications, in: M.C. Morris (Ed.) *Fluorescence Based Biosensors: From Concepts to Applications*, Academic Press, San Diego, CA, USA, 2013, pp. 313-348.
28. M. Araya-Farias, M. Taverna, M. Woytasik, F. Bayle, M. Guerrouache, I. Ayed, H.H. Cao, B. Carbonnier, N.T. Tran, A new strategy for simultaneous synthesis and efficient anchorage of polymer monoliths in native PDMS microchips, *Polymer*, 66 (2015) 249-258.

29. K. Faure, M. Bias, O. Yassine, N. Delaunay, G. Cretier, M. Albert, J.-L. Rocca, Electrochromatography in poly(dimethyl)siloxane microchips using organic monolithic stationary phases, *Electrophoresis*, 28 (2007) 1668-1673.
30. Q.-S. Kang, Y. Li, J.-Q. Xu, L.-J. Su, Y.-T. Li, W.-H. Huang, Polymer monolith-integrated multilayer poly(dimethylsiloxane) microchip for online microextraction and capillary electrophoresis, *Electrophoresis*, 31 (2010) 3028-3034.
31. Q.-S. Kang, X.-F. Shen, N.-N. Hu, M.-J. Hu, H. Liao, H.-Z. Wang, Z.-K. He, W.-H. Huang, A 3D porous polymer monolith-based platform integrated in poly(dimethylsiloxane) microchips for immunoassay, *Analyst*, 138 (2013) 2613-2619.
32. E.L. Pfaunmiller, M.L. Paulemond, C.M. Dupper, D.S. Hage, Affinity monolith chromatography: a review of principles and recent analytical applications, *Anal. Bioanal. Chem.*, 405 (2013) 2133-2145.
33. E.L. Pfaunmiller, M. Hartmann, C.M. Dupper, S. Soman, D.S. Hage, Optimization of human serum albumin monoliths for chiral separations and high-performance affinity chromatography, *J. Chromatogr. A*, 1269 (2012) 198-207.
34. A. Pingoud, C. Urganke, J. Hoggett, A. Jeltsch, *Biochemical Methods - A Concise Guide for Students and Researches*, Wiley VCH, Weinheim, Germany, 2002.
35. F. Sipieter, P. Vandame, C. Spriet, A. Leray, P. Vincent, D. Trinel, J. Bodart, F.B. Riquet, L. Héliot, From FRET imaging to practical methodology for kinase activity sensing in living cells, in: M.C. Morris (Ed.) *Fluorescence Based Biosensors: From*

Concepts to Applications, Academic Press, San Diego, CA, USA, 2013, pp. 145-216.

36. S.M. Nie, S.R. Emery, Probing single molecules and single nanoparticles by surface-enhanced Raman scattering, *Science*, 275 (1997) 1102-1106.
37. K. Kneipp, Y. Wang, H. Kneipp, L.T. Perelman, I. Itzkan, R. Dasari, M.S. Feld, Single molecule detection using surface-enhanced Raman scattering (SERS), *Phys. Rev. Lett.*, 78 (1997) 1667-1670.
38. J.P. Anderson, M. Griffiths, V.R. Boveia, Near-infrared fluorescence enhancement using silver island films, *Plasmonics*, 1 (2006) 103-110.
39. C.F. Duan, H. Cui, Z.F. Zhang, B. Liu, J.Z. Guo, W. Wang, Size-dependent inhibition and enhancement by gold nanoparticles of luminol-ferricyanide chemiluminescence, *J. Phys. Chem. C*, 111 (2007) 4561-4566.
40. Y.P. Kim, Y.H. Oh, E. Oh, S. Ko, M.K. Han, H.S. Kim, Energy transfer-based multiplexed assay of proteases by using gold nanoparticle and quantum dot conjugates on a surface, *Anal. Chem.*, 80 (2008) 4634-4641.
41. G.K. Kouassi, J. Irudayaraj, Magnetic and gold-coated magnetic nanoparticles as a DNA sensor, *Anal. Chem.*, 78 (2006) 3234-3241.
42. Z.H. Mo, X.C. Yang, K.P. Guo, Z.Y. Wen, A nanogold-quenched fluorescence duplex probe for homogeneous DNA detection based on strand displacement, *Anal. Bioanal. Chem.*, 389 (2007) 493-497.

43. M.C. Daniel, D. Astruc, Gold nanoparticles: Assembly, supramolecular chemistry, quantum-size-related properties, and applications toward biology, catalysis, and nanotechnology, *Chem. Rev.*, 104 (2004) 293-346.
44. O. Stranik, H.M. McEvoy, C. McDonagh, B.D. MacCraith, Plasmonic enhancement of fluorescence for sensor applications, *Sensors Actuators B Chem.*, 107 (2005) 148-153.
45. S.M. Tabakman, L. Lau, J.T. Robinson, J. Price, S.P. Sherlock, H. Wang, B. Zhang, Z. Chen, S. Tangsombatvisit, J.A. Jarrell, P.J. Utz, H. Dai, Plasmonic substrates for multiplexed protein microarrays with femtomolar sensitivity and broad dynamic range, *Nature Commun.*, 2 (2011).
46. J.L. Chen, A.F. Zheng, A.H. Chen, Y.C. Gao, C.Y. He, X.M. Kai, G.H. Wu, Y.C. Chen, A functionalized gold nanoparticles and Rhodamine 6G based fluorescent sensor for high sensitive and selective detection of mercury(II) in environmental water samples, *Anal. Chim. Acta*, 599 (2007) 134-142.
47. K. Sokolov, G. Chumanov, T.M. Cotton, Enhancement of molecular fluorescence near the surface of colloidal metal films, *Anal. Chem.*, 70 (1998) 3898-3905.
48. Q.Q. Fu, Y. Tang, C.Y. Shi, X.L. Zhang, J.J. Xiang, X. Liu, A novel fluorescence-quenching immunochromatographic sensor for detection of the heavy metal chromium, *Biosens. Bioelectron.*, 49 (2013) 399-402.
49. P. Bharadwaj, P. Anger, L. Novotny, Nanoplasmonic enhancement of single-molecule fluorescence, *Nanotechnol.*, 18 (2007).

50. L. Zhao, T. Ming, H. Chen, Y. Liang, J. Wang, Plasmon-induced modulation of the emission spectra of the fluorescent molecules near gold nanorods, *Nanoscale*, 3 (2011) 3849-3859.
51. J.R. Lakowicz, J. Malicka, I. Gryczynski, Z. Gryczynski, C.D. Geddes, Radiative decay engineering: the role of photonic mode density in biotechnology, *J. Physics D Appl. Physics*, 36 (2003) R240-R249.
52. M.I. Stockman, Nanoplasmonics: past, present, and glimpse into future, *Optics Express*, 19 (2011) 22029-22106.
53. P. Bharadwaj, B. Deutsch, L. Novotny, Optical antennas, *Adv. Optics Photonics*, 1 (2009) 438-483.
54. C.D. Geddes, I. Gryczynski, J. Malicka, Z. Gryczynski, J.R. Lakowicz, Metal-enhanced fluorescence: potential applications in HTS, *Combin. Chem. High Throughput Screening*, 6 (2003) 109-117.
55. E. Pfaunmiller, A.C. Moser, D.S. Hage, Biointeraction analysis of immobilized antibodies and related agents by high-performance immunoaffinity chromatography, *Methods*, 56 (2012) 130-135.

CHAPTER 6.

SUMMARY AND FUTURE WORK

6.1. SUMMARY

The entrapment method for immobilizing biologically-related compounds in chromatographic supports has been shown to be useful for preparing affinity ligands where the ligand retains essentially full activity. The work in this dissertation included the development of new approaches for increasing the amount of proteins that can be placed in supports prepared by entrapment for high performance affinity chromatography (HPAC) and the application of the newly developed supports for studying the interactions between drugs and proteins. As shown in this dissertation, HPAC with supports made by entrapment can be used to investigate how the binding of proteins to drugs and small solutes is affected by glycation. The use of microfluidics in HPAC and with monolithic supports and using metal-based fluorescence enhancement for detection was also considered.

The first chapter provided a general introduction to HPAC and the methods of zonal elution and frontal analysis. Background information on the entrapment method was also provided, along with a description of the potential advantages of this method over covalent immobilization methods.

Chapter 2 examined ways of increasing the protein coverage, and therefore the overall activity, of supports made by entrapment. This work included modifying the conditions of the entrapment process in a slurry-based format. Human serum albumin

(HSA) was used as a model protein for these studies. The protein content for several batches of silica supports that were made by entrapment was measured and the retention of HPLC columns that were made with these supports was measured for solutes that bind to HSA. Alternative ways of measuring the protein content of such supports, such as fluorescence of labelled HSA and thermogravimetric analysis, were investigated as well.

Chapter 3 dealt with the development of a flow-based format for the entrapment of proteins. The optimum conditions for obtaining supports with high protein contents with this on-column entrapment method were found. The supports that were made by this method were used in the study of interactions between HSA or lectins and probe compounds that are known to bind these proteins. By using probes with known binding constants for these proteins, it was possible to estimate the protein content of these supports in columns without the need for disassembling these columns or destroying the support.

Changes in the bloodstream can occur during metabolic diseases, such as diabetes, and produce modifications in serum proteins. One important example is the glycation of HSA that occurs in diabetes. This modification can influence the binding of this protein with some drugs, such as many sulfonylurea drugs that are used to treat type II diabetes. In Chapter 4, samples of normal HSA and HSA with glycation levels characteristic of patients with pre-diabetes, controlled diabetes or advanced diabetes were placed into supports made by entrapment and the on-column method. The high protein contents that were achieved by the on-column method, and the fact that the activity of this protein was maintained in these supports, allowed the use of this method in a simplified approach for measuring drug-protein interactions at specific sites on normal HSA or glycated HSA. This

was achieved by using competing agents for the given sites and measuring the shifts in retention that occurred for a given drug in the presence of this competing agent.

The development of a microfluidic device that was suitable for use in on-column or post-column detection in HPAC was discussed in Chapter 5. A monolith based on glycidyl methacrylate-ethylene dimethacrylate (GMA/EDMA) co-polymer was placed into such a device for use as a chromatographic support and a near infrared scanning fluorescence microscope was used as the detector. The conditions that were needed with this system for measuring a NIR fluorescent dye were established when using monoliths and when the monoliths were placed into microchannels. This chapter also examined the fluorescence enhancement that was obtained for the NIR fluorescent dye when silver nanoparticles (AgNPs) were added to GMA/EDMA monoliths. The limit of detection was decreased for monoliths contained AgNPs when compared to monoliths without AgNPs. Overall, these results indicated that fluorescence enhancement by AgNPs was feasible in microfluidic devices containing EGA/EDMA monoliths. These devices are attractive for future use in biointeraction systems that may contain proteins or antibodies that are immobilized into monolithic supports.

6.2. FUTURE WORK

The work in this dissertation involved the development of high capacity supports containing entrapped proteins for use in HPAC. This work has shown that an on-column method of entrapment can provide the highest protein contents in column affinities while also having minimal reagent consumption. The creation of encapsulated protein columns with high protein contents has opened up many possible options for further implementation

of the entrapment immobilization method. For example, it should be feasible to study analytes with low affinities by using columns with high protein coverage or to reduce the column size for studying the interactions of drugs or metabolites with proteins that are either expensive or that are isolated from a small amount of a sample (e.g., a serum sample from a human or animal). It should also be possible with these small columns to combine several columns together in microfluidic devices and to use them with fluorescence detection to analyze samples with sizes in the sub-microliter range and target analytes at sub-nanomolar concentrations.

The next logical step, after the implementation of the on-column method of entrapment in this dissertation, would be the automation of the entrapment process. This could be done by using a system of pumps for applying the reagents through a hydrazide-activated silica column, and a system of valves that can switch between the various reagent solutions. One further step in automation would be to make a complete on-line entrapment system where the protein that is to be entrapped (e.g., HSA) could also be isolated from a biological sample (e.g., human serum) by using an antibody column for the protein, followed by elution of the captured protein directly into the hydrazide-activated silica support, where entrapment is then performed. Such a system would minimize loss of the protein during sample handling steps and would provide a convenient way of entrapping proteins or other biologically-related agents that are obtained from *in vivo* samples.

The fact that the protein remains fully active when it is immobilized by entrapment should also make it possible with this method to create fast screening methods that can be used to obtain the binding affinities for solutes with the entrapped proteins. As shown in Chapter 4, this might be accomplished by simply measuring retention time shifts when this

solute is injected in the presence or absence of the entrapped protein. The entrapment method could also be extended to additional ligands besides those examined in this dissertation. Examples include other serum proteins (e.g., variants of the protein α_1 -acid glycoprotein) or other lectins (e.g., jacalin or *Sambucus nigra* agglutinin). These lectin columns could be used in studies for glycoproteomics in which the binding of the entrapped lectins might be used for the isolation of glycopeptides or glycans prior to the analysis of these analytes by methods such as mass spectrometry.

ACKNOWLEDGMENTS

The work described in this dissertation was supported, in part, by the National Institutes of Health (grants R01 GM044931 and R01 DK069629), and by the National Science Foundation/EPSCoR program (grant EPS-1004094). Support for the remodeled facilities that were used to perform these experiments was provided under NIH grant RR015468-001.